NASA TECHNICAL NOTE

NASA TN D-5727

C. 1



NASA TN D-5727



# INDUCED INTERFERENCE EFFECTS ON THE AERODYNAMIC CHARACTERISTICS OF A 0.16-SCALE SIX-JET V/STOL MODEL IN TRANSITION



*by Matthew M. Winston*

*Langley Research Center*
*Langley Station, Hampton, Va.*

NATIONAL AERONAUTICS AND SPACE ADMINISTRATION • WASHINGTON, D. C. • MARCH 1970

| 1. Report No. NASA TN D-5727 | 2. Government Accession No. | 3. Recipient's Catalog No. |
|---|---|---|
| 4. Title and Subtitle<br>INDUCED INTERFERENCE EFFECTS ON THE AERODYNAMIC CHARACTERISTICS OF A 0.16-SCALE SIX-JET V/STOL MODEL IN TRANSITION | | 5. Report Date<br>March 1970<br>6. Performing Organization Code |
| 7. Author(s)<br>Matthew M. Winston | | 8. Performing Organization Report No.<br>L-6921<br>10. Work Unit No.<br>721-01-11-00-23 |
| 9. Performing Organization Name and Address<br>NASA Langley Research Center<br>Hampton, Va. 23365 | | 11. Contract or Grant No.<br>13. Type of Report and Period Covered<br>Technical Note |
| 12. Sponsoring Agency Name and Address<br>National Aeronautics and Space Administration<br>Washington, D.C. 20546 | | 14. Sponsoring Agency Code |

15. Supplementary Notes

16. Abstract

The investigation was conducted in the 17-foot (5.18-meter) test section of the Langley 300-MPH 7- by 10-foot tunnel. The model was powered by six cold-air ejectors simulating four direct-lift and two lift-cruise jet engines. The jet-induced interference effects are analyzed for the pure-lift and lift-cruise propulsion modes for effective velocity ratios from 0 to about 0.12 over ranges of angle of attack and sideslip angle. The effects of horizontal-tail configuration, thrust vectoring, and ground proximity are examined. Also, results of a limited investigation of the inlet-mass-flow contribution to the total induced effects are included.

17. Key Words Suggested by Author(s)
Jet-induced effects
V/STOL
Static stability characteristics
Horizontal-tail surfaces

18. Distribution Statement
Unclassified – Unlimited

| 19. Security Classif. (of this report) | 20. Security Classif. (of this page) | 21. No. of Pages | 22. Price* |
|---|---|---|---|
| Unclassified | Unclassified | 73 | $3.00 |

*For sale by the Clearinghouse for Federal Scientific and Technical Information
Springfield, Virginia 22151

# INDUCED INTERFERENCE EFFECTS ON THE AERODYNAMIC CHARACTERISTICS OF A 0.16-SCALE SIX-JET V/STOL MODEL IN TRANSITION

By Matthew M. Winston
Langley Research Center

## SUMMARY

An investigation was conducted to determine the jet-induced interference effects on a model of a jet-lift research airplane during low-speed transition. The data were obtained in the 17-foot (5.18-meter) test section of the Langley 300-MPH 7- by 10-foot tunnel. Effects of engine inlet mass flow and jet efflux were examined for angles of attack from about $-7^{\circ}$ to $28^{\circ}$, sideslip angles from about $-28^{\circ}$ to $6^{\circ}$, and effective velocity ratios from 0 to about 0.12. Results are presented for conditions simulating operation with six direct-lift engines and also for conditions simulating simultaneous operation of four lift engines and two cruise engines. The effects of horizontal-tail configuration, thrust vectoring, and ground proximity are included.

Similar induced lift losses and nose-up pitching moments are indicated for both the pure-lift and lift-cruise propulsion modes, and the overall interference effects on the lateral-directional characteristics are shown to be positive. The induced effects attributed to inlet mass flow provided a large positive contribution to effective dihedral and increased both the total drag and nose-up pitching moments.

## INTRODUCTION

Extensive studies of jet-propelled vertical or short take-off and landing (V/STOL) aircraft have shown that jet-induced effects on basic aircraft characteristics can be significant, particularly in the speed range for transition from vertical to cruise flight (refs. 1 to 7). The effects of engine inlet flow and the interaction of jet efflux with free-stream flow have been shown not only to affect the magnitude of the resultant overall forces and moments but also to cause appreciable changes in stability and trim.

The emphasis of most of the presently available information is on the jet-induced effects on longitudinal aerodynamic characteristics for vertically oriented lifting jets. Also, a limited amount of information is available on the induced effects from vectored

nozzle configurations which rotate the jet efflux through a wide angular range ($90^{o}$ or more) to provide thrust for both lift and cruise (refs. 5 and 6).

The present investigation was conducted with a 0.16-scale model of a V/STOL research aircraft which is powered by four direct-lift engines mounted vertically in the fuselage and two lift-cruise engines mounted horizontally in nacelles alongside the fuselage. The flow from the two lift-cruise engines can be diverted to exhaust through vertically oriented lift nozzles in the fuselage; this thus provides six lifting elements for vertical flight. The lift nozzles for all six engines can be vectored through a limited angular range. The unique feature of this airplane is that one of its normal operational modes employs simultaneous application of horizontal and vertical thrust from the lift-cruise and direct-lift engines, respectively. The induced effects associated with this particular combination of jet operations are, therefore, of special interest. Basic force data from the present model are given in reference 8, and an analysis of some of the static stability characteristics in the cruise mode is given in reference 9. The present paper is concerned primarily with the jet-induced interference effects associated with the low-speed portion of the transition speed range. The effects of thrust vectoring, engine modes, horizontal-tail configuration, and ground proximity are analyzed for ranges of angle of attack and sideslip angle. The measured force and moment parameters are included together with the calculated interference data.

## SYMBOLS

The data are referred to the stability system of axes. Moments are referred to a point in the plane of symmetry 0.1 wing mean aerodynamic chord aft of the wing leading edge and 0.088 wing mean aerodynamic chord above the wing-chord plane. (See fig. 1.) Units for the physical quantities used herein are presented in both the U.S. Customary Units and the International System of Units. Factors relating these two systems of units may be found in reference 10.

$A$ cross-sectional area, feet$^2$ (meters$^2$)

$b$ wing span, feet (meters)

$C_D$ drag coefficient, $\frac{D}{qS}$

$C_L$ lift coefficient, $\frac{L}{qS}$

$C_l$ rolling-moment coefficient, $\frac{\text{Rolling moment}}{qSb}$

$\Delta C_l$ increment in $C_l$ due to jet interference

$C_m$ pitching-moment coefficient, $\frac{M}{qS\bar{c}}$

$C_n$ yawing-moment coefficient, $\frac{\text{Yawing moment}}{qSb}$

$\Delta C_n$ increment in $C_n$ due to jet interference

$C_T$ thrust coefficient, $\frac{T}{qS}$

$C_Y$ side-force coefficient, $\frac{\text{Side force}}{qS}$

$\Delta C_Y$ increment in $C_Y$ due to jet interference

$\bar{c}$ wing mean aerodynamic chord, feet (meters)

D drag, pounds (newtons)

$\Delta D$ drag increment due to jet interference, pounds (newtons)

h height of model center of gravity above ground plane, feet (meters)

$i_t$ horizontal-tail incidence angle, positive when leading edge is up, degrees

L lift, pounds (newtons)

$\Delta L$ lift increment due to jet interference, pounds (newtons)

M pitching moment, foot-pounds (meter-newtons)

$\Delta M$ pitching-moment increment due to jet interference, foot-pounds (meter-newtons)

q free-stream dynamic pressure, pounds/foot$^2$ (newtons/meter$^2$)

S wing planform area, feet$^2$ (meters$^2$)

| | |
|---|---|
| T | total measured thrust of engine simulator, pounds (newtons) |
| V | velocity, feet/second (meters/second) |
| $\alpha$ | angle of attack, degrees |
| $\beta$ | angle of sideslip, degrees |
| $\delta_n$ | resultant thrust angle less $10^o$ achieved by orientation of lift nozzles |
| $\rho$ | mass density of air, slugs/foot$^3$ (kilograms/meter$^3$) |

Subscripts:

| | |
|---|---|
| a | power-off measurement |
| j | jet exit |
| m | power-on measurement |
| T | calculated force or moment due to a component of thrust |
| $\infty$ | free stream |

## MODEL, APPARATUS, AND INSTRUMENTATION

The model used in this investigation was a 0.16-scale model of a jet V/STOL research airplane powered by four direct-lift and two lift-cruise engines. Sketches and geometric characteristics of the model are presented in figure 1. The wing incorporates 30-percent-chord single-slotted flaps which extend from 35 percent to 78 percent of the wing semispan. The flaps were deflected $40^o$ for the present investigation. Horizontal-tail incidence is manually adjustable from $-10^o$ to $15^o$ in $5^o$ increments. During a portion of the tests, a fixed-incidence auxiliary horizontal tail was installed below the basic horizontal tail. (See ref. 9.) A sketch of this auxiliary tail is given in figure 2, and photographs of the model with the basic and auxiliary horizontal tails installed are presented as figure 3. Manually adjustable elevator and rudder were also incorporated into the empennage; for the present investigation, however, they were set at $0^o$. Boundary-layer transition was fixed on the wing, vertical tail, basic horizontal tail, and auxiliary horizontal tail by strips of No. 70 carborundum grit at 0.10 local chord of these surfaces.

The model was powered by six cold-air ejectors, four ejectors simulating direct-lift engines and two ejectors simulating lift-cruise engines. A complete description and a typical calibration of the type of ejector used are given in reference 11. Compressed air (primary air) was distributed to each ejector from a plenum chamber in the model. Secondary air was entrained through the model inlets (on the fuselage upper surface and in the nacelles) and ducted to the ejector faces. The combined primary and secondary air was then ducted through the exit nozzles into the free stream. Instrumentation in the exit nozzles was used to determine the thrust of each ejector. Two different sets of ducts were used with the nacelle-mounted ejectors. One set directed the flow straight through the nacelles for cruise-engine simulation, and the other set directed the flow through the fuselage to the lift nozzles for lift-engine simulation.

In the pure-lift mode, the three pairs of lift nozzles were variably inclined in the longitudinal plane, so that the resultant of the six thrust vectors passed through the assumed center of gravity at an inclination $10^{\circ}$ forward of the vertical axis. On the full-scale airplane, this arrangement provides a basic hovering attitude of $10^{\circ}$ (nose up). This nozzle configuration is designated herein as $\delta_n = 0^{\circ}$. The nozzles could also be deflected to two other positions which rotated the resultant vector $10^{\circ}$ farther forward of the basic setting for a $20^{\circ}$ total inclination or to $10^{\circ}$ aft of the basic setting for a $0^{\circ}$ inclination; these deflections are designated as $\delta_n = 10^{\circ}$ and $\delta_n = -10^{\circ}$, respectively. All nozzles were inclined $10^{\circ}$ away from the plane of symmetry.

The model was mounted on a six-component strain-gage balance and was supported on a sting which contained an internal air-supply line to power the ejectors. Details of the air supply and balance installation are given in figure 1(b). The sting was supported by a telescoping strut, so that the model could be moved through a range of pitch and yaw angles and heights above the moving-belt ground plane described in reference 12.

Forces and moments were measured with the six-component balance, pitch angles were measured with an electronic gravity-sensing device, and the sideslip angles were measured with a calibrated gearing arrangement on the support drive mechanism. Ejector operating variables, such as pressures and mass flows, were measured with standard types of pressure transducers and flowmeters.

## TESTS AND CORRECTIONS

The investigation was conducted in the 17-foot (5.18-meter) test section of the Langley 300-MPH 7- by 10-foot tunnel. The maximum free-stream velocity was about 57 knots which corresponds to a Reynolds number based on wing mean aerodynamic chord of $0.43 \times 10^6$. All the data were obtained with the model in the normal transition configuration where the flaps were set at $40^{\circ}$ and the jet exit doors on the fuselage

underside were open. For the tests out of ground effect, the landing gear was removed. For the tests in ground effect, the landing gear was installed. The primary model variables were horizontal-tail configuration and incidence and jet nozzle arrangement and setting. Test variables were angles of attack and sideslip, free-stream velocity, model thrust, and model height above the ground. The various model thrust levels were obtained by setting the primary air supply pressure at the entrance to the support sting in accordance with a previously determined relationship between sting pressure and static thrust. At selected points during a given test, electrical signals from the six-component balance, pitch-angle sensor, pressure transducers, and fixed tunnel instrumentation were fed into a digital readout and recording system. Other variables, such as sideslip angle and model height, were manually fed into the recording system.

The data have been corrected for deadweight tares, for the loads exerted on the balance by the air supply-line installation, and for the effects of varying air pressure on the balance. No corrections have been made to the data to account for the wind-tunnel wall effects, since these effects are believed to be small for a model of this size in the 17-foot (5.18-meter) test section. (See ref. 13.)

## PRESENTATION OF RESULTS

The results of this investigation are presented to show the effects of jet-induced loads for various model configurations and operational conditions in the transition speed range. Generally, the range of effective velocity ratio $\sqrt{\frac{\rho_\infty V_\infty^2}{\rho_j V_j^2}}$ for transition of jet V/STOL airplanes is from 0 to about 0.3. Most of the data presented herein, however, were obtained up to velocity ratios of only about 0.12 and, consequently, represent the low-speed portion of the normal transition speed range. As indicated by most of the references cited herein, the magnitude of the induced effects for a given configuration at a velocity ratio of 0.12 can be expected to be less than one-half of that obtained at a velocity ratio of 0.3.

The longitudinal data are presented as forces nondimensionalized by thrust and as moments nondimensionalized by the product of thrust and wing mean aerodynamic chord. The lateral-directional data are presented in standard coefficient form. For each configuration and flight condition, the measured data are presented together with the calculated jet-induced force and moment increments. The jet-induced interference increments were calculated from the following equations:

$$\frac{\Delta L}{T} = \frac{L_m}{T} - \left(\frac{L_T}{T} + \frac{C_{L,a}}{C_T}\right)$$

$$\frac{\Delta D}{T} = \frac{D_m}{T} - \left(\frac{D_T}{T} + \frac{C_{D,a}}{C_T}\right)$$

$$\frac{\Delta M}{T\bar{c}} = \frac{M_m}{T\bar{c}} - \left(\frac{M_T}{T\bar{c}} + \frac{C_{m,a}}{C_T}\right)$$

$$\Delta C_l = C_{l,m} - \left(C_{l,T} + C_{l,a}\right)$$

$$\Delta C_n = C_{n,m} - \left(C_{n,T} + C_{n,a}\right)$$

$$\Delta C_Y = C_{Y,m} - \left(C_{Y,T} + C_{Y,a}\right)$$

The jet interference increments thus obtained include both inlet momentum effects and jet exit effects. The individual induced effects of inlet and exit flow are discussed subsequently in this paper.

Since the data are identified by either the thrust coefficient $C_T$ or the effective velocity ratio $\sqrt{\frac{\rho_\infty V_\infty^2}{\rho_j V_j^2}}$ or both, figure 4 is given to show the relationship between these two parameters for this model with all six ejectors operating. The curve is defined by the following equation:

$$C_T = \frac{2A_j/S}{\left(\sqrt{\frac{\rho_\infty V_\infty^2}{\rho_j V_j^2}}\right)^2}$$

The data are presented in the following figures:

## DISCUSSION OF RESULTS

### Effects of Engine Mode and Nozzle Setting

Engine mode.- The model longitudinal aerodynamic characteristics in the pure-lift and lift-cruise modes are given in figure 5 over a range of effective velocity ratio for both tail on and tail off. The most unexpected result is that the longitudinal interference increments in the lift mode are nearly equal to those in the lift-cruise mode over most of the range of effective velocity ratio. (See fig. 5(b).) It should be pointed out here that the lift-cruise engine mode is generally not employed at speeds represented by these low effective velocity ratios. The lower measured values of $L/T$ would be compensated by additional aerodynamic lift, and the negative $D/T$ values would represent forward acceleration at the speeds for which the lift-cruise mode is normally employed.

Three different engine configurations are compared in figure 6 through an angle-of-attack range. Although operation with only four lift engines is not an intended propulsion mode for this airplane, the model characteristics in this mode are of interest for comparison. The lift-thrust and drag-thrust ratios for the four-lift-engine and six-lift-engine configurations are in close agreement, and the pitching-moment parameter with only four engines operating is slightly larger over the entire range of angle of attack. A small part of this pitching-moment increase is due to a forward shift of the resultant thrust vector when the center pair of nozzles is inoperative. The major contribution to these larger pitching moments, however, is from induced effects. Of the three propulsion modes shown, both the lift losses and induced pitching-moment increments are greatest for the four-lift-engine configuration.

Nozzle setting.- The effect of lift nozzle setting for the six-lift-engine mode is given in figure 7 over a range of effective velocity ratio. The values of L/T and D/T in figure 7(a) can be interpreted as a measure of the accelerating and decelerating capability obtainable from nozzle vectoring at fixed attitude and thrust setting through a range of forward speeds. At the higher effective velocity ratios, the untrimmed pitching moments for the accelerating conditions (i.e., D/L is negative at $\delta_n = 10^o$) are due primarily to interference, and the trim requirements for the decelerating condition (positive D/L at $\delta_n = -10^o$) are reduced by interference effects (fig. 7(b)). The lift losses for the two accelerating conditions are nearly equal, whereas those for the decelerating condition are greater by from 2 to 5 percent of the thrust over the range of effective velocity ratio.

Combined effects.- Comparisons of the effects of nozzle setting at two different effective velocity ratios for the pure-lift mode (fig. 8) and the lift-cruise mode (fig. 9) indicate the extent to which both the nozzle setting and effective velocity ratio affect the magnitude and variation of longitudinal parameters and the corresponding interference increments. Data from the pure-lift configuration (figs. 8(a) and (c)) show generally equal changes in D/T and $M/T\bar{c}$ for equal deflections in nozzle angles at both the lower and higher effective velocity ratios. At the higher effective velocity ratios, however, the lift-curve slope, maximum lift, and pitching moments are greater. Also at the higher velocity ratios, the interference increments (figs. 8(b) and (d)) are larger as expected, and the more pronounced stall is accompanied by a sharp decrease in the lift losses. The results shown in figure 9 for the lift-cruise configuration exhibit trends similar to those obtained for the pure-lift configuration. The magnitudes of several of the effects differ, however. First, the drag and pitching-moment increments due to changes in lift nozzle angles are only about one-half of those obtained for the pure-lift mode. Second, for comparable conditions, the lift-curve slopes for the lift-cruise mode are higher prior to stall, but as expected the maximum lift-thrust ratios are lower for this mode than for the pure-lift mode.

Significance of data.- The foregoing results regarding variations in interference effects for different configurations and flight conditions are generally regarded as indicative of the nature and extent of jet-induced pressures on the lower surfaces of the model. In general, the larger nose-up pitching-moment increments accompany the larger lift losses; this indicates that the major lift loss is incurred aft of the moment center where not only the horizontal tail but also most of the wing area is located. Similar results have been noted throughout the literature on this subject. Since only very small changes in the induced effects occur with changes in angle of attack and since considerably larger effects result from changing nozzle configuration or setting, the influence of the free stream on the induced effects is apparently minimal within the range of

effective velocity ratio of this investigation. The data on jet paths from reference 14 indicate that at low velocity ratios the path of the mixed jet and free stream and the associated vorticity may pass sufficiently far beneath the model (out of ground effect) so that its effects are small relative to the direct effects of the high energy jet on the flow close to the model. Extension of this investigation to include measurement of induced pressures on the model and jet-wake visualizations up to higher effective velocity ratios would provide worthwhile additional data.

## Effects of Horizontal Tail

Basic tail.- The effectiveness of the basic high tail is shown in figure 10 for three different nozzle settings in the lift mode. Tail effectiveness was somewhat better at $\delta_n = 10^o$ than at the other two nozzle angles within the normal cruise range of angle of attack. This result indicates that the nozzles exhausting at their most rearward inclination provide the most favorable downwash and dynamic-pressure environment in the region of the tail. An unexpected result was that at $\delta_n = 10^o$ the configuration incurring the least loss of lift ($i_t = -10^o$) had the largest increment in pitching-moment interference. One possible explanation for this result could be that the primary lift loss for this particular configuration occurred at the tail, and that this small lift loss in combination with a long moment arm was sufficient to produce a large moment increment.

Auxiliary tail.- The effects of an auxiliary horizontal tail used to improve the longitudinal stability in cruise flight (ref. 9) are shown in figure 11 for the pure-lift engine mode and in figure 12 for the lift-cruise engine mode. For the speed range of this investigation, there is little or no contribution to stability from the auxiliary tail in either mode, as expected. In the pure-lift mode, there is no lift interference attributable to the auxiliary tail; however, the data from the lift-cruise mode, where the auxiliary tail is directly in the wake of the cruise engine exhaust, show a significant lift loss prior to stall without the expected increment in nose-up moment (fig. 12(b)).

## Aerodynamic Characteristics and Interference Effects in Sideslip

Horizontal and vertical tails.- The horizontal and vertical tails added to the wing and body (fig. 13) caused the expected changes in lateral-directional characteristics. The directional stability and increased dihedral effect provided by the tail are largely due to interference, but the differences between the magnitudes of the increments for the two configurations are small. The lift and drag parameters and interference increments were relatively constant over the range of sideslip angle, but nose-down pitching moments and decreased pitching-moment interference were exhibited at the high negative sideslip angles. A similar effect is expected at high positive sideslip angles.

Effective velocity ratio.- The model characteristics in sideslip at three different effective velocity ratios are given in figure 14(a). The effective dihedral and rolling-moment trim requirements are considerably greater at the lowest velocity ratio (0.050) at sideslip angles greater than $-12^{\circ}$, and the directional stability and yawing-moment trim requirements show a similar trend at sideslip angles less than $-12^{\circ}$. The large contributions of the induced effects to these results are shown in figure 14(b). The longitudinal data of figures 14(c) and (d) show that the increased diving-moment tendency at high negative sideslip angles is a direct function of velocity ratio. Therefore, in the critical areas of hovering and low-speed transition, the potential piloting problems associated with this effect are significantly reduced.

Nozzle setting.- The effects of nozzle setting on the lateral-directional characteristics are shown to be small at sideslip angles between $-16^{\circ}$ and $5^{\circ}$ (figs. 15(a) and (b)). Where significant effects of nozzle setting are evident in figure 15(a), they are shown to result almost entirely from the induced effects given in figure 15(b).

Significance of data.- Perhaps the most significant results of the sideslip investigation are that the interference effects at a given velocity ratio always increased the effective dihedral and directional stability and that all the lateral-directional interference increments varied with sideslip angle; these increments are unlike the longitudinal increments which, at a given velocity ratio, do not vary considerably with either angle of attack or sideslip. These results are not surprising, however, considering the increased asymmetry of both the free stream and flow from the exhaust nozzle with an increase in sideslip angle. In fact, since the lift nozzles are canted $10^{\circ}$ outboard, half of the exhaust is passed initially toward the upstream side of the airplane while the other half passes downstream; this effect becomes a maximum at $\beta = 90^{\circ}$. The data of reference 14 indicate that the flow from the upstream nozzles should have reasonably small effects, whereas the flow from the downstream nozzles is blown back under the downstream wing (which is already operating at a lower lift) where the resultant lift losses cause the increased dihedral effect. Similarly, the differences in the induced effects from the two sets of nozzles are believed to account for the variations in side-force and yawing-moment increments. Similar lateral-directional interference effects are expected from configurations having different outboard cant of the lift nozzles, but perhaps the degree of effect would differ from that shown herein.

## Ground Effects

Angle of attack.- The variations of model longitudinal aerodynamic characteristics with height above the ground at $\alpha = 0^{\circ}$ and $10^{\circ}$ are given in figure 16 where the lowest value of $h/\bar{c}$ shown ($h/\bar{c} \approx 1.45$) represents a distance of about 0.52 foot (0.158 meter) to the bottom of the wheels on the full-scale airplane. The data show nearly a constant

increment in L/T between the two angles of attack throughout the range of height above the ground. The difference in the pitching-moment parameter between the two angles of attack at the lower heights becomes negligible above about $h/\bar{c} = 3.5$. About 60 percent of the difference in the lift-thrust ratio is due to the greater lift losses incurred at $\alpha = 0^{\circ}$ than at $\alpha = 10^{\circ}$, and practically all of the measured pitching moment at $\alpha = 10^{\circ}$ results from the induced effects.

Sideslip angle.- Figure 17 presents data for three sideslip angles over a range of effective velocity ratio in ground effect. Essentially all the rolling moments at the three sideslip angles are due to jet-induced interference; except at $\beta = 0^{\circ}$, both the magnitudes of the yawing-moment and side-force coefficients and the variations of these coefficients with effective velocity ratio indicate very large contributions from the induced effects. Also, the magnitudes of the lateral-directional interference increments appear to be direct functions of sideslip angle at the higher effective velocity ratios. The sideslip angle had only small effects on the longitudinal parameters, especially at the lower velocity ratios. The mechanisms by which ground proximity influences induced interference is well documented in the available literature (for example, see refs. 5 and 6).

## Inlet-Mass-Flow Effects

The effects of inlet mass flow are shown in figures 18, 19, and 20. Longitudinal characteristics and interference increments for the six-lift-engine mode are given in figure 18 for a range of effective velocity ratio. With the inlets closed, no entrainment of free-stream air occurs and the only interference effects result from the jet efflux. It is indicated that the differences in the measured characteristics (fig. 18(a)) result from the differences in interference increments (fig. 18(b)) due to inlet mass flow. The pitching-moment increments due to exit effects (inlets closed) result primarily from the lift losses since the drag increment does not vary with effective velocity ratio. On the other hand, the pitching-moment increments with the inlets open result from a combination of lift loss and inlet drag, both of which vary with effective velocity ratio. Consequently, the inlets provide a constant positive lift increment, an increasing drag penalty, and increasing nose-up moments as forward speed increases. At a fixed velocity ratio (fig. 19), the longitudinal interference increments due to inlet mass flow are essentially constant over a range of angle of attack.

Lateral-directional and longitudinal characteristics and interference increments are given in figure 20 for a range of sideslip angle. The positive contribution of interference to effective dihedral discussed previously is a result largely of inlet-mass-flow effects. Even though there is an inlet flow contribution to the side-force variation, its point of application under the particular conditions of this figure is very near the model moment center, inasmuch as there is essentially no effect of inlet mass flow on the

magnitude or variation of the yawing-moment increments. Inlet-mass-flow effects on directional stability have been shown to be large, however. A vectored-jet configuration where all the inlet area was on the sides of the fuselage experienced negative directional stability at speeds up to about 60 knots (ref. 15); this instability was entirely attributable to inlet-mass-flow effects. The instability in this particular flight investigation was severe enough to require the installation of audio-warning devices for safety of flight. The results shown in figure 20(d) indicate that the inlet-mass-flow contribution to longitudinal interference was essentially constant over the range of sideslip angles for the present investigation.

## CONCLUSIONS

The results of an investigation of the aerodynamic characteristics and induced interference effects on a jet V/STOL model in low-speed transition flight indicate the following conclusions:

1. For low transition speeds, there were only negligible differences between the longitudinal interference effects obtained when operating in either the pure-lift or lift-cruise propulsion modes. Induced lift losses and nose-up trim changes with negligible effects on longitudinal stability were obtained for either mode.

2. Although the basic horizontal tail was mounted high on the vertical fin, the horizontal-tail effectiveness was influenced by relatively moderate changes in orientation of the lift-engine efflux (nozzle setting from $-10^{\circ}$ to $10^{\circ}$).

3. The contributions of the induced effects to effective dihedral and directional stability were positive for all test conditions. Lateral-directional interference increments varied with sideslip angle, whereas longitudinal interference increments varied negligibly with either angle of attack or sideslip angle.

4. The positive lift increment attributed to inlet mass flow only was essentially constant for a range of velocity ratio, angle of attack, and sideslip angle. The inlet drag and pitching moments varied with effective velocity ratio but also remained fairly constant over the ranges of angles of attack and sideslip of interest.

5. The inlet mass flow provided the major contribution to the positive induced dihedral effect. For the particular conditions herein, however, the side-force interference increment caused by the inlet mass flow had only a negligible effect on directional stability.

Langley Research Center,
National Aeronautics and Space Administration,
Langley Station, Hampton, Va., January 13, 1970.

## REFERENCES


1. Otis, James H., Jr.: Induced Interference Effects on a Four-Jet VTOL Configuration With Various Wing Planforms in the Transition Speed Range. NASA TN D-1400, 1962.

2. Vogler, Raymond D.: Interference Effects of Single and Multiple Round or Slotted Jets on a VTOL Model in Transition. NASA TN D-2380, 1964.

3. Margason, Richard J.: Jet-Induced Effects in Transition Flight. Conference on V/STOL and STOL Aircraft, NASA SP-116, 1966, pp. 177-189.

4. Margason, Richard J.; and Gentry, Garl L., Jr.: Aerodynamic Characteristics of a Five-Jet VTOL Configuration in the Transition Speed Range. NASA TN D-4812, 1968.

5. Krenz, Günter; and Barche, Jürgen: Jet Influence on V/STOL-Aircraft in the Transitional and High Speed Flight Regime. Integration of Propulsion Systems in Airframes, AGARD CP No. 27, Sept. 1967, pp. 2-1 – 2-25.

6. Wood, M. N.: Jet V/STOL Aircraft Aerodynamics. Ann. N.Y. Acad. Sci., vol. 154, art. 2, Nov. 22, 1968, pp. 893-920.

7. Carter, Arthur W.: Effects of Jet-Exhaust Location on the Longitudinal Aerodynamic Characteristics of a Jet V/STOL Model. NASA TN D-5333, 1969.

8. Winston, Matthew M.: Wind-Tunnel Data From a 0.16-Scale V/STOL Model With Direct-Lift and Lift-Cruise Jets. NASA TM X-1758, 1969.

9. Winston, Matthew M.: Static Stability Characteristics of a 0.16-Scale Model of a Jet-Lift V/STOL Research Airplane in Cruise. NASA TM X-1835, 1969.

10. Mechtly, E. A.: The International System of Units – Physical Constants and Conversion Factors. NASA SP-7012, 1964.

11. Margason, Richard J.; and Gentry, Garl L.: Static Calibration of an Ejector Unit for Simulation of Jet Engines in Small-Scale Wind-Tunnel Models. NASA TN D-3867, 1967.

12. Turner, Thomas R.: A Moving-Belt Ground Plane for Wind-Tunnel Ground Simulation and Results for Two Jet-Flap Configurations. NASA TN D-4228, 1967.

13. Heyson, Harry H.: Linearized Theory of Wind-Tunnel Jet-Boundary Corrections and Ground Effect for VTOL-STOL Aircraft. NASA TR R-124, 1962.

14. Margason, Richard J.: The Path of a Jet Directed at Large Angles to a Subsonic Free Stream. NASA TN D-4919, 1968.

15. Fisher, Ian A.: Experience of and Methods To Be Used in Clearing a Jet-Lift Aircraft for Service Use. J. Amer. Helicopter Soc., vol. 13, no. 3, July 1968, pp. 70-78.

GEOMETRIC CHARACTERISTICS

| | Wing | Horizontal tail | Vertical tail |
|---|---|---|---|
| Area | 2.67 $ft^2$ (.25 $m^2$) | .68 $ft^2$ (.06 $m^2$) | .70 $ft^2$ (.07 $m^2$) |
| Span | 48.00 (121.92) | 20.48 (52.02) | 11.68 (29.67) |
| Root chord | 11.52 (29.26) | 6.80 (17.27) | 11.44 (29.06) |
| Tip chord | 4.48 (11.38) | 2.72 (6.91) | 5.90 (14.99) |
| Mean aerodynamic chord | 8.52 (21.64) | 5.05 (12.83) | 8.96 (22.76) |
| Aspect ratio | 5.90 | 4.30 | 1.35 |
| Taper ratio | .39 | .40 | .52 |
| Sweep (.25 chord line) | 4.18° | 12.37° | 32.13° |
| Airfoil section | | NACA 0010 (modified) | NACA 64A012 |
| Root | NACA 64A012 | | |
| Tip | NACA 64A212 | | |
| Tail length | | 30.82 (78.28) | 25.10 (63.75) |

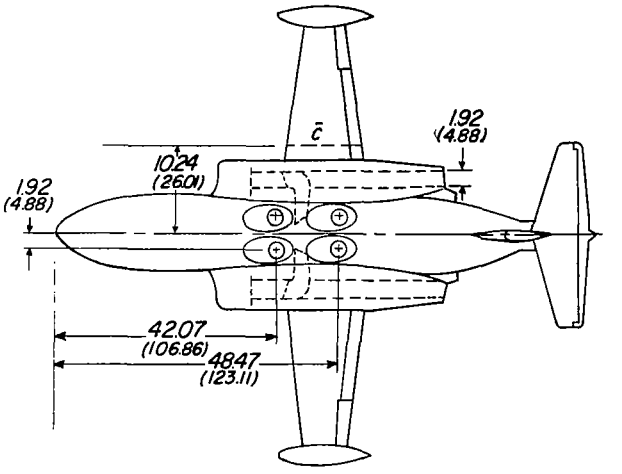


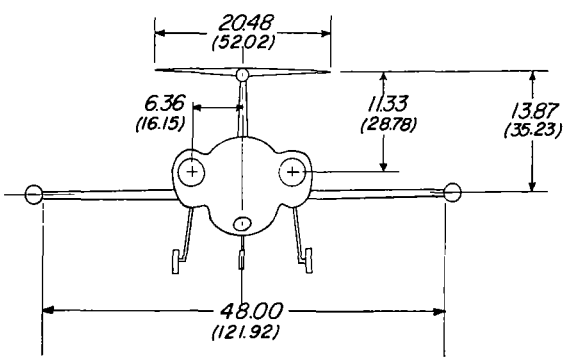


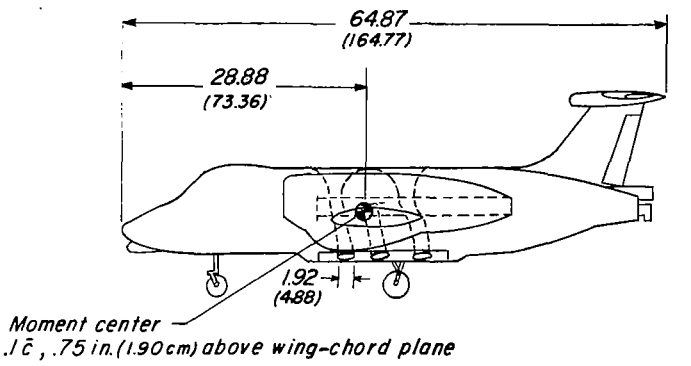


(a) Principal dimensions and geometric characteristics.

Figure 1.- Model details. All dimensions are in inches (centimeters) unless otherwise specified.

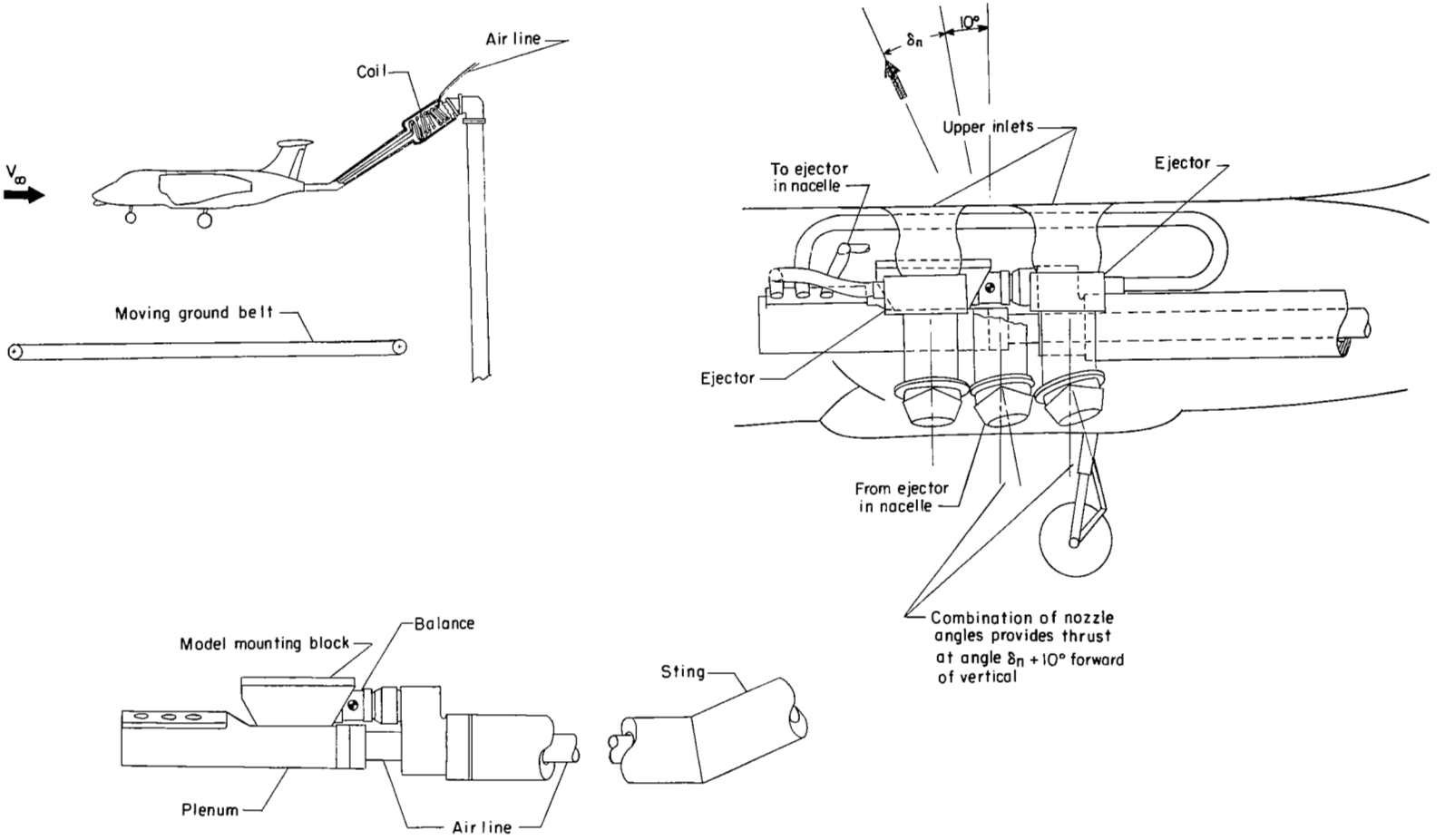


(b) Balance and propulsion system.

Figure 1.- Concluded.

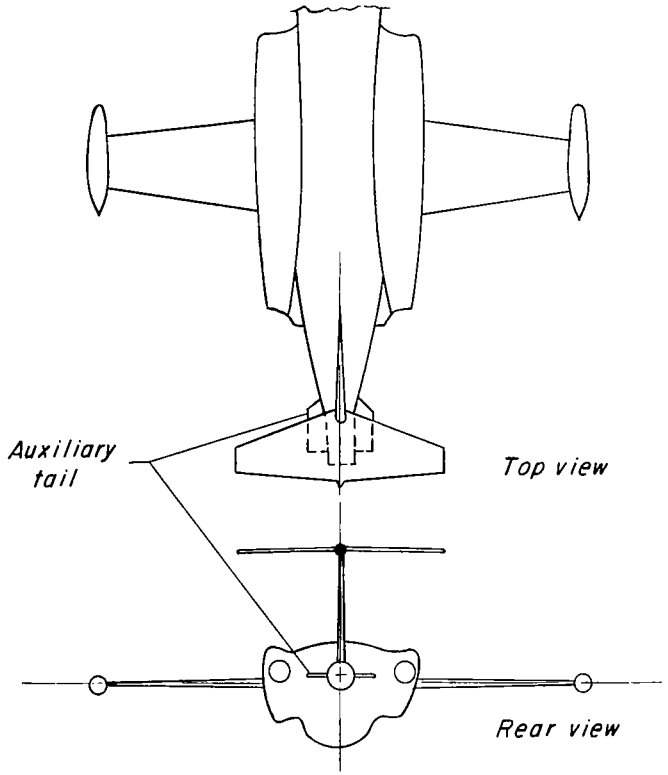


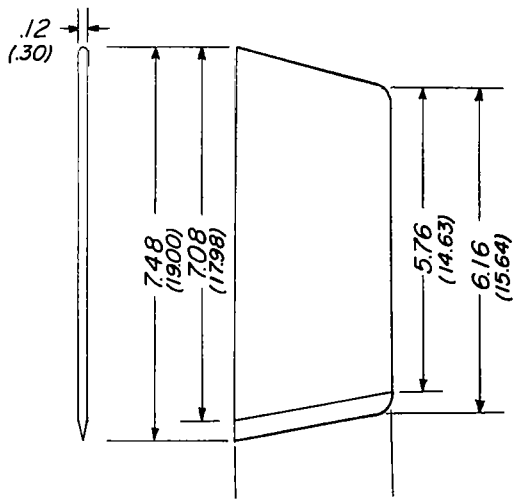


Figure 2.- Auxiliary tail installation and dimensions. Dimensions are in inches (centimeters).

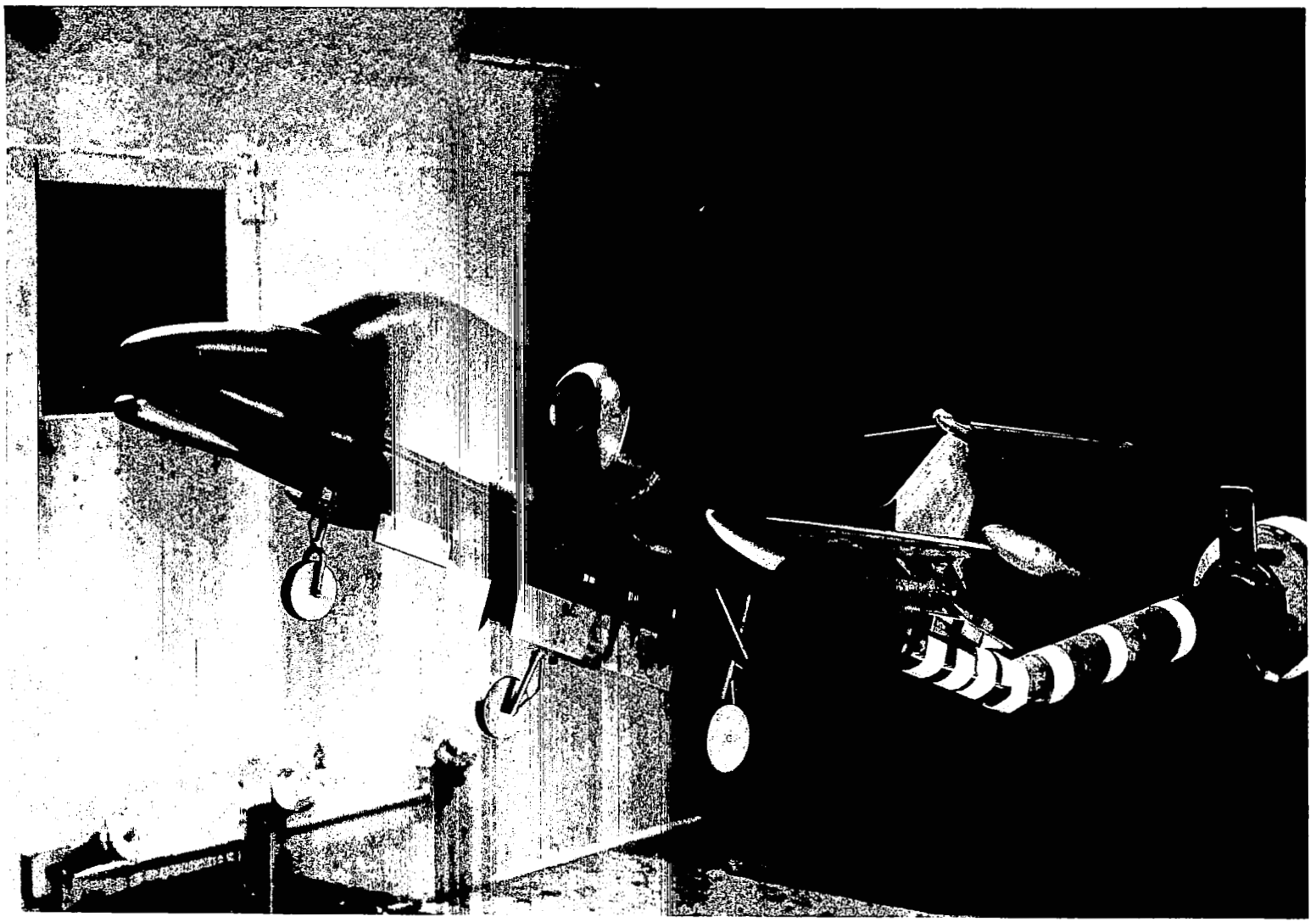

(a) View showing cruise engine inlet. L-68-1528

Figure 3.- Model in the 17-foot (5.18 meter) test section of the Langley 300-MPH 7- by 10-foot tunnel.

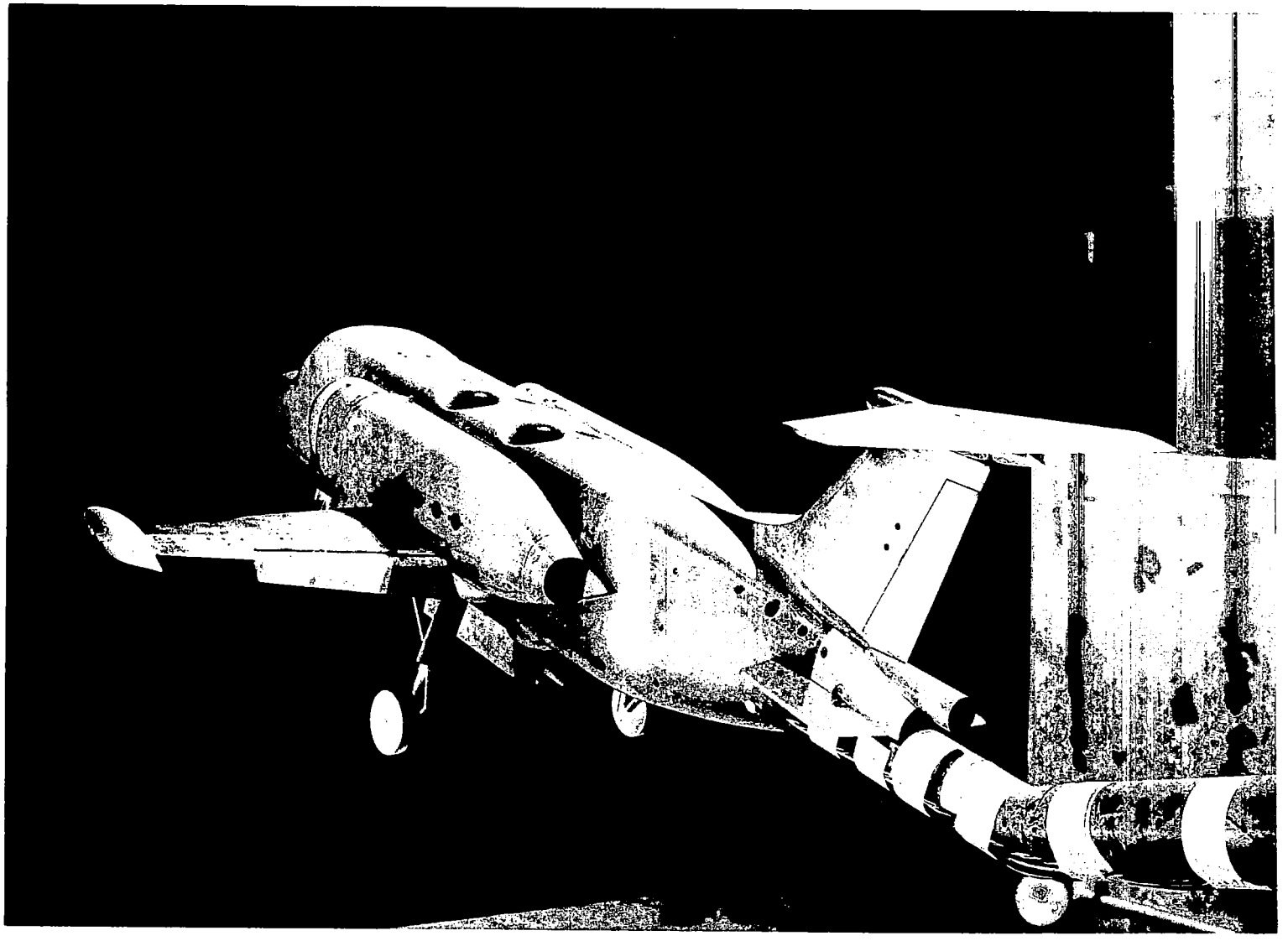

(b) View showing lift engine inlets. L-68-1526

Figure 3.- Continued.

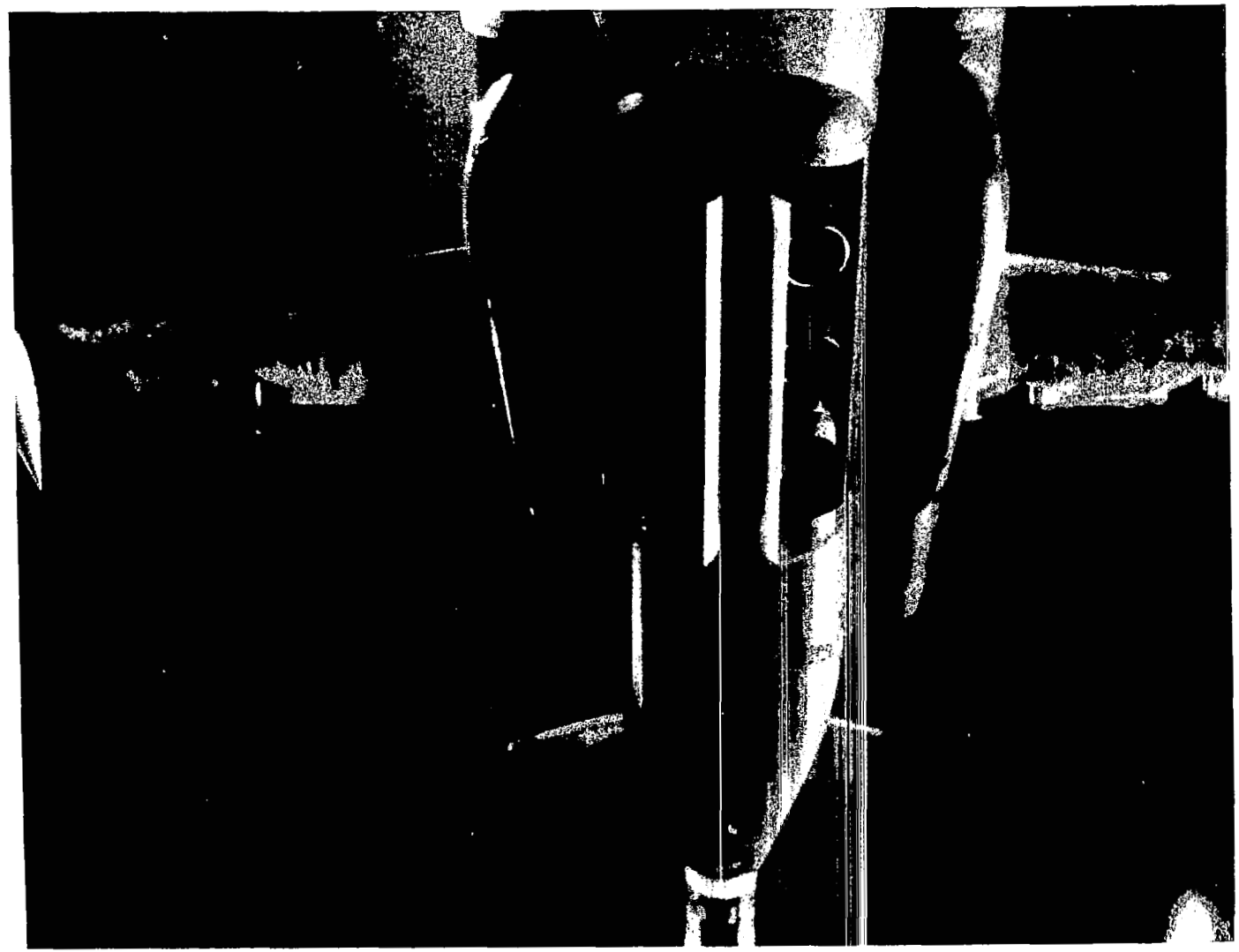

(c) View showing lift engine exit nozzles. L-70-1503

Figure 3.- Concluded.

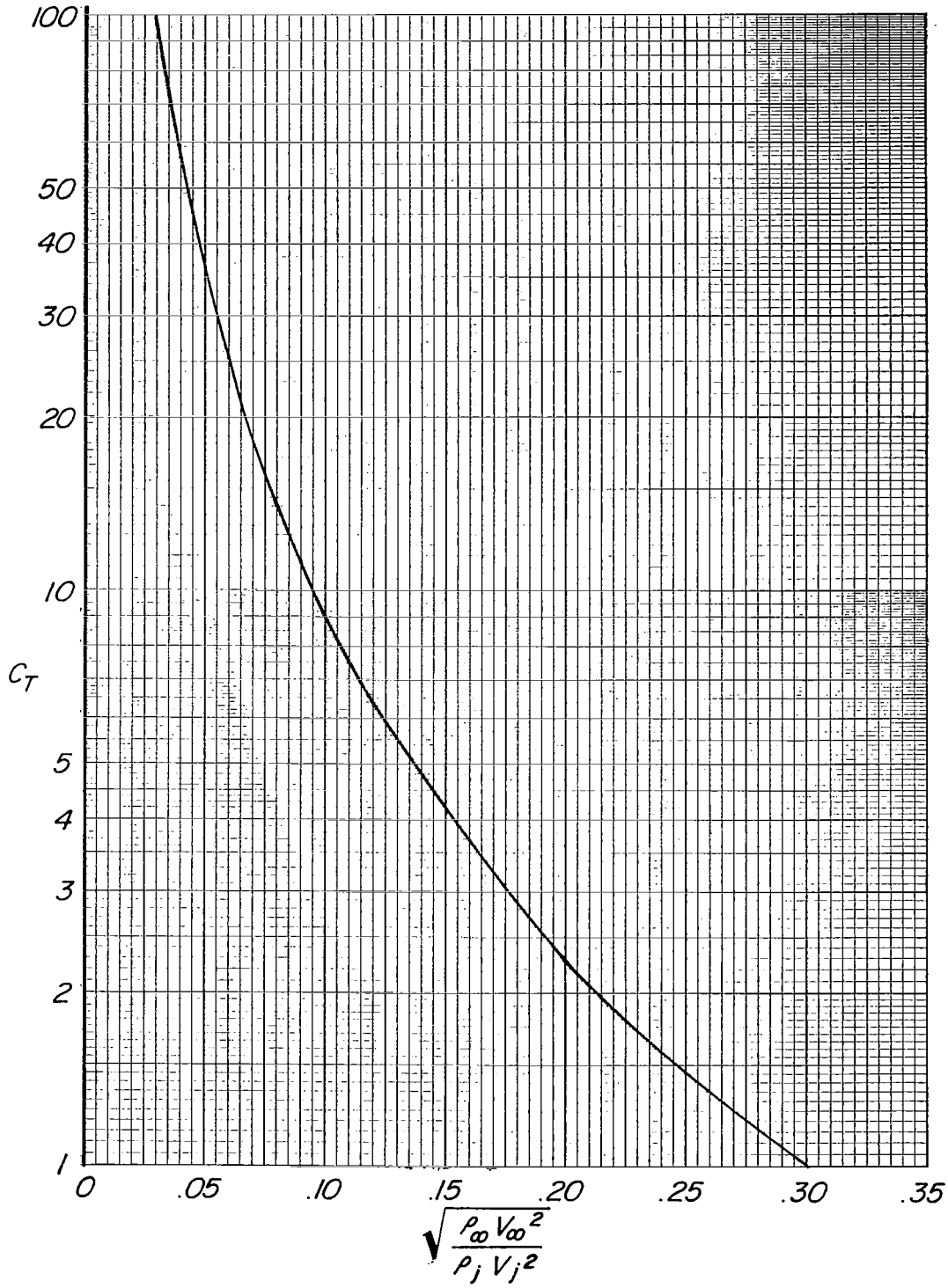


Figure 4.- Variation of thrust coefficient with effective velocity ratio. Six nozzles operating.

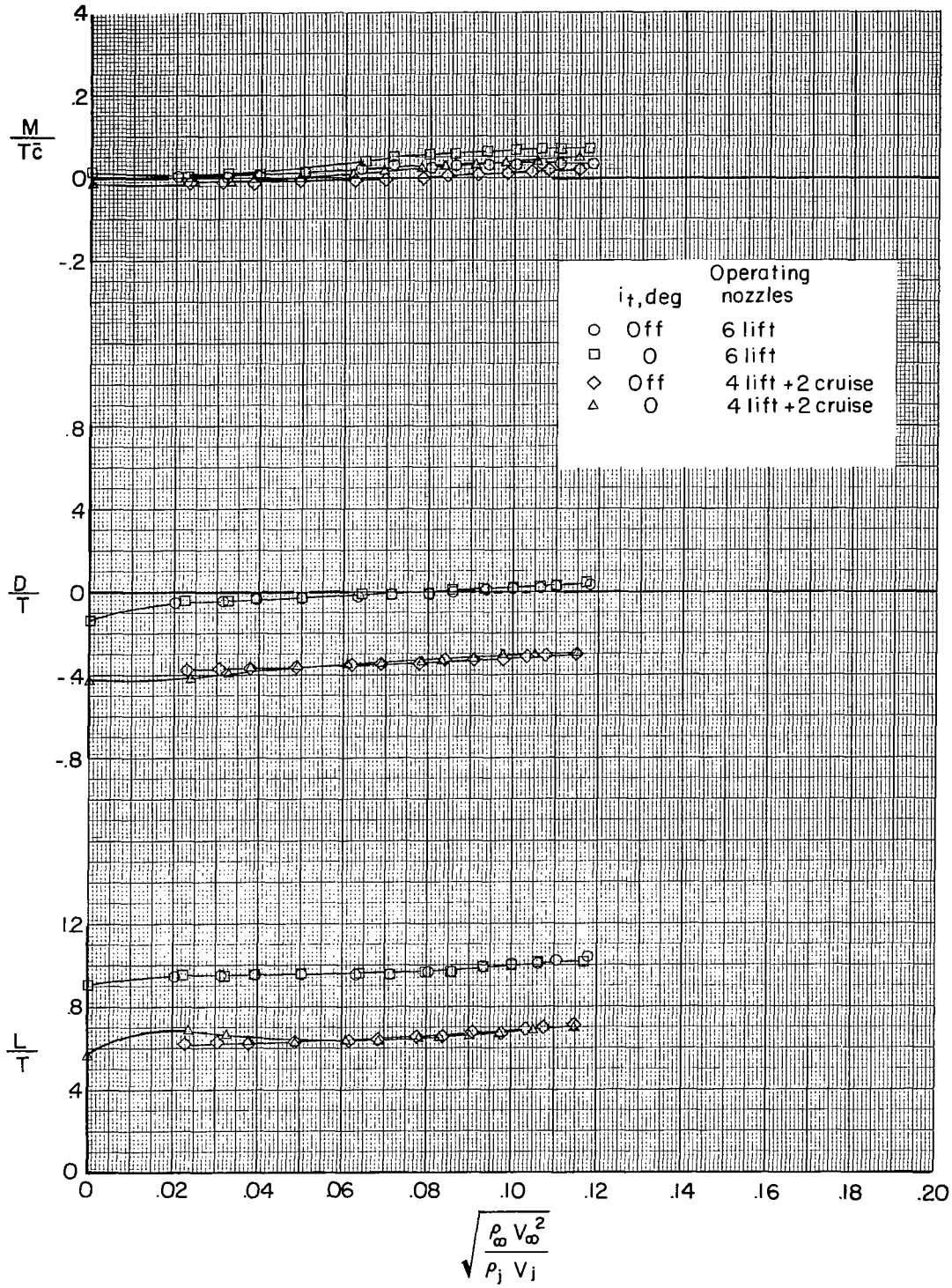


(a) Measured characteristics.

Figure 5.- Variation of M/Tc̄, D/T, and L/T with effective velocity ratio showing effect of horizontal tail and engine mode. Auxiliary tail on; $\alpha = 5^0$; $\beta = 0^0$; $\delta_n = 0^0$.

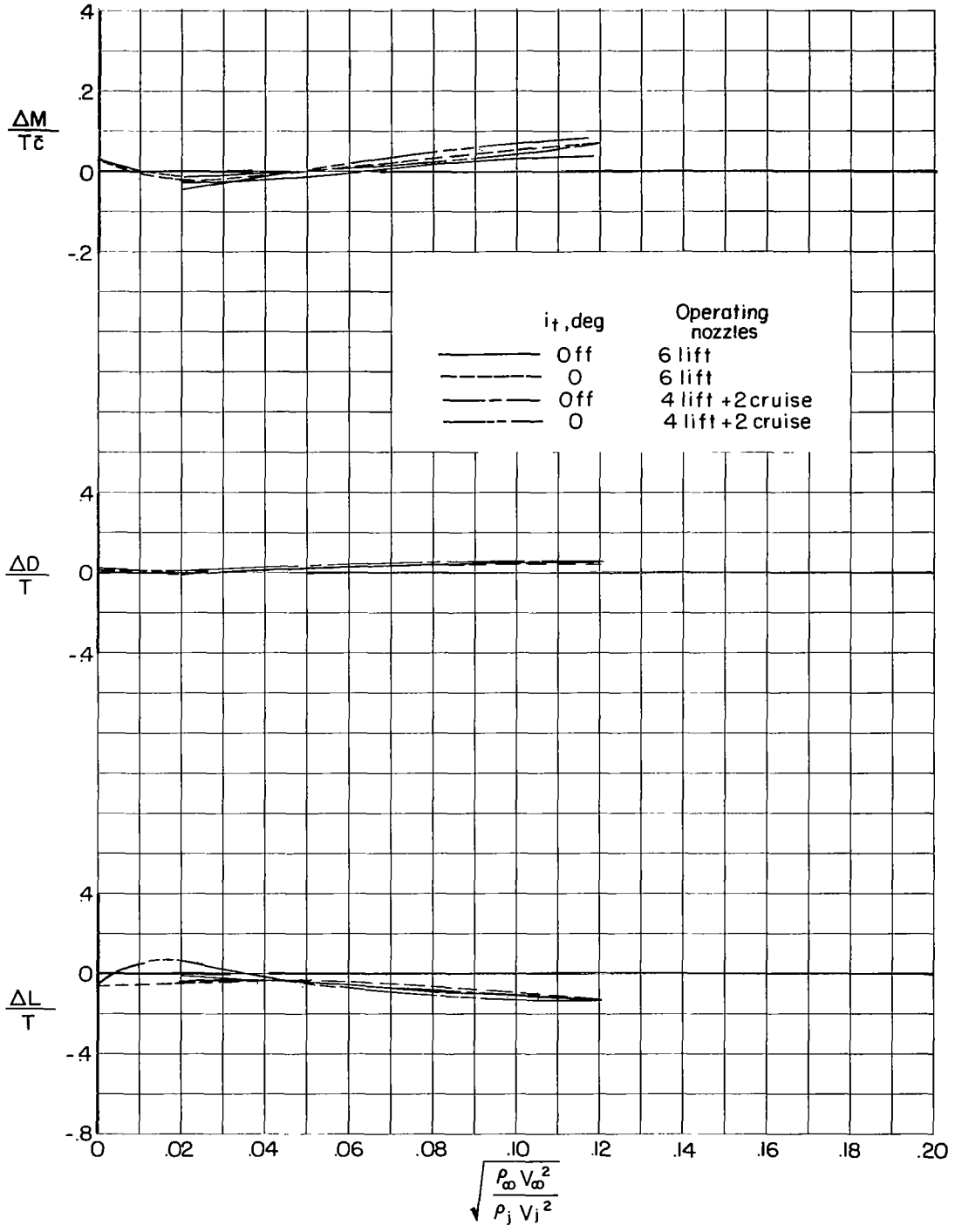


(b) Interference increments.

Figure 5.- Concluded.

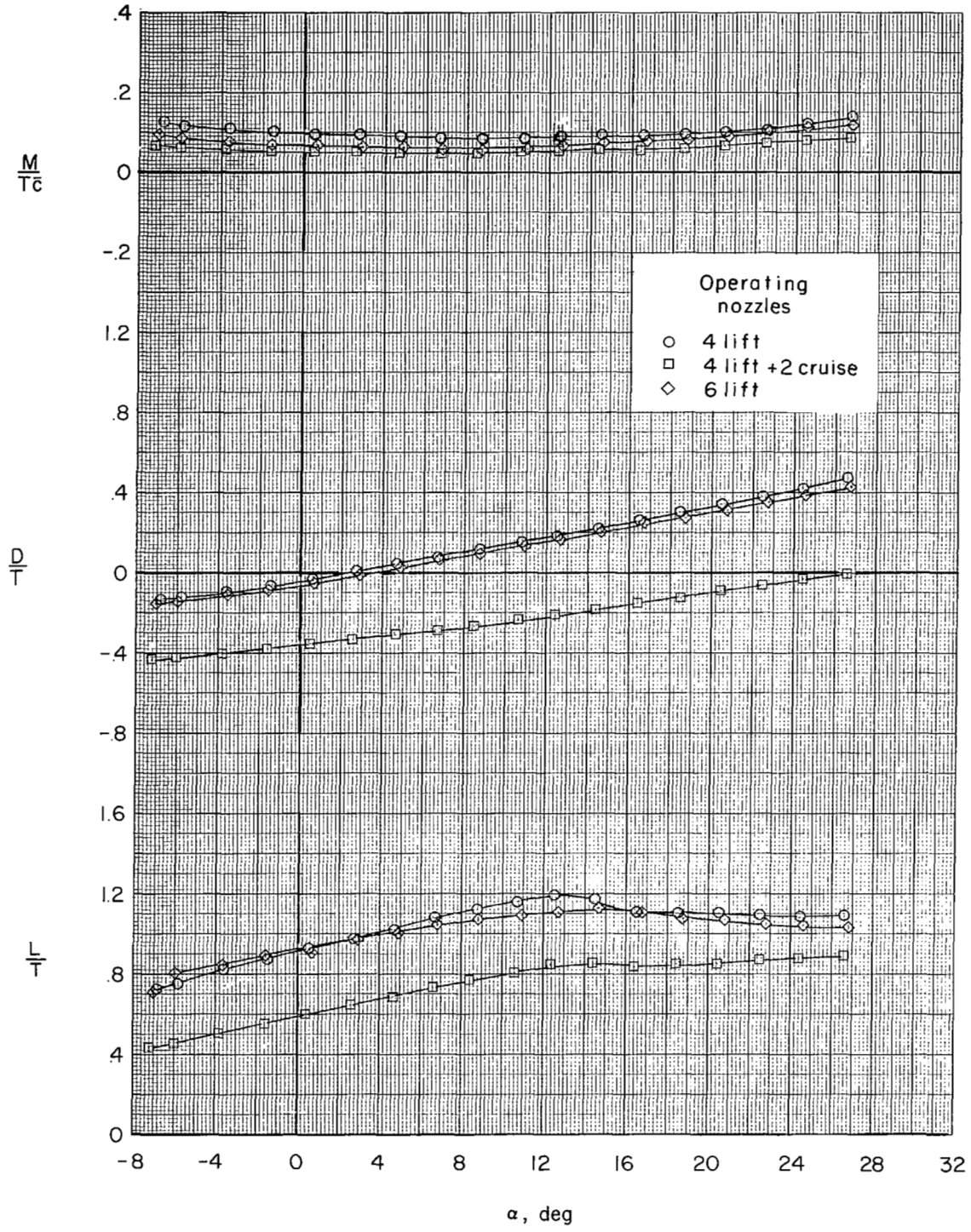


(a) Measured characteristics.

Figure 6.- Variation of $M/T\bar{c}$, D/T, and L/T with angle of attack showing effect of engine mode. Auxiliary tail on; effective velocity ratio, 0.115; $\beta = 0^0$; $\delta_n = 0^0$.

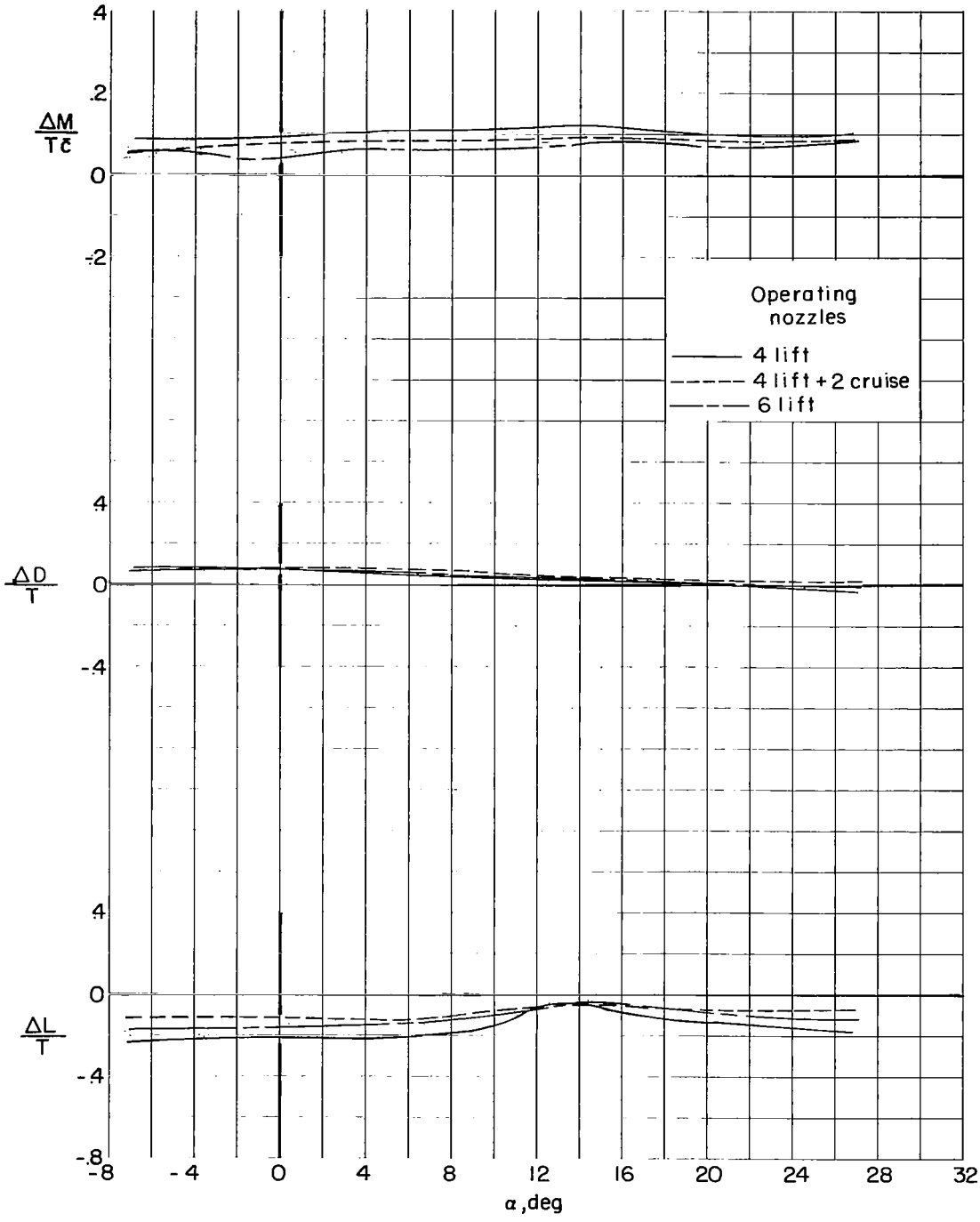


(b) Interference increments.

Figure 6.- Concluded.

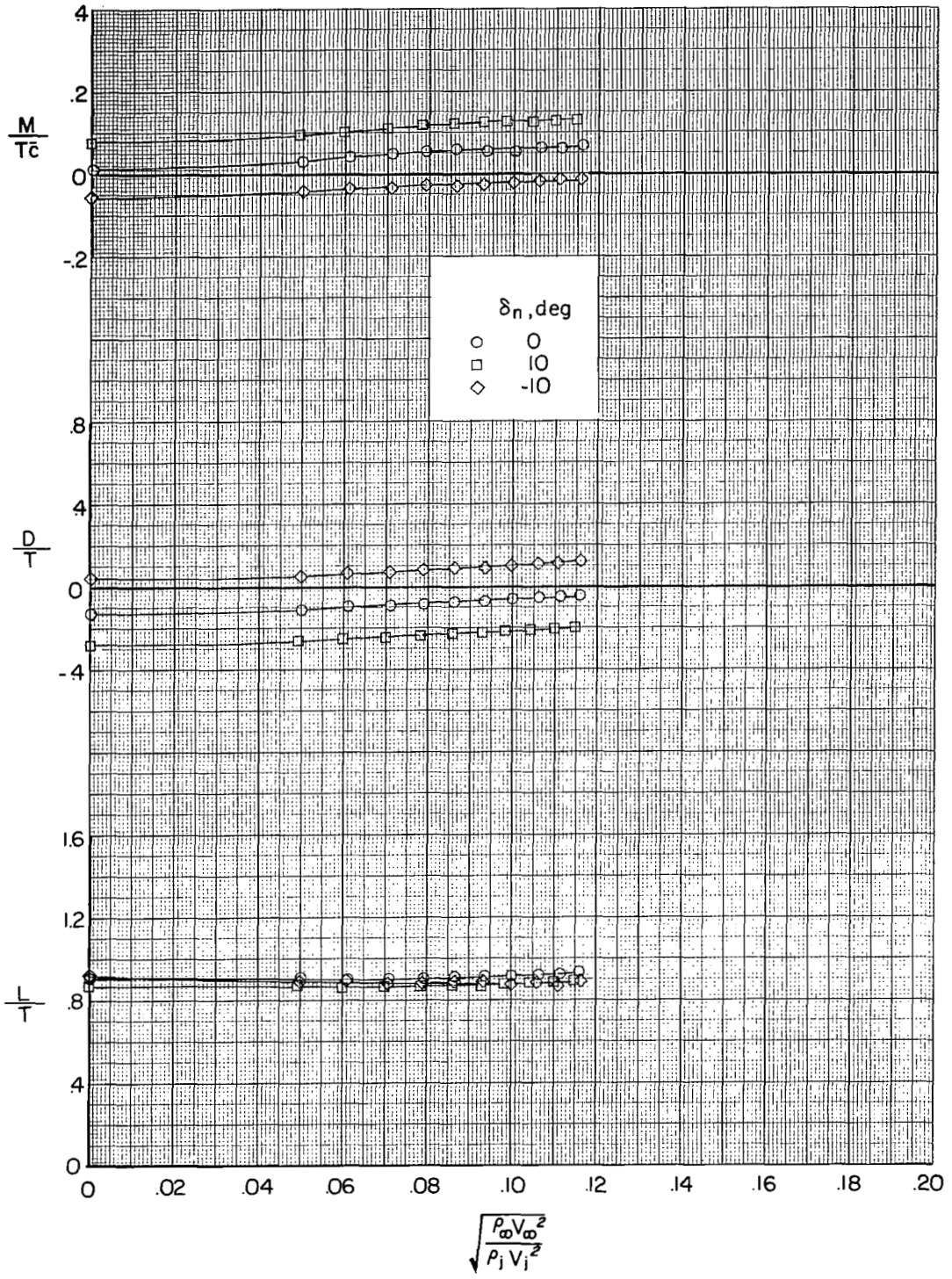


(a) Measured characteristics.

Figure 7.- Variation of $M/T\bar{c}$, D/T, and L/T with effective velocity ratio showing effect of nozzle setting. Six lift engines; $\alpha = 0^0$; $\beta = 0^0$.

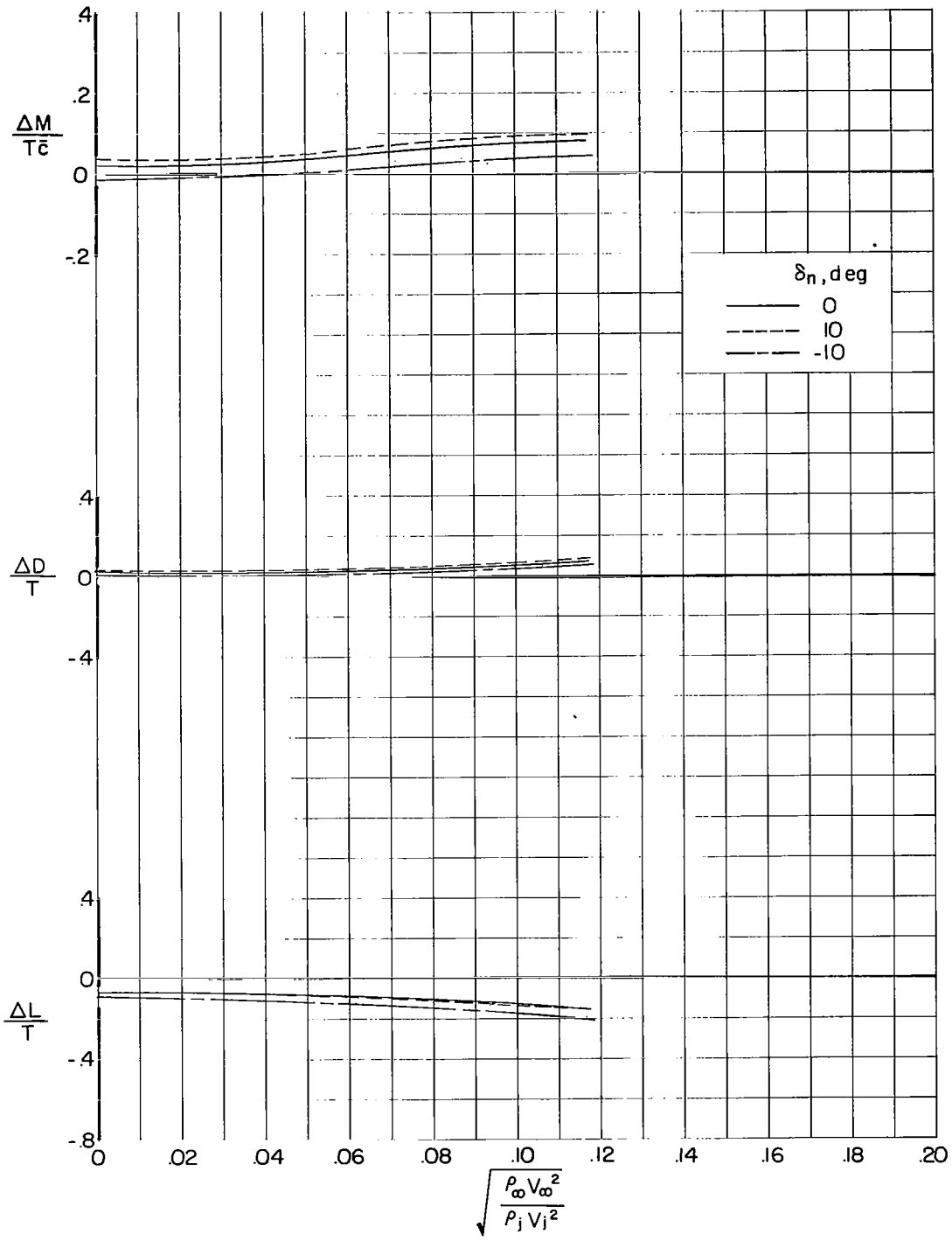


(b) Interference increments.

Figure 7.- Concluded.

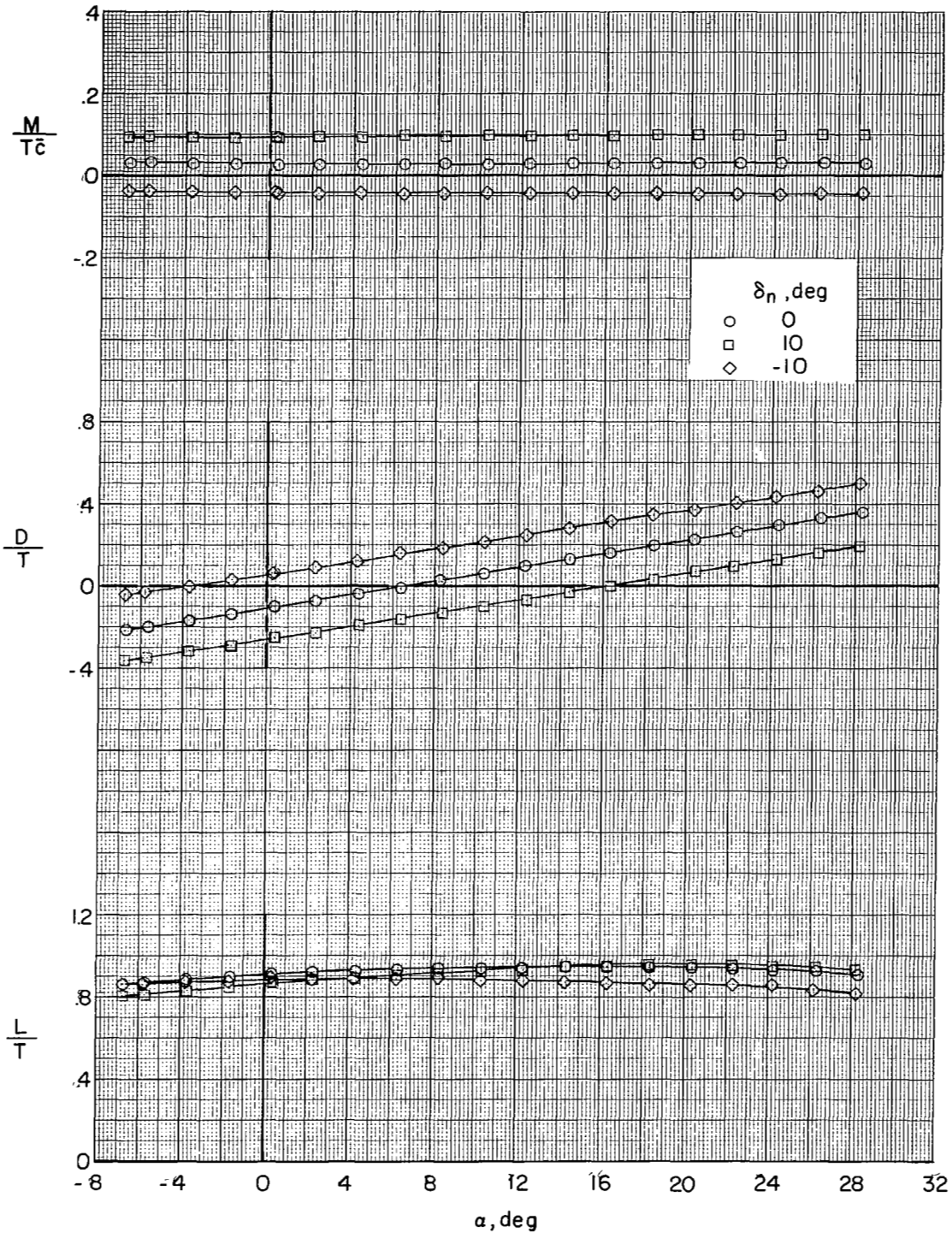


(a) Measured characteristics at effective velocity ratio of 0.050.

Figure 8.- Effect of nozzle setting on longitudinal aerodynamic characteristics. Six lift engines; $\beta = 0^0$.

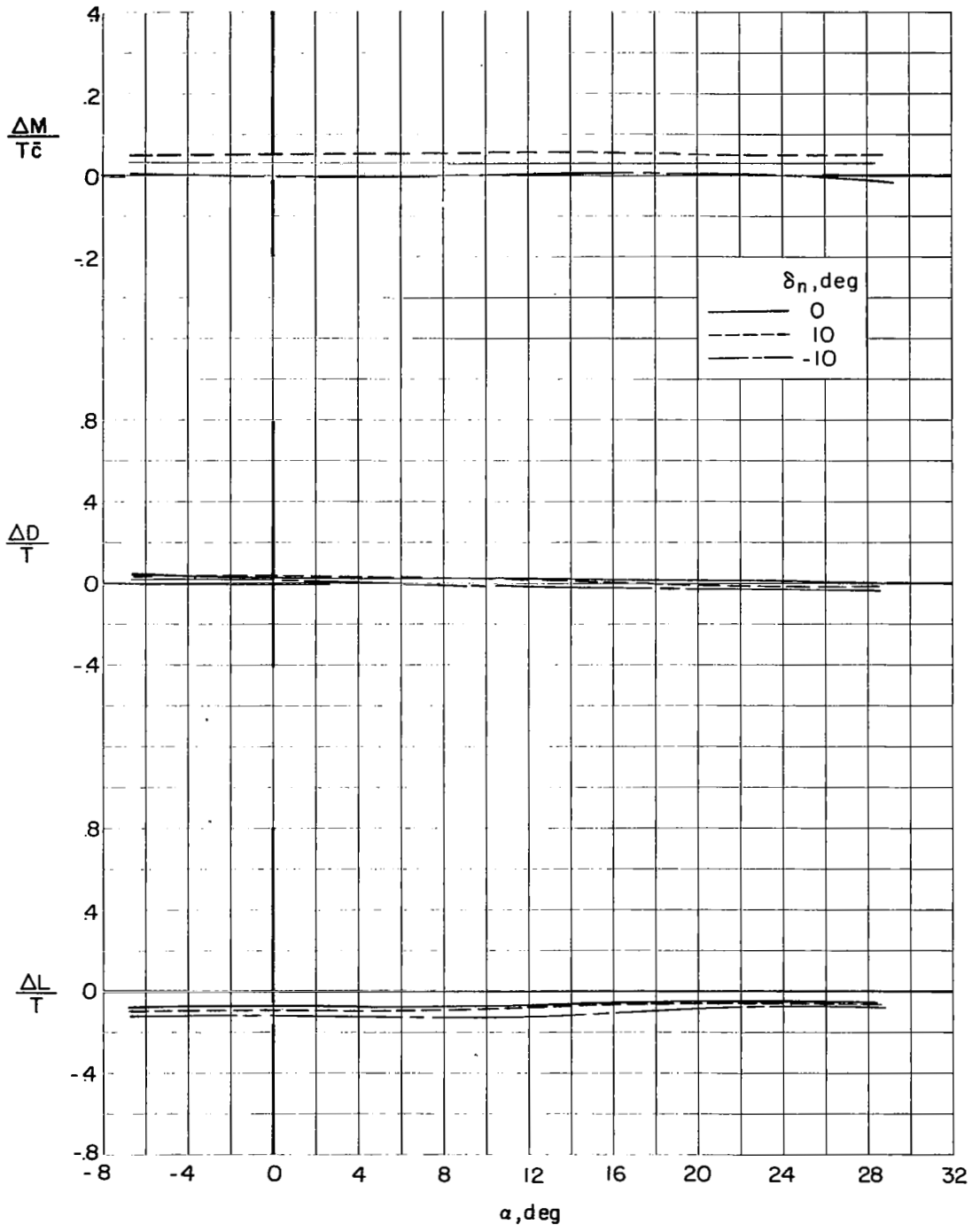


(b) Interference increments at effective velocity ratio of 0.050.

Figure 8.- Continued.

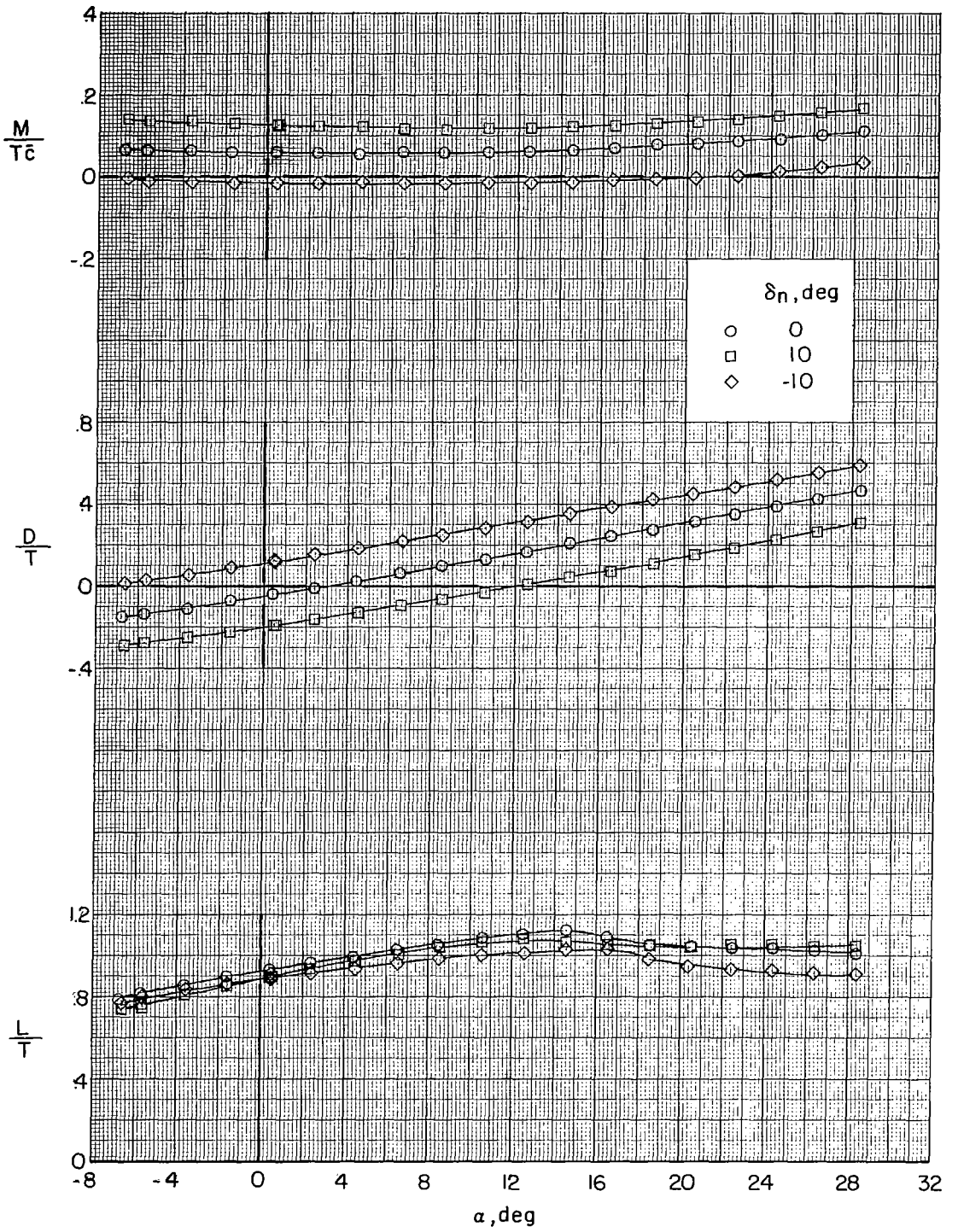


(c) Measured characteristics at effective velocity ratio of 0.115.

Figure 8.- Continued.

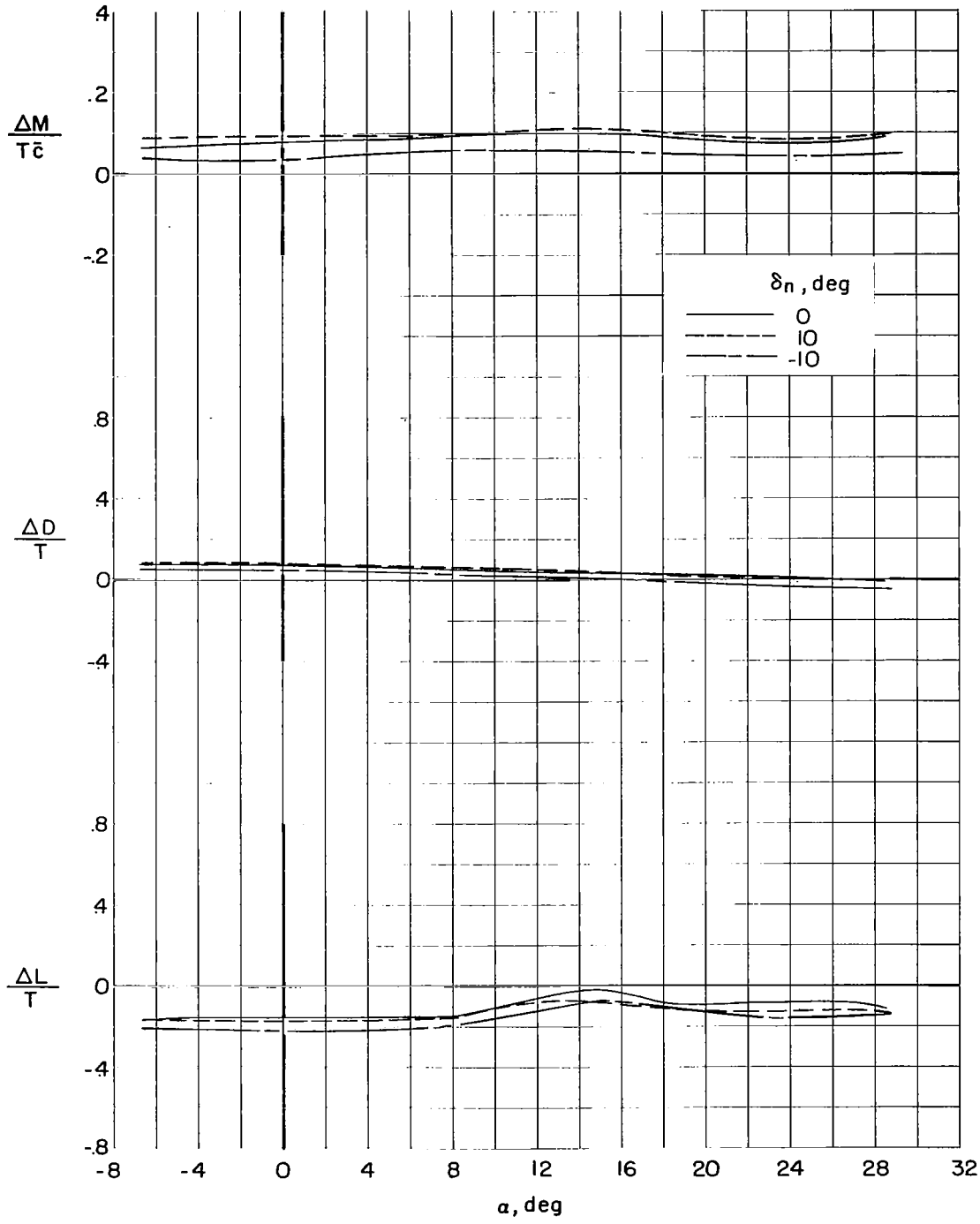


(d) Interference increments at effective velocity ratio of 0.115.

Figure 8.- Concluded.

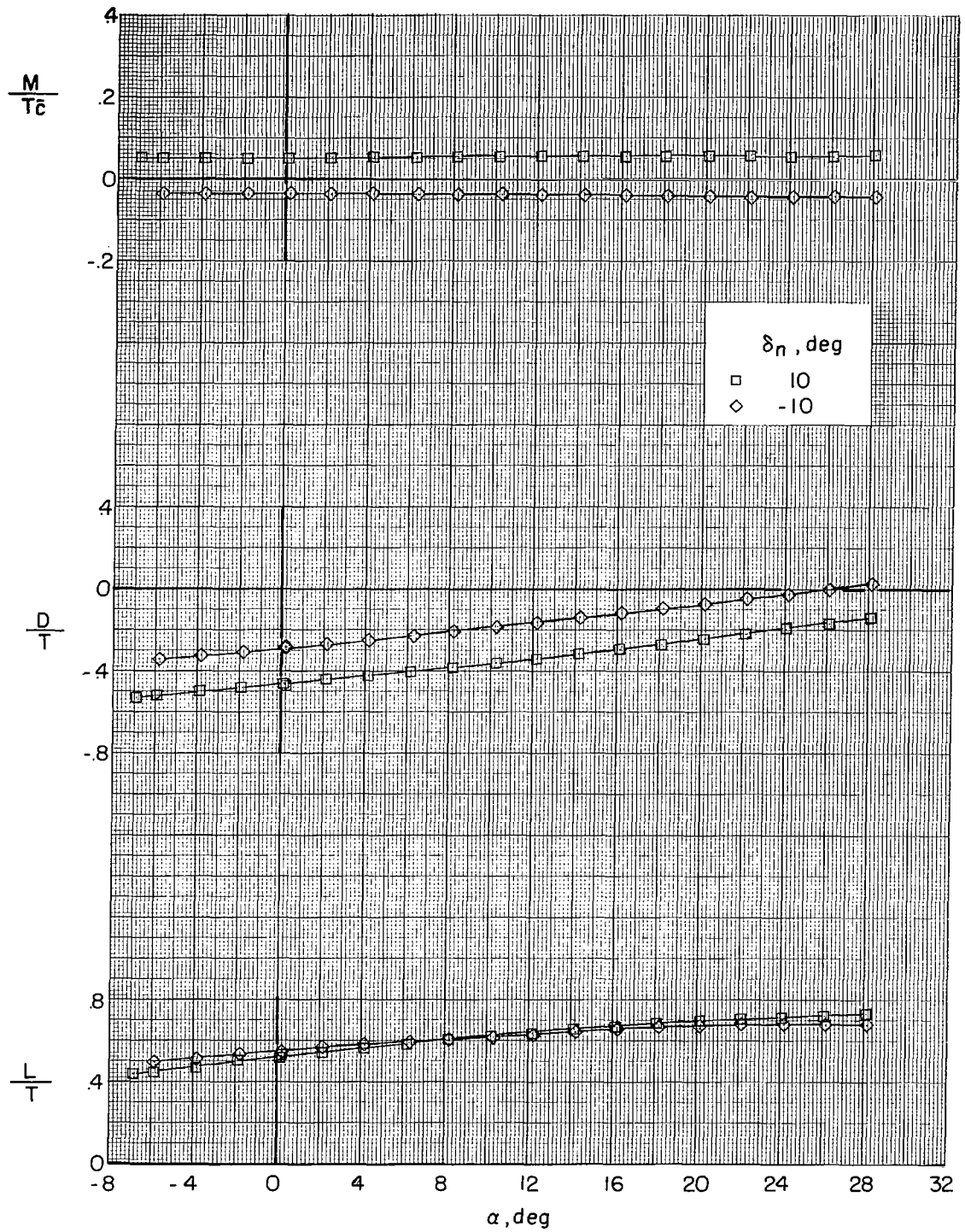


(a) Measured characteristics at effective velocity ratio of 0.050.

Figure 9.- Effect of nozzle setting on longitudinal aerodynamic characteristics. Four lift engines and two cruise engines; $\beta = 0^0$.

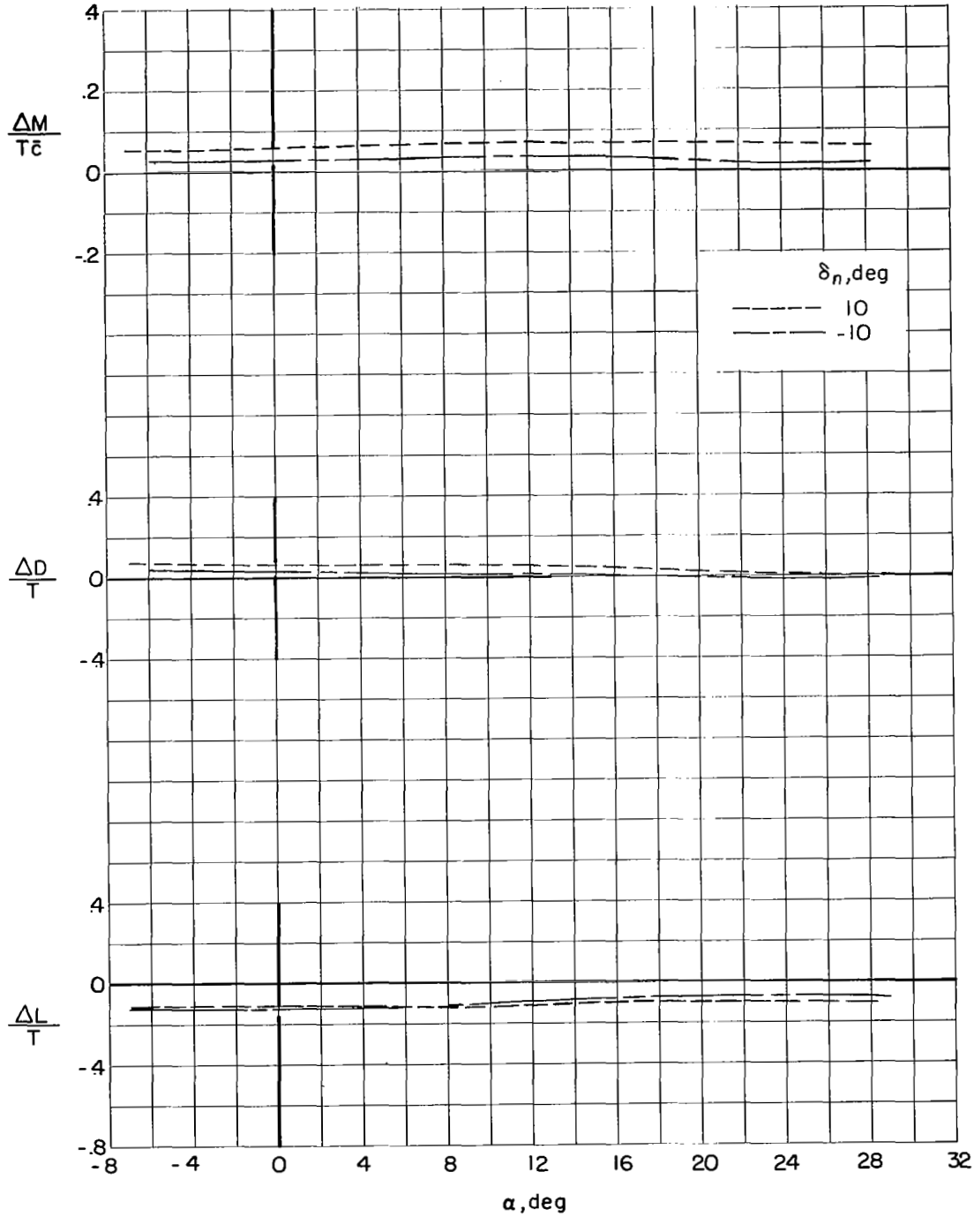


(b) Interference increments at effective velocity ratio of 0.050.

Figure 9.- Continued.

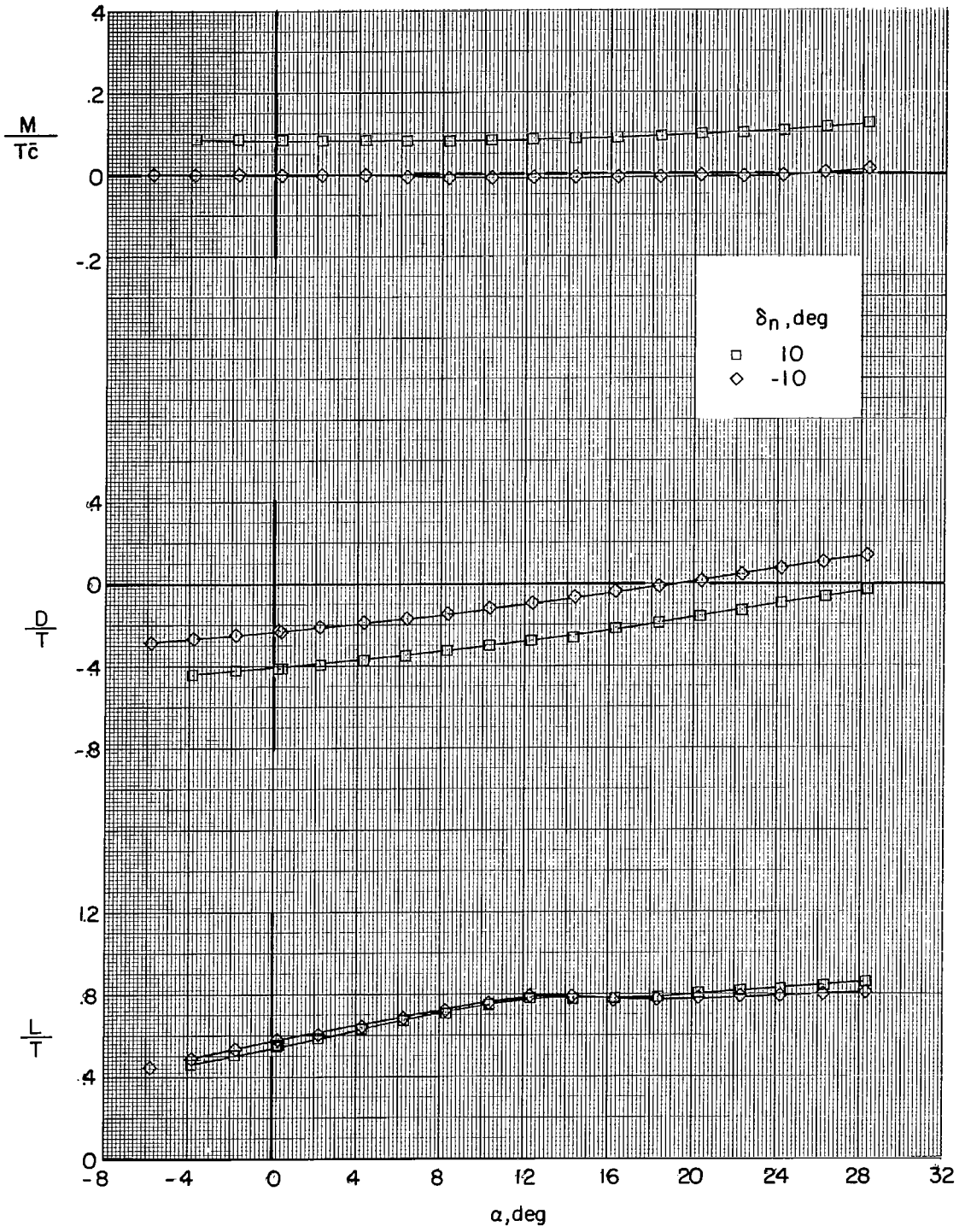


(c) Measured characteristics at effective velocity ratio of 0.115.

Figure 9.- Continued.

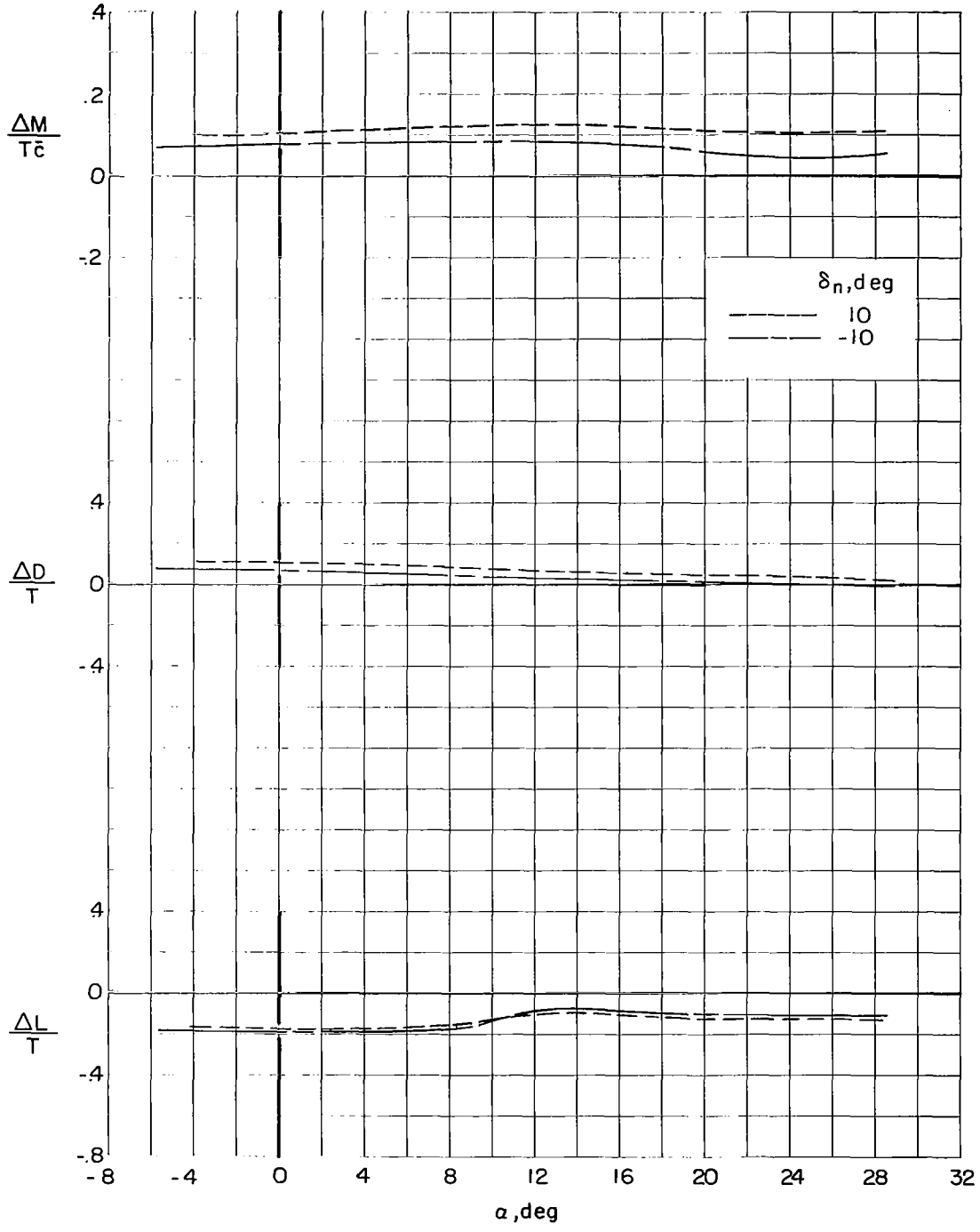


(d) Interference increments at effective velocity ratio of 0.115.

Figure 9.- Concluded.

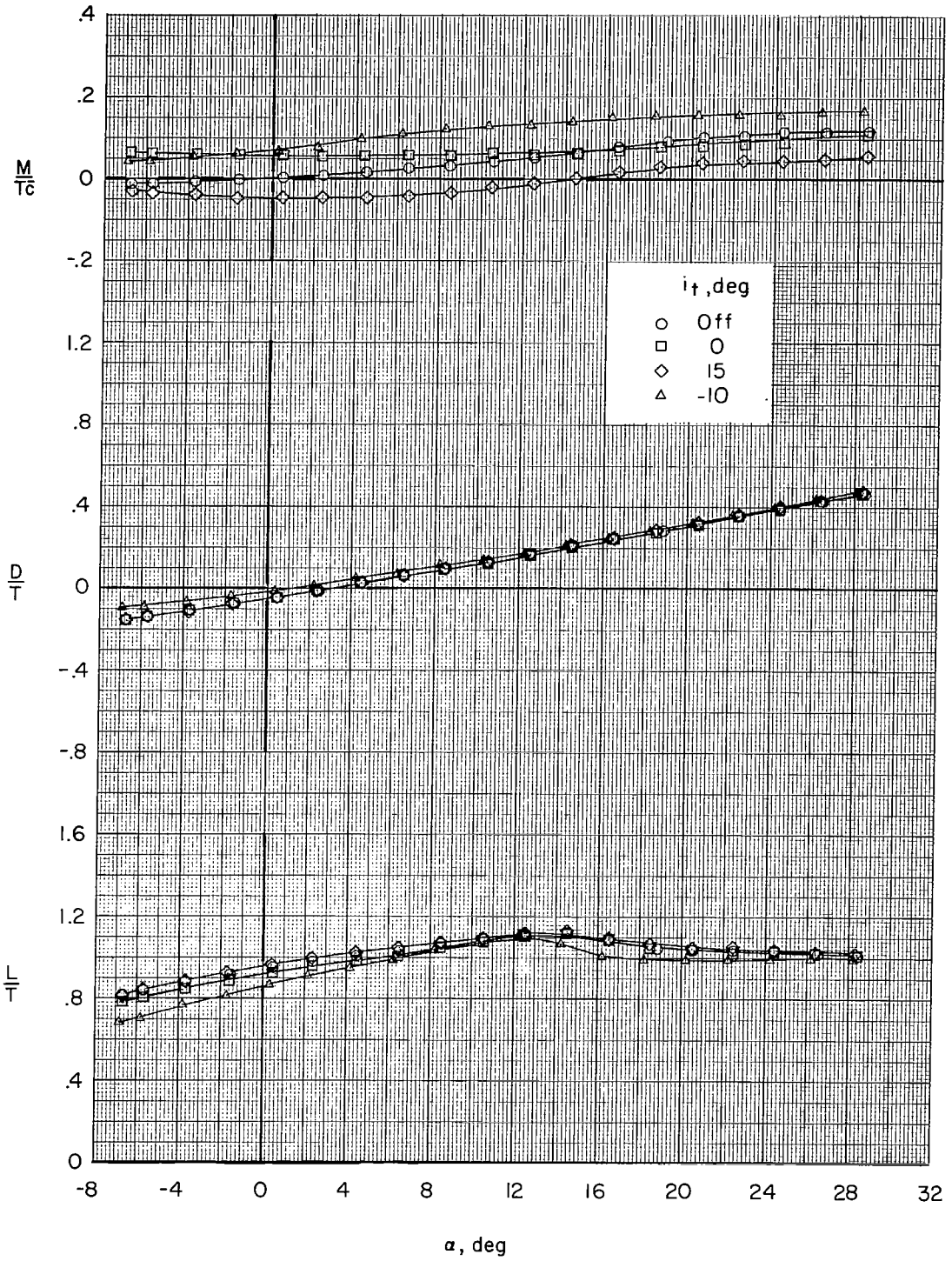


(a) Measured characteristics at $\delta_n = 0^0$.

Figure 10.- Effect of basic-horizontal-tail incidence on longitudinal aerodynamic characteristics. Six lift engines; $\beta = 0^0$; effective velocity ratio, 0.115.

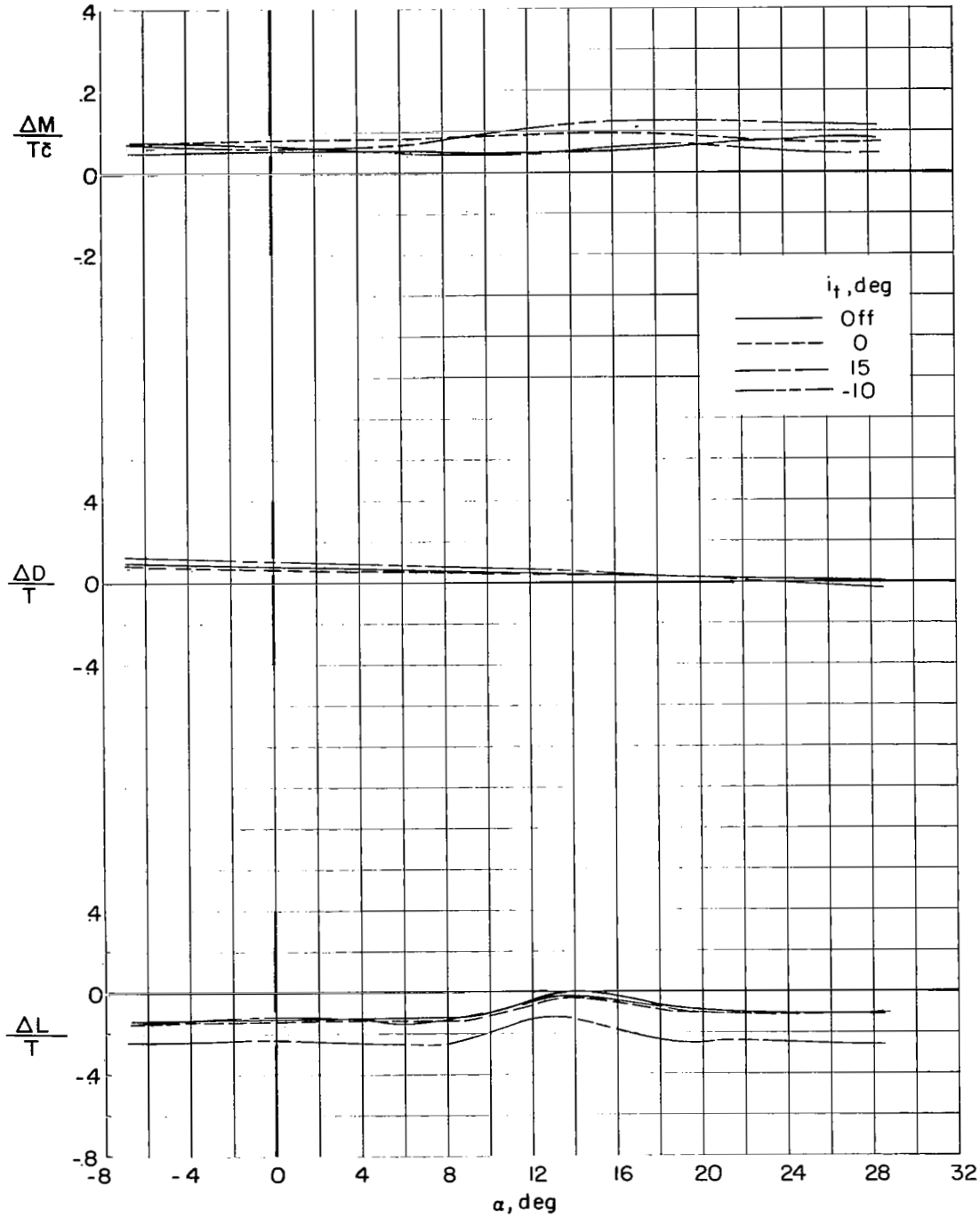


(b) Interference increments at $\delta_n = 0^0$.

Figure 10.- Continued.

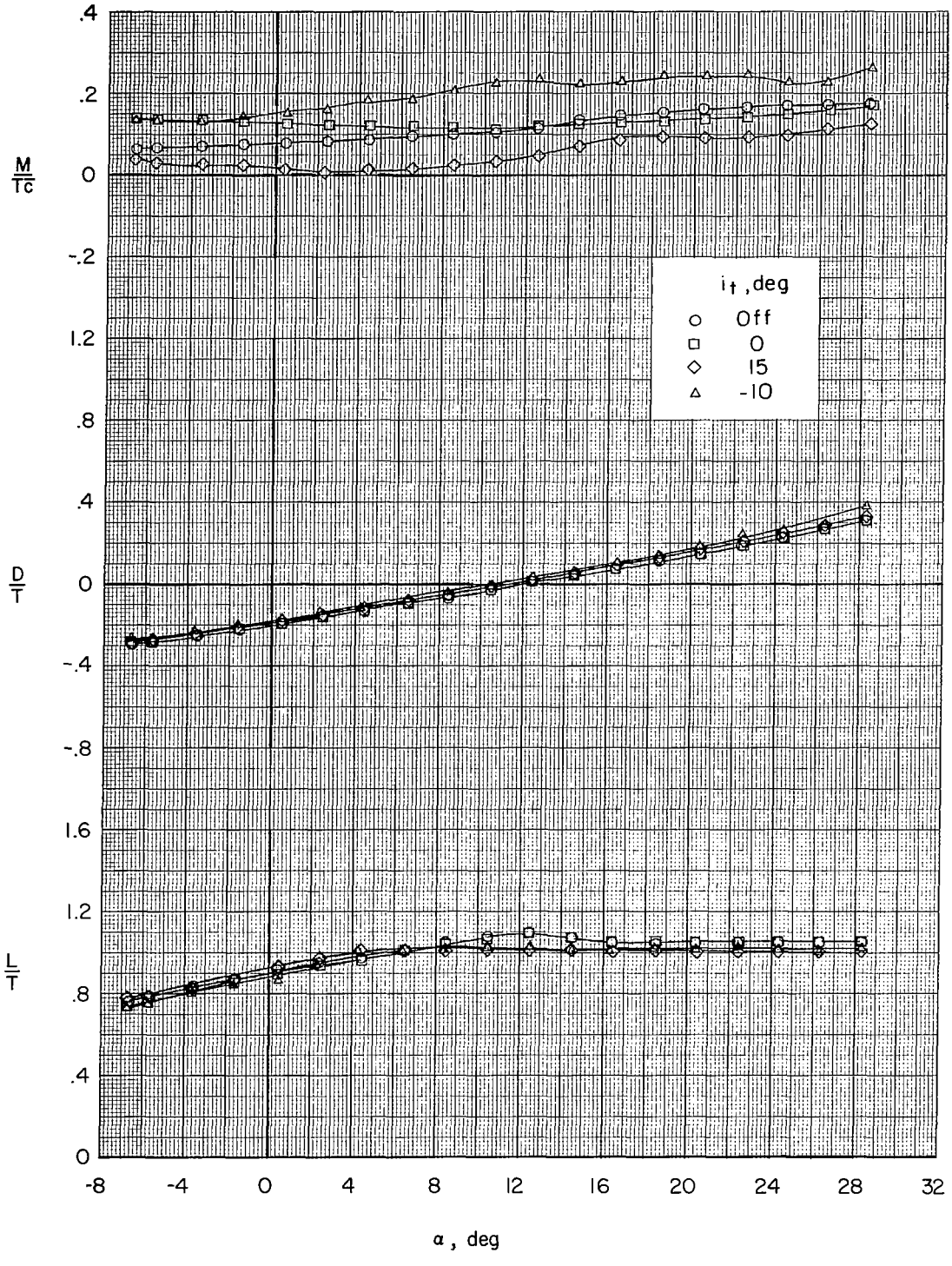


(c) Measured characteristics at $\delta_n = 10^0$.

Figure 10.- Continued.

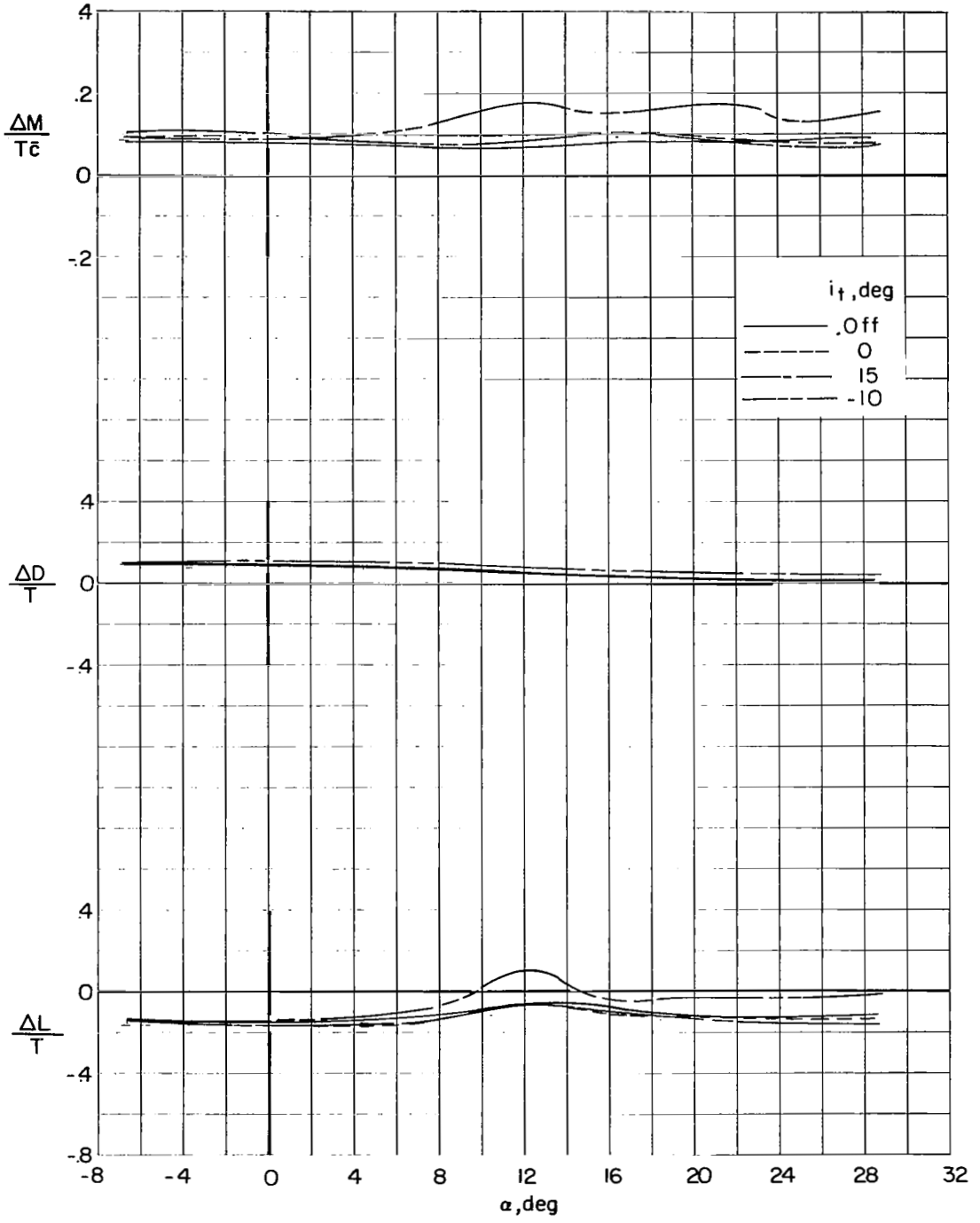


(d) Interference increments at $\delta_n = 10^0$.

Figure 10.- Continued.

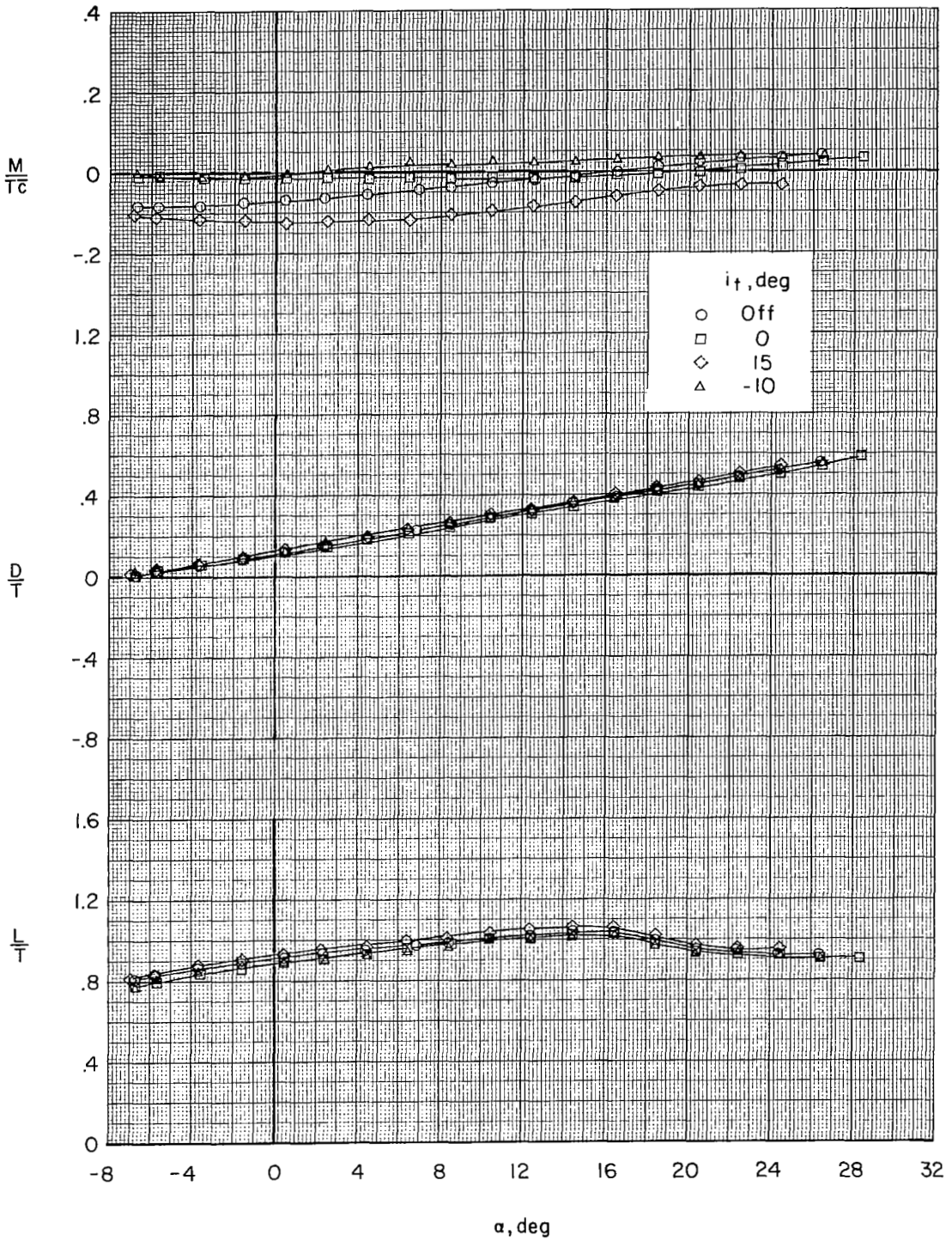


(e) Measured characteristics at $\delta_n = -10^0$.

Figure 10.- Continued.

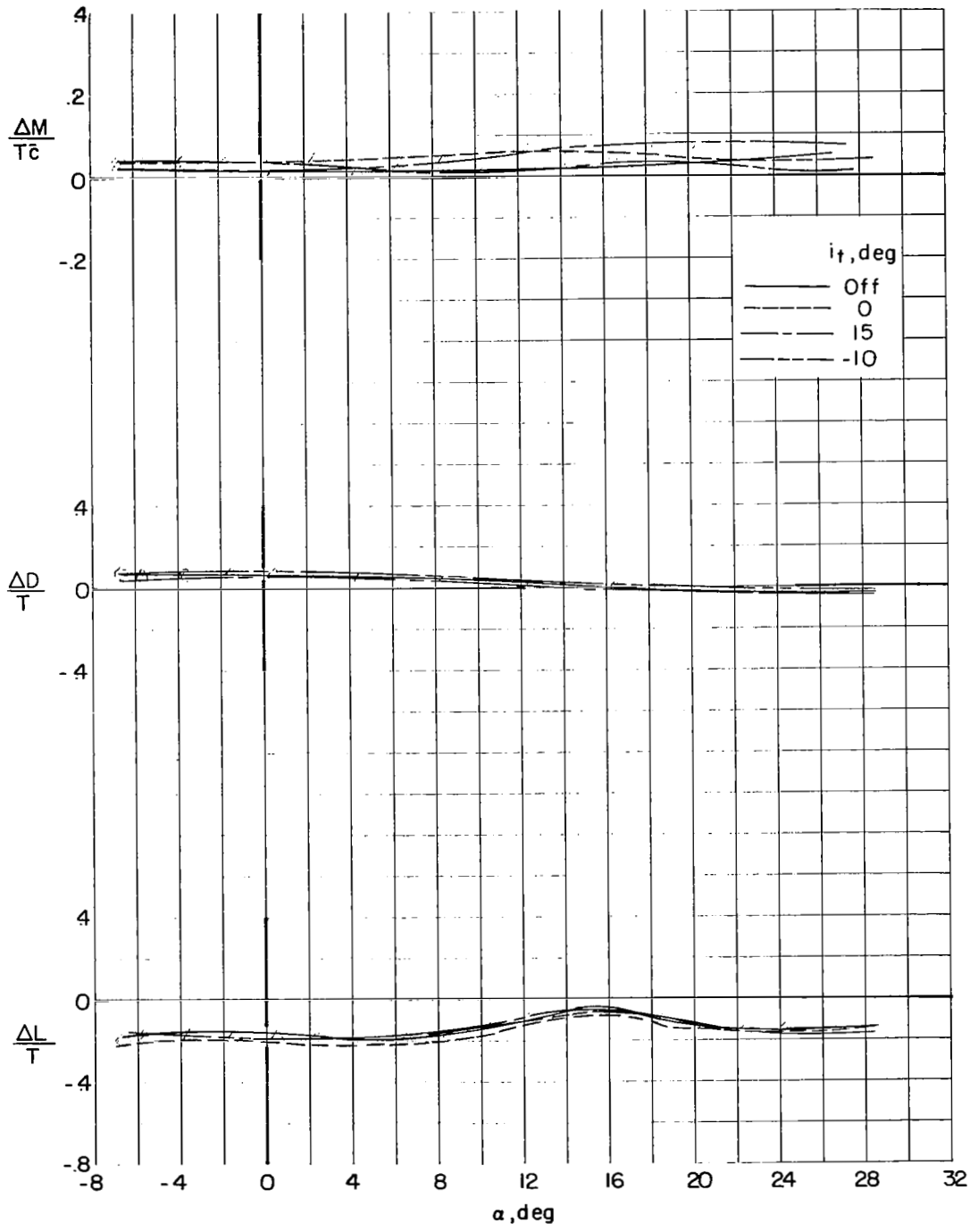


(f) Interference increments at $\delta_n = -10^0$.

Figure 10.- Concluded.

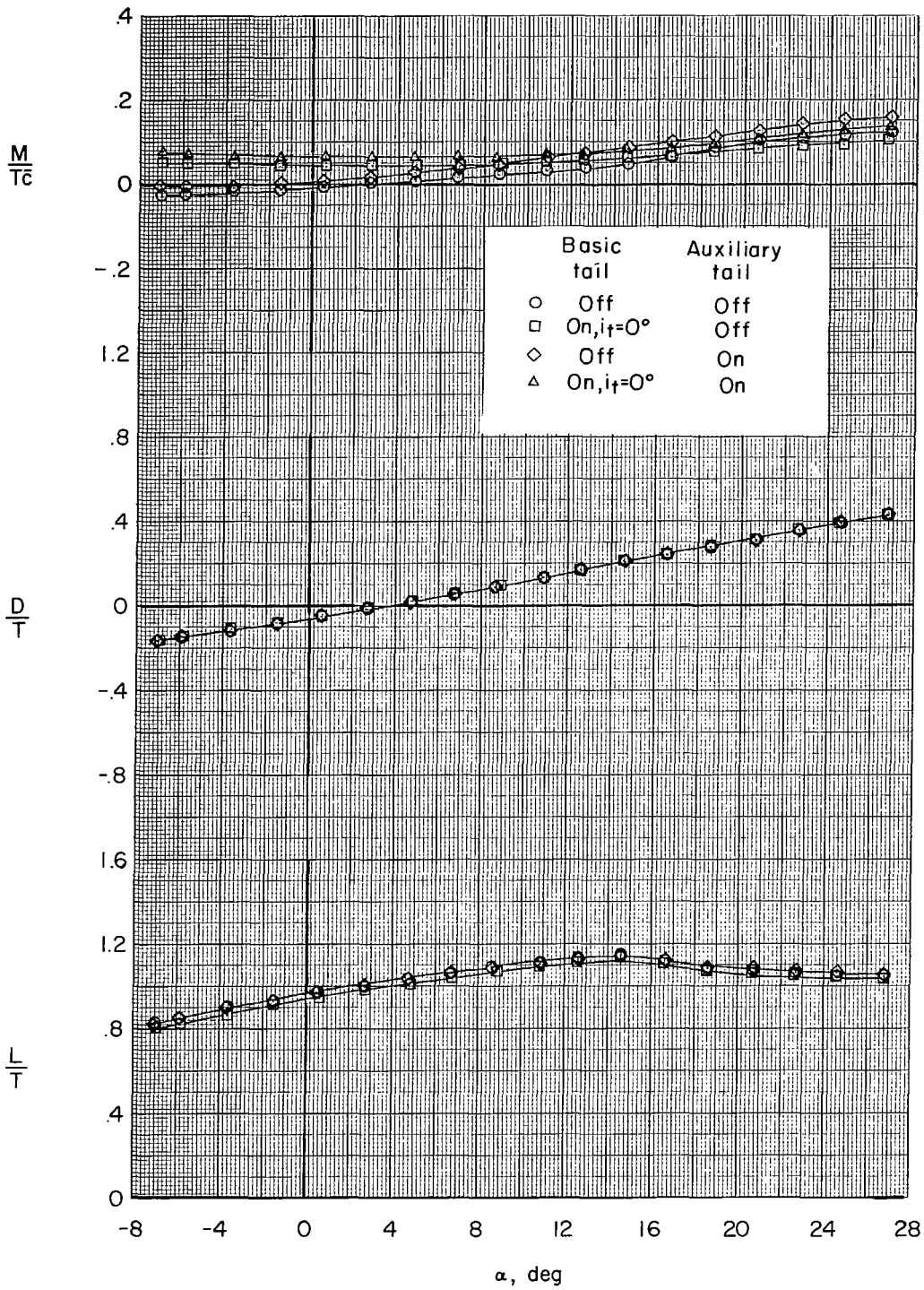


(a) Measured characteristics.

Figure 11.- Effect of basic and auxiliary horizontal tails on longitudinal aerodynamic characteristics. Six lift engines; $\beta = 0^0$; $\delta_n = 0^0$; effective velocity ratio, 0.115.

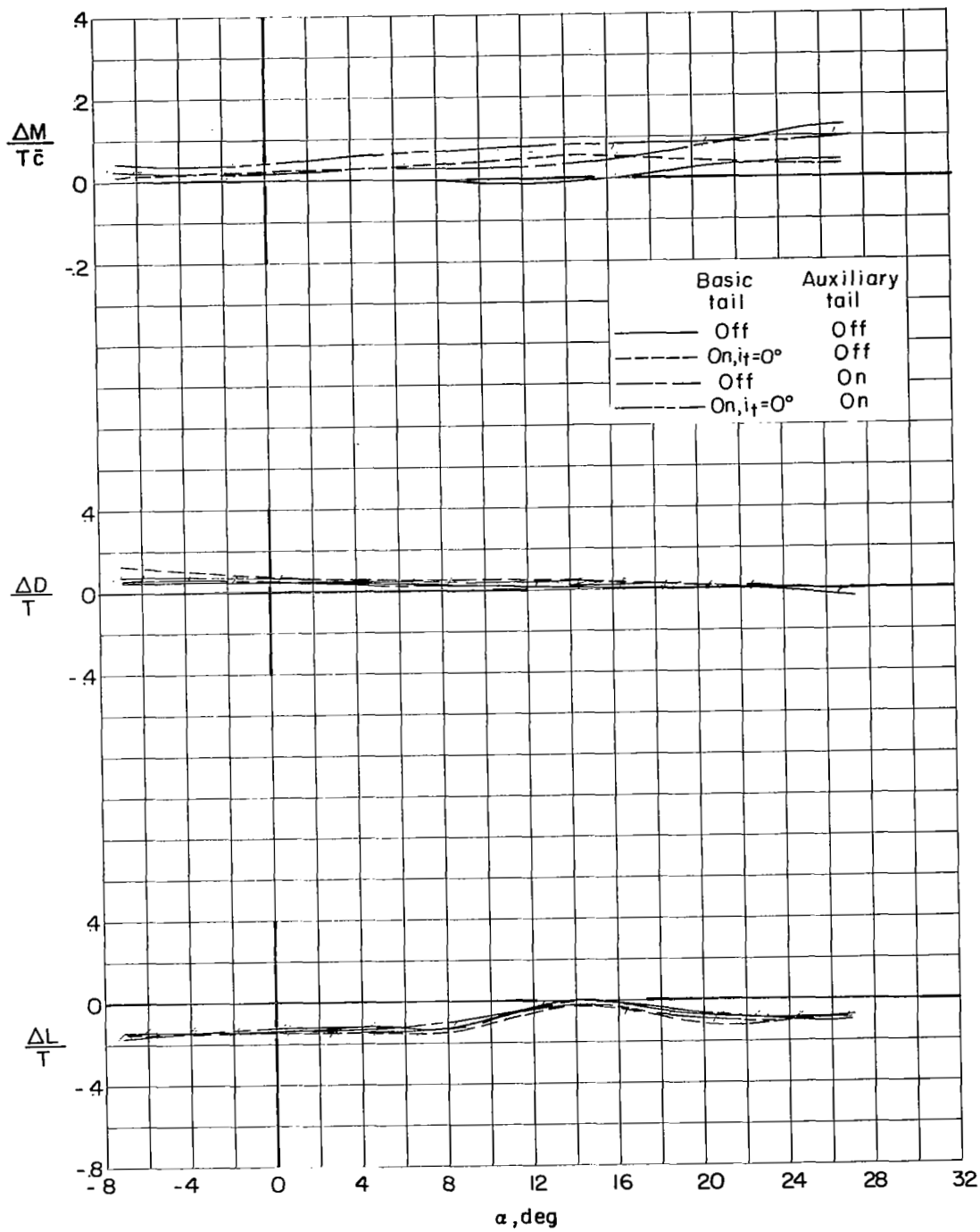


(b) Interference increments.

Figure 11.- Concluded.

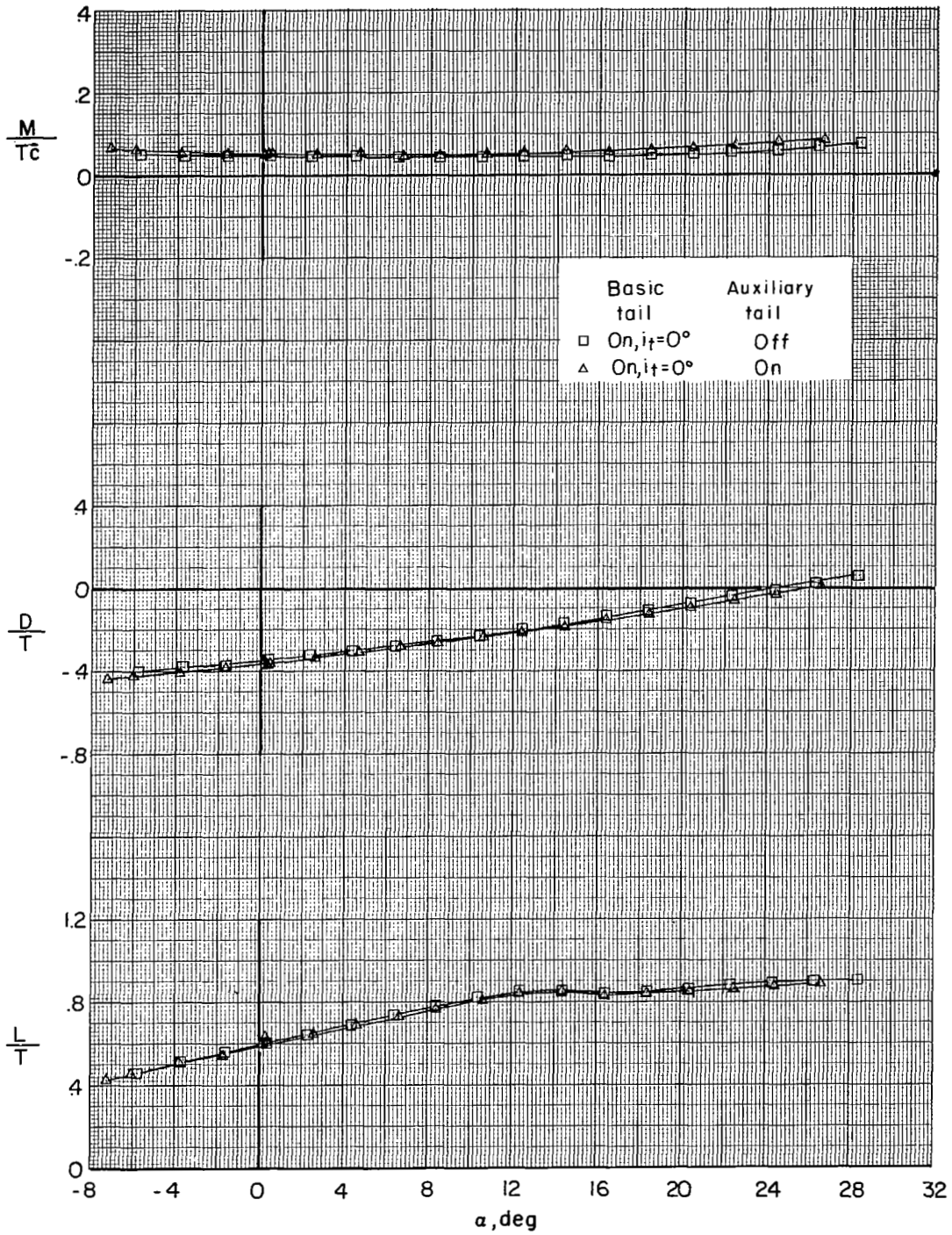


(a) Measured characteristics.

Figure 12.- Effect of auxiliary tail on longitudinal aerodynamic characteristics. Four lift engines and two cruise engines; $\beta = 0^0$; $\delta_n = 0^0$; effective velocity ratio, 0.115.

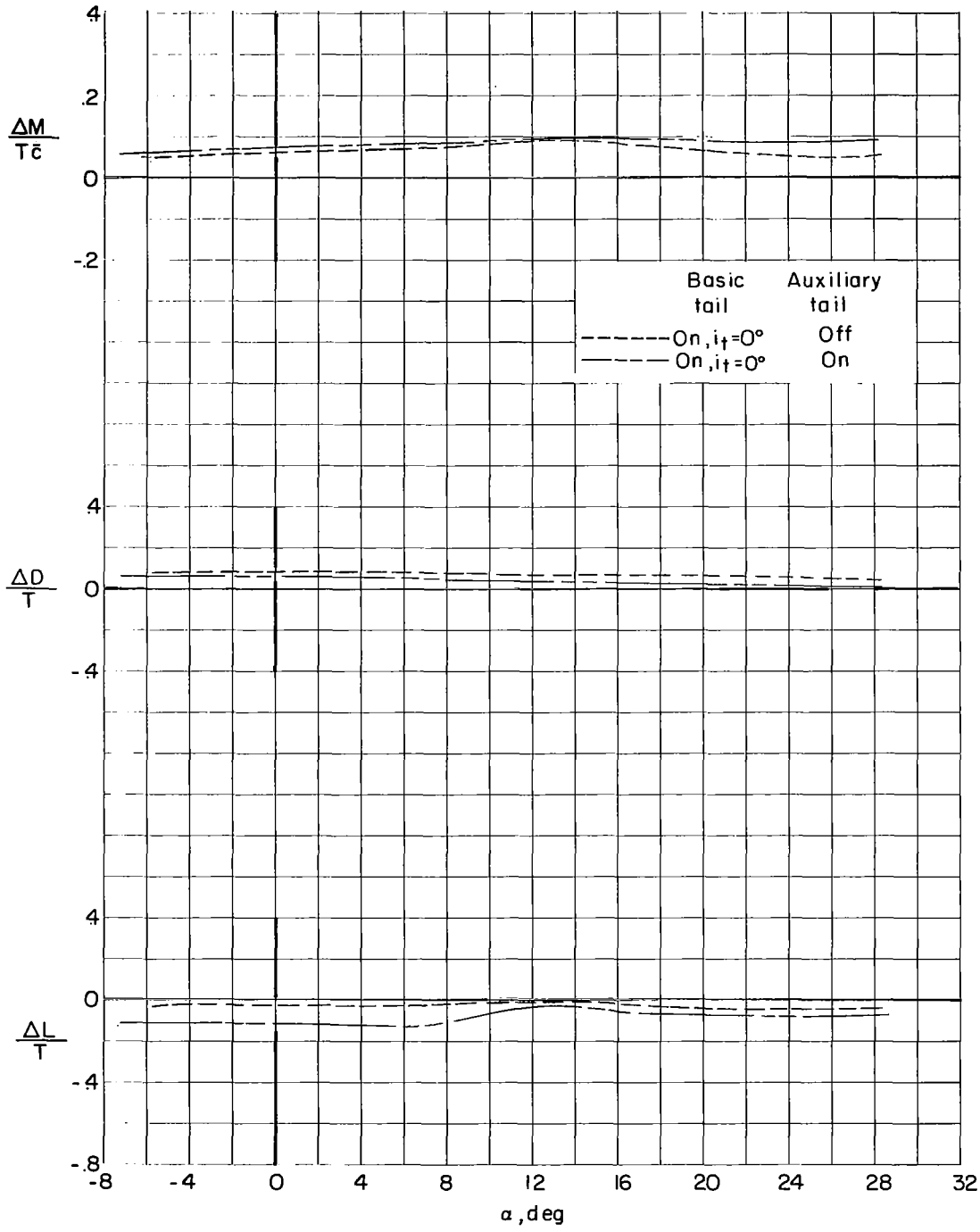


(b) Interference increments.

Figure 12.- Concluded.

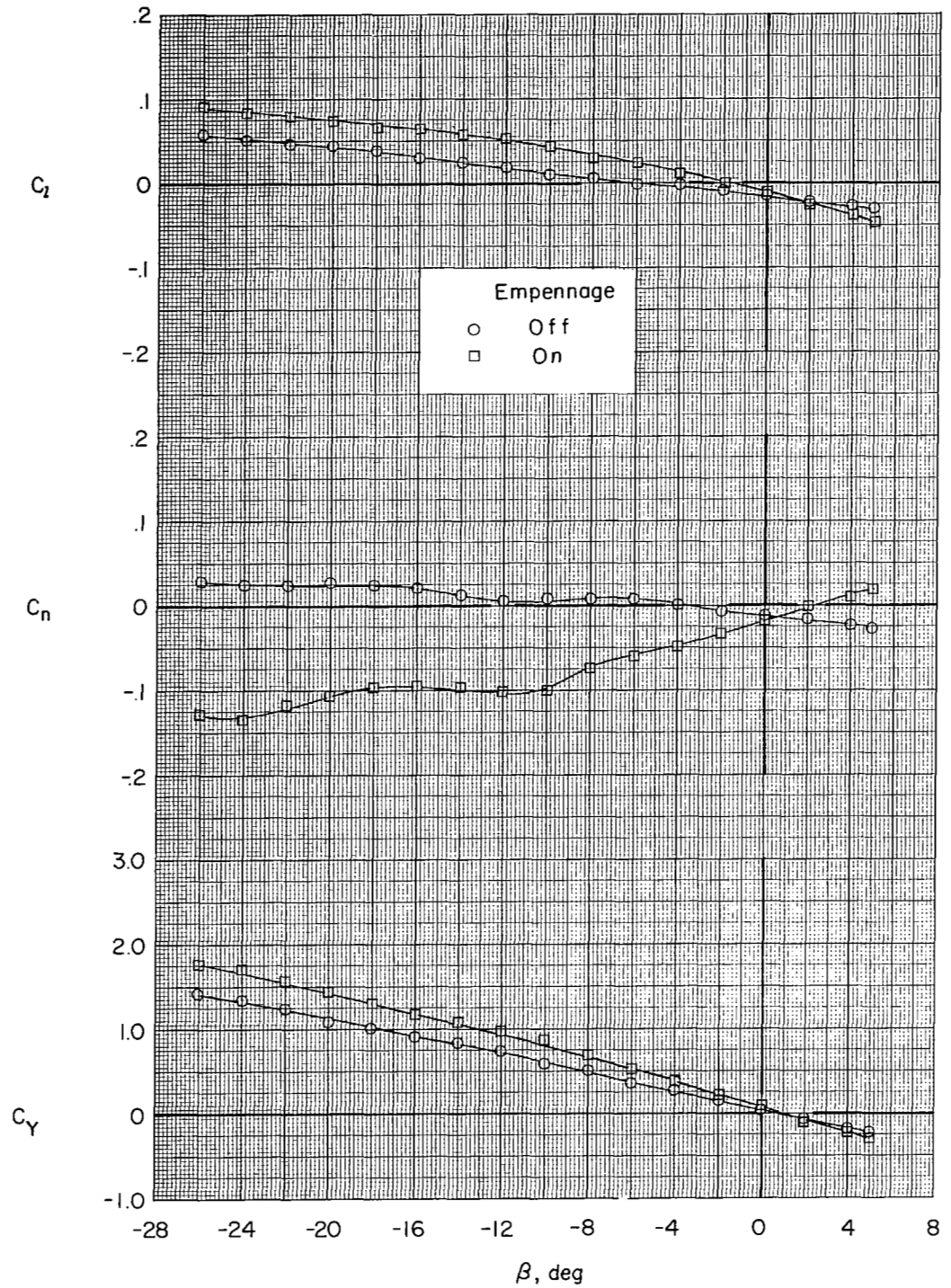


(a) Measured lateral-directional characteristics.

Figure 13.- Aerodynamic characteristics in sideslip showing effect of basic empennage. Six lift engines; effective velocity ratio, 0.115; $\alpha = 0^0$; $\delta_n = 0^0$.

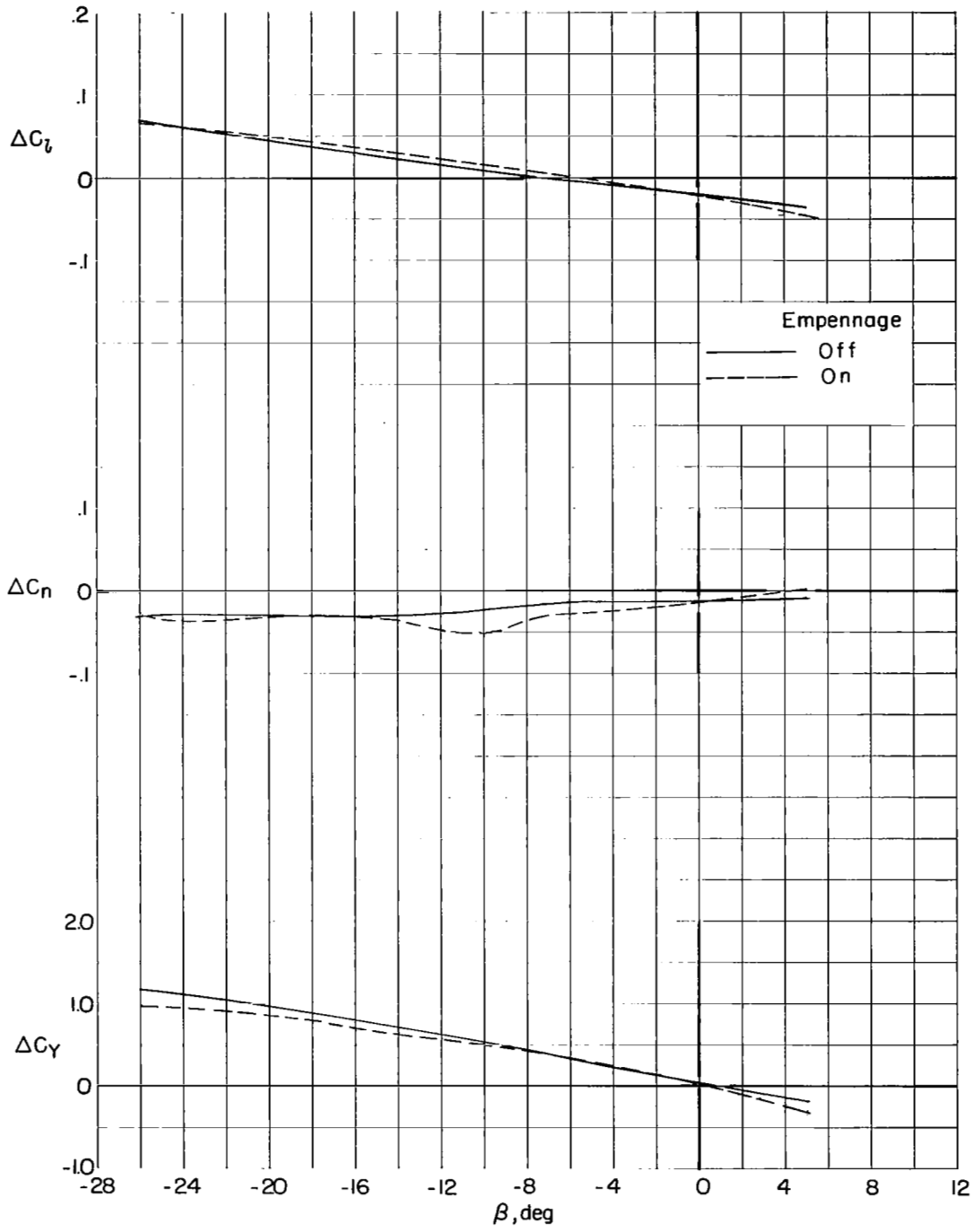


(b) Lateral-directional interference increments.

Figure 13.- Continued.

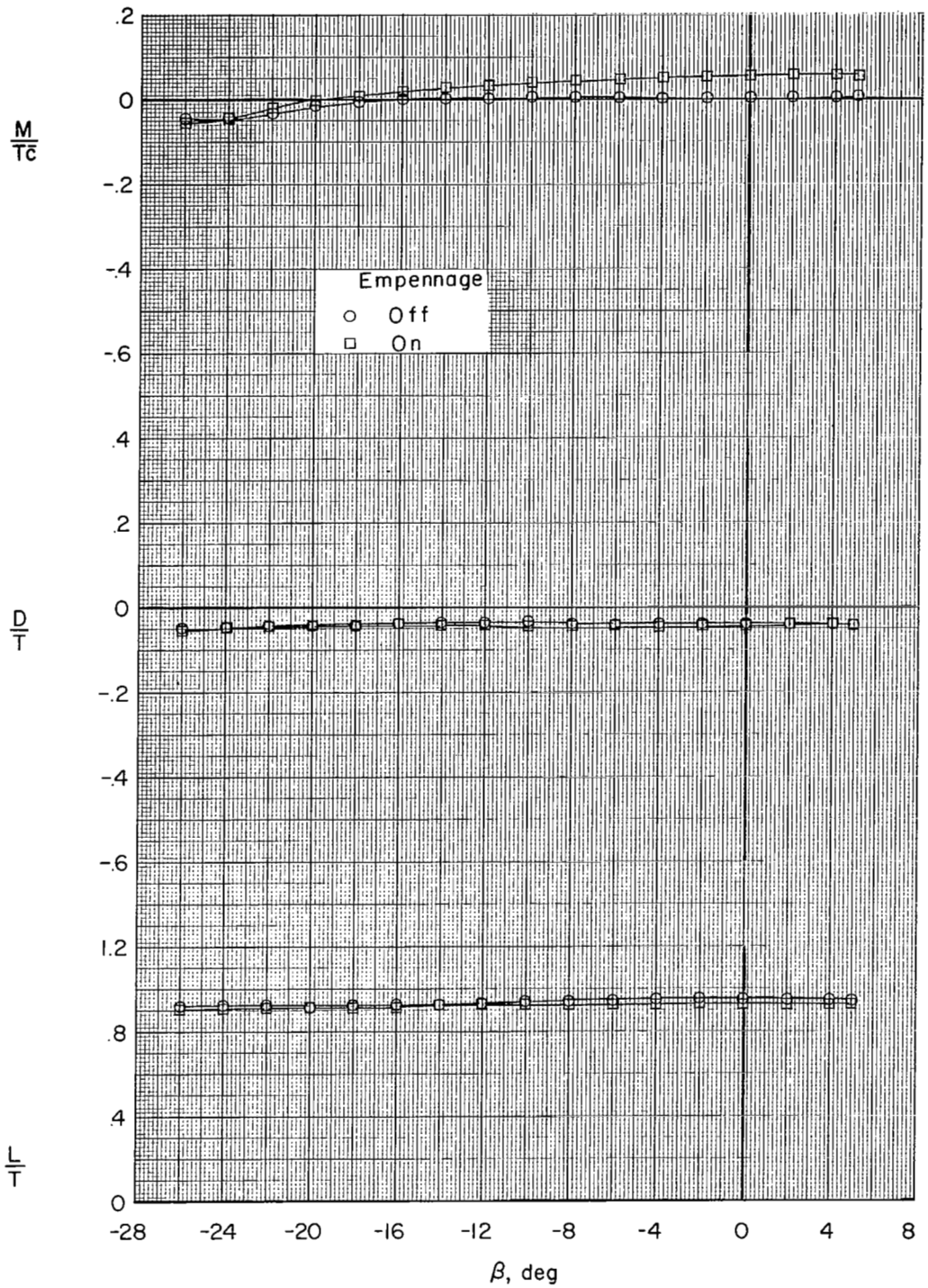


(c) Measured longitudinal characteristics.

Figure 13.- Continued.

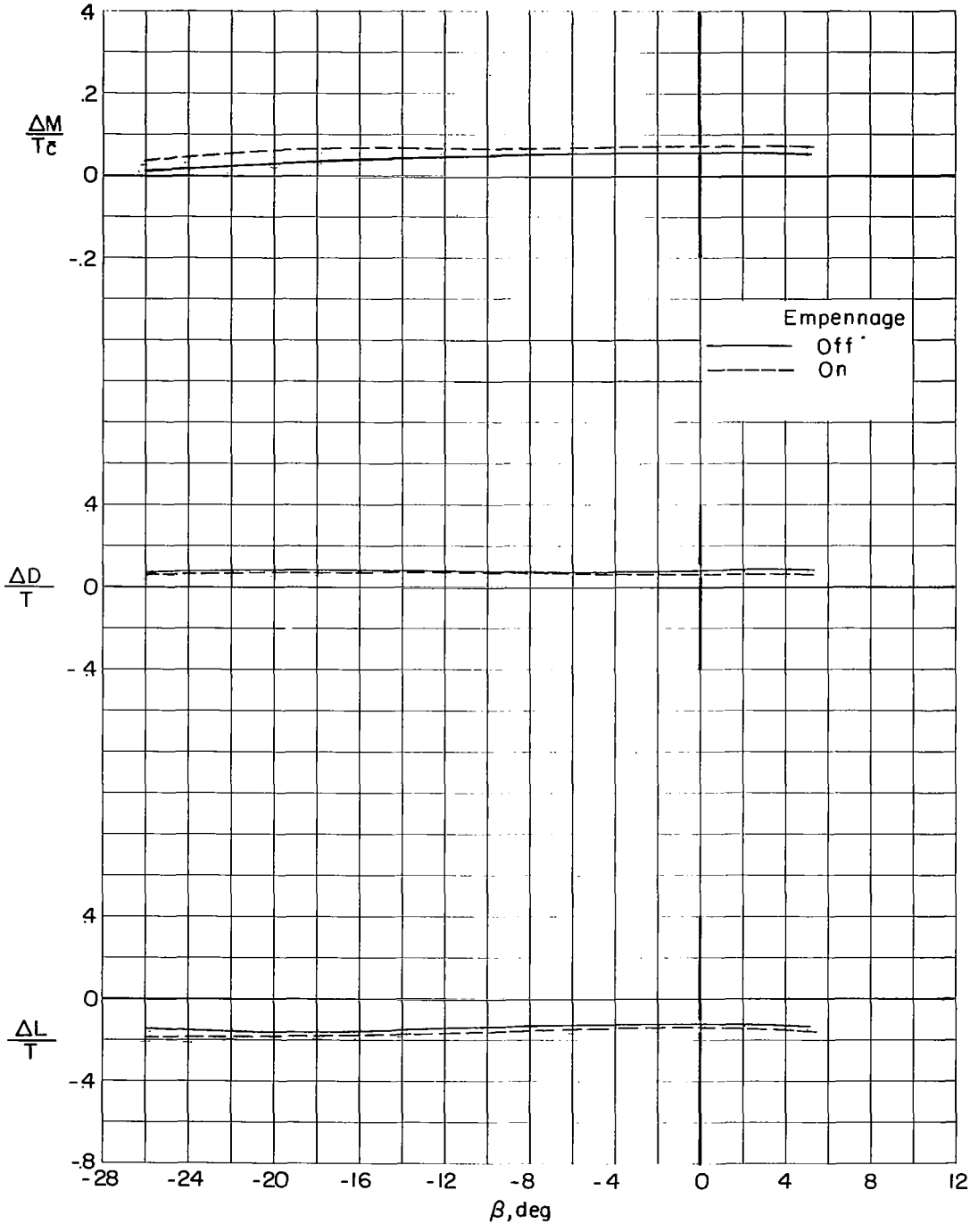


(d) Longitudinal interference increments.

Figure 13.- Concluded.

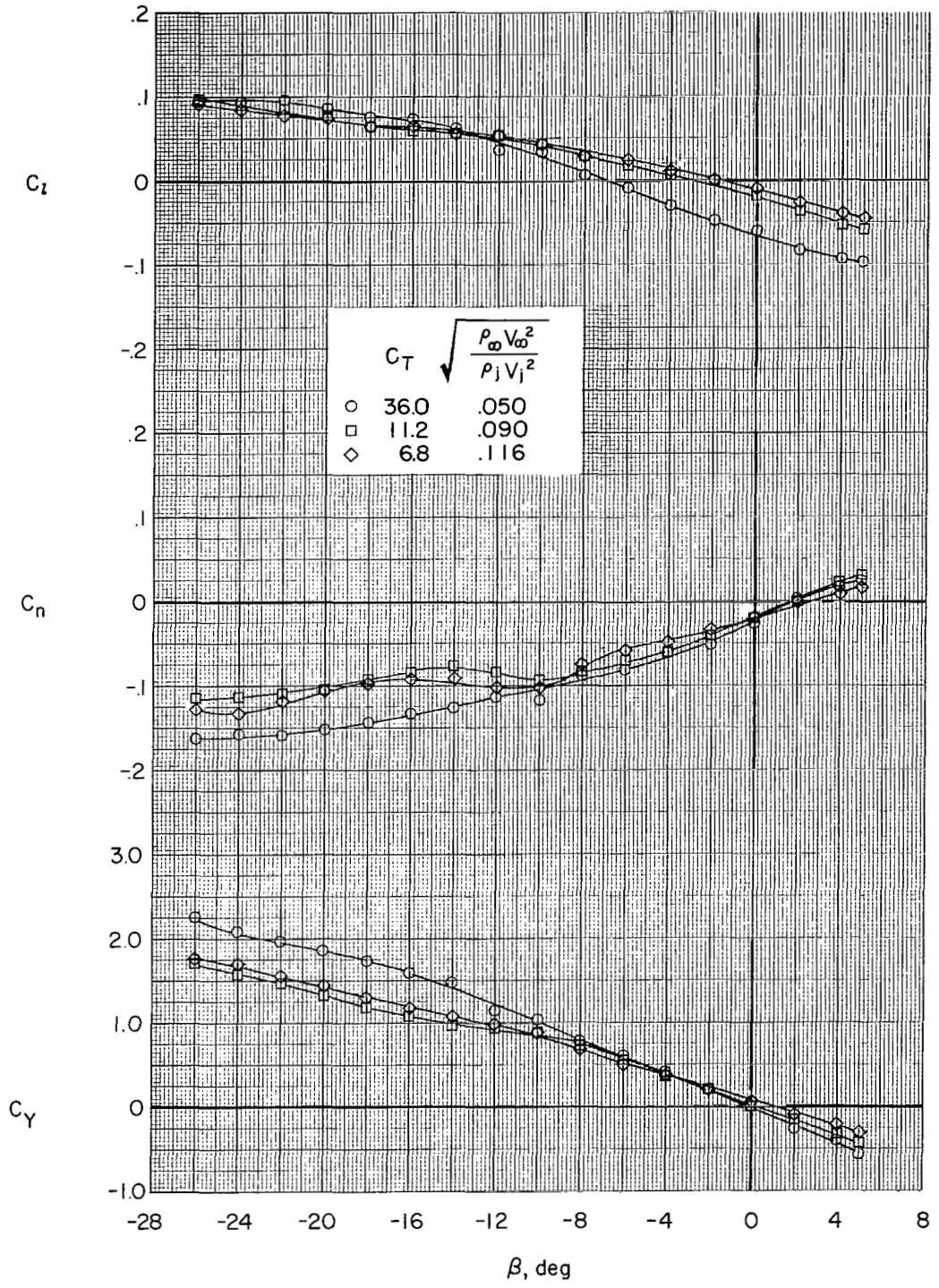


(a) Measured lateral-directional characteristics.

Figure 14.- Aerodynamic characteristics in sideslip showing effect of effective velocity ratio. Six lift engines; $\alpha = 0^0$; $\delta_n = 0^0$.

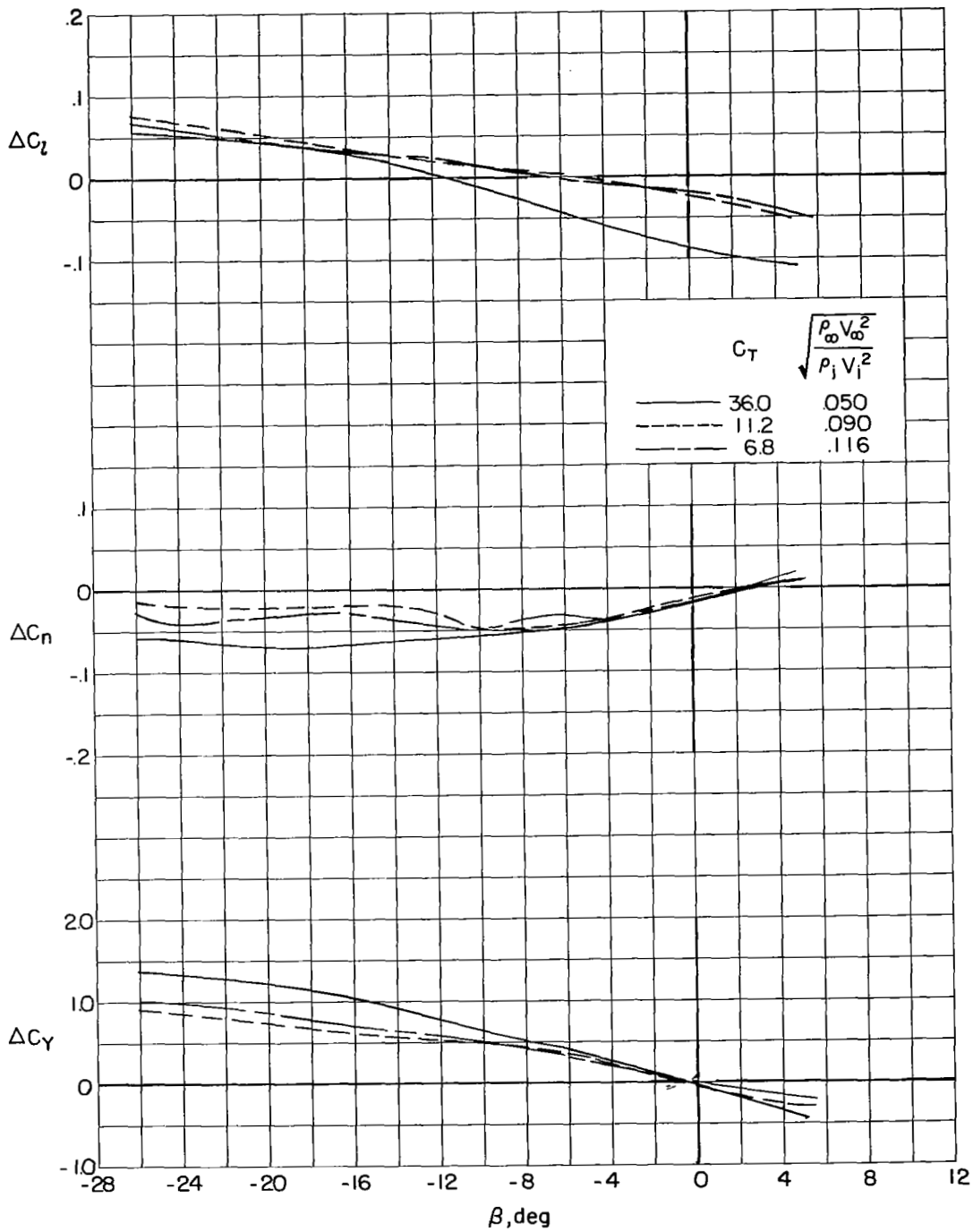


(b) Lateral-directional interference increments.

Figure 14.- Continued.

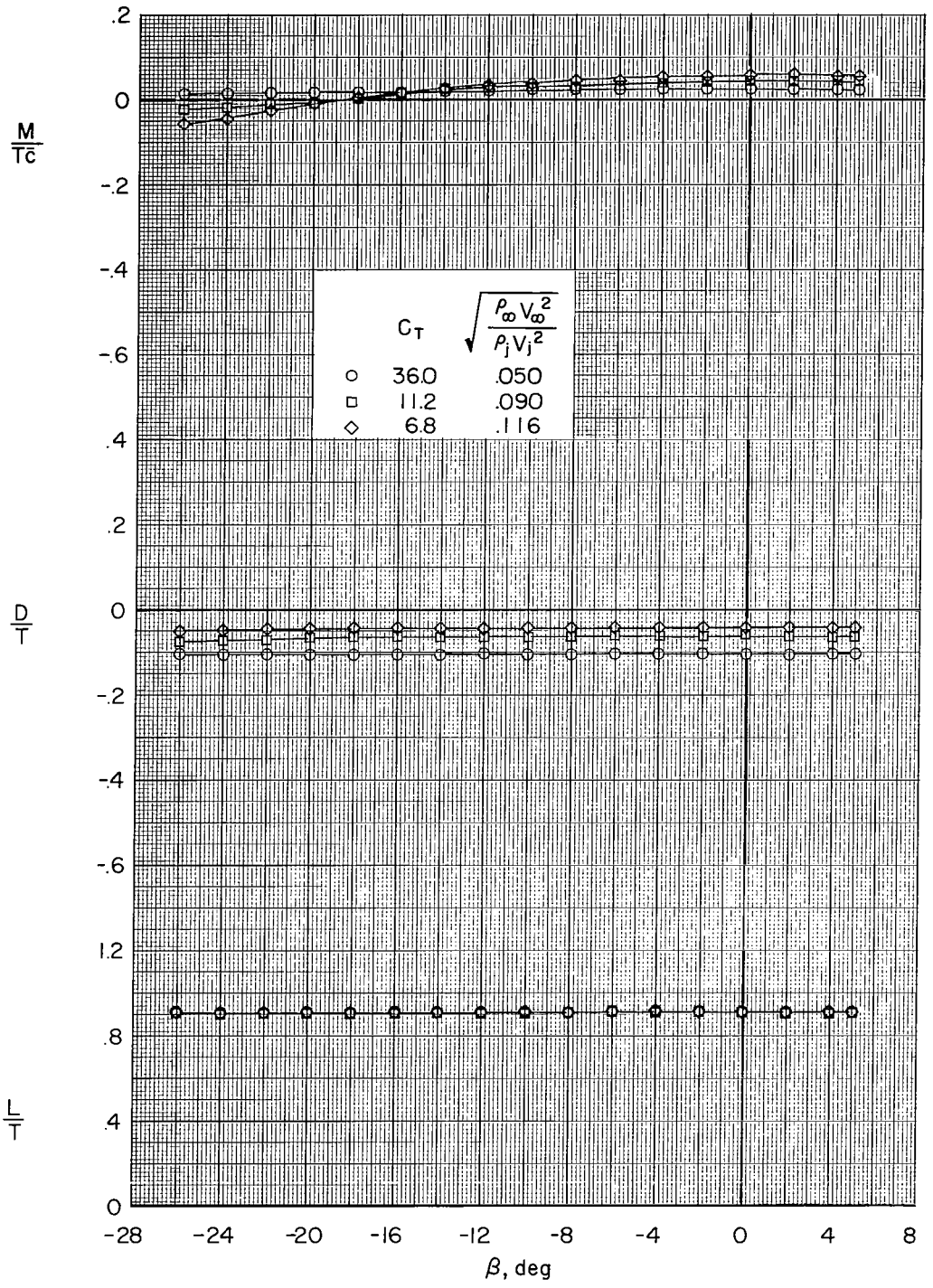


(c) Measured longitudinal characteristics.

Figure 14.- Continued.

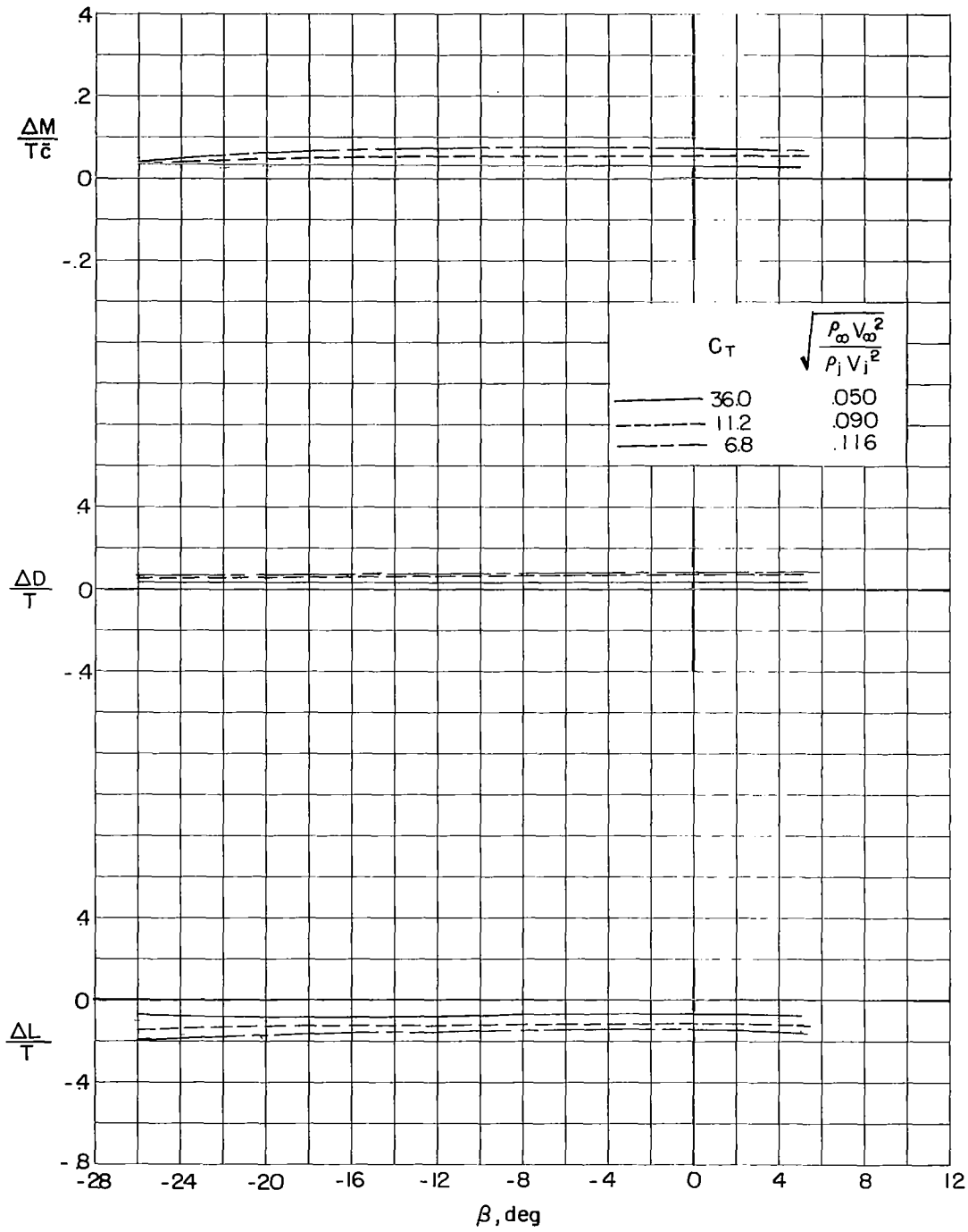


(d) Longitudinal interference increments.

Figure 14.- Concluded.

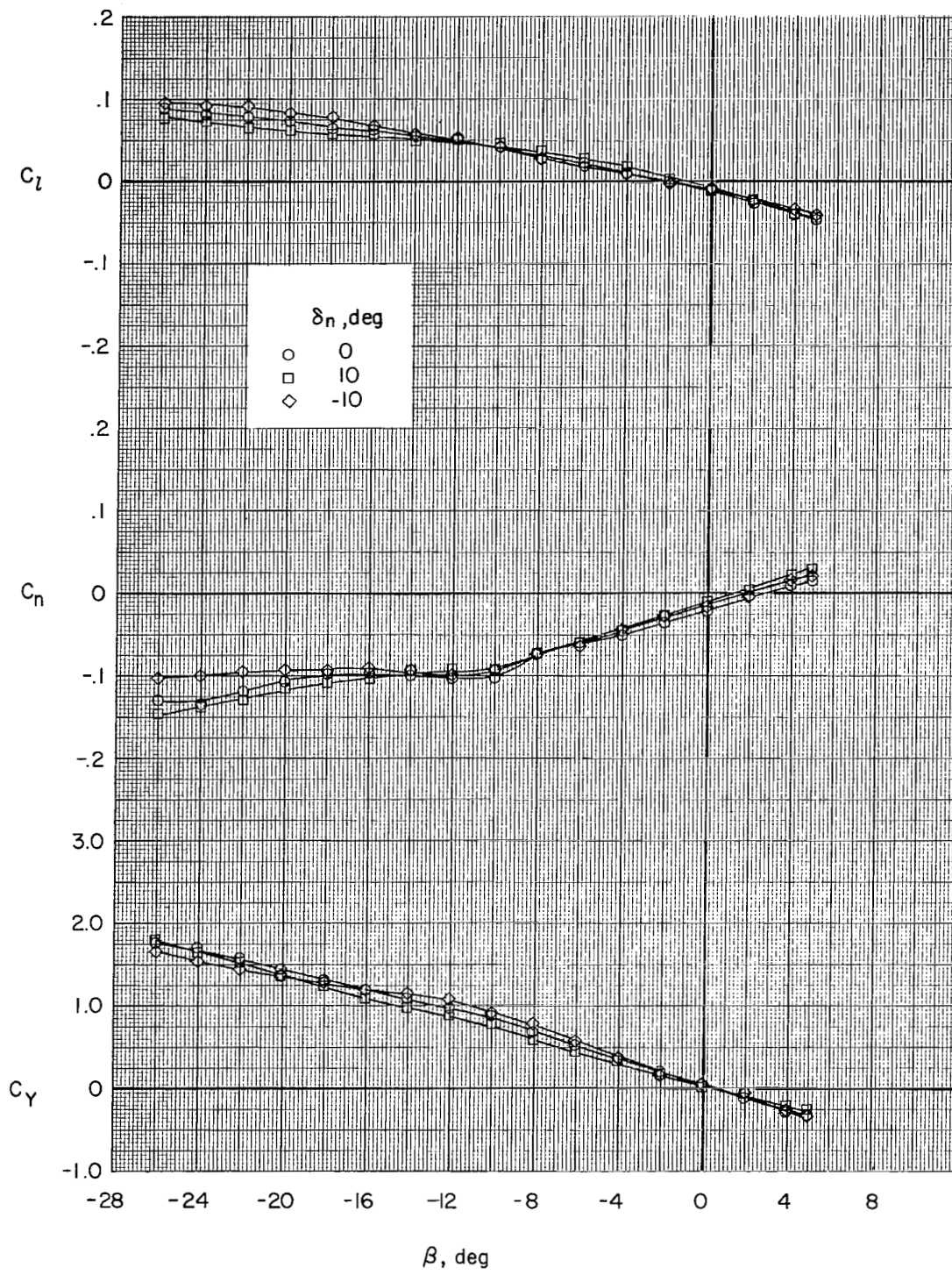


(a) Measured lateral-directional characteristics.

Figure 15.- Aerodynamic characteristics in sideslip showing effect of nozzle setting. Six lift engines; $\alpha = 0^0$; effective velocity ratio, 0.115.

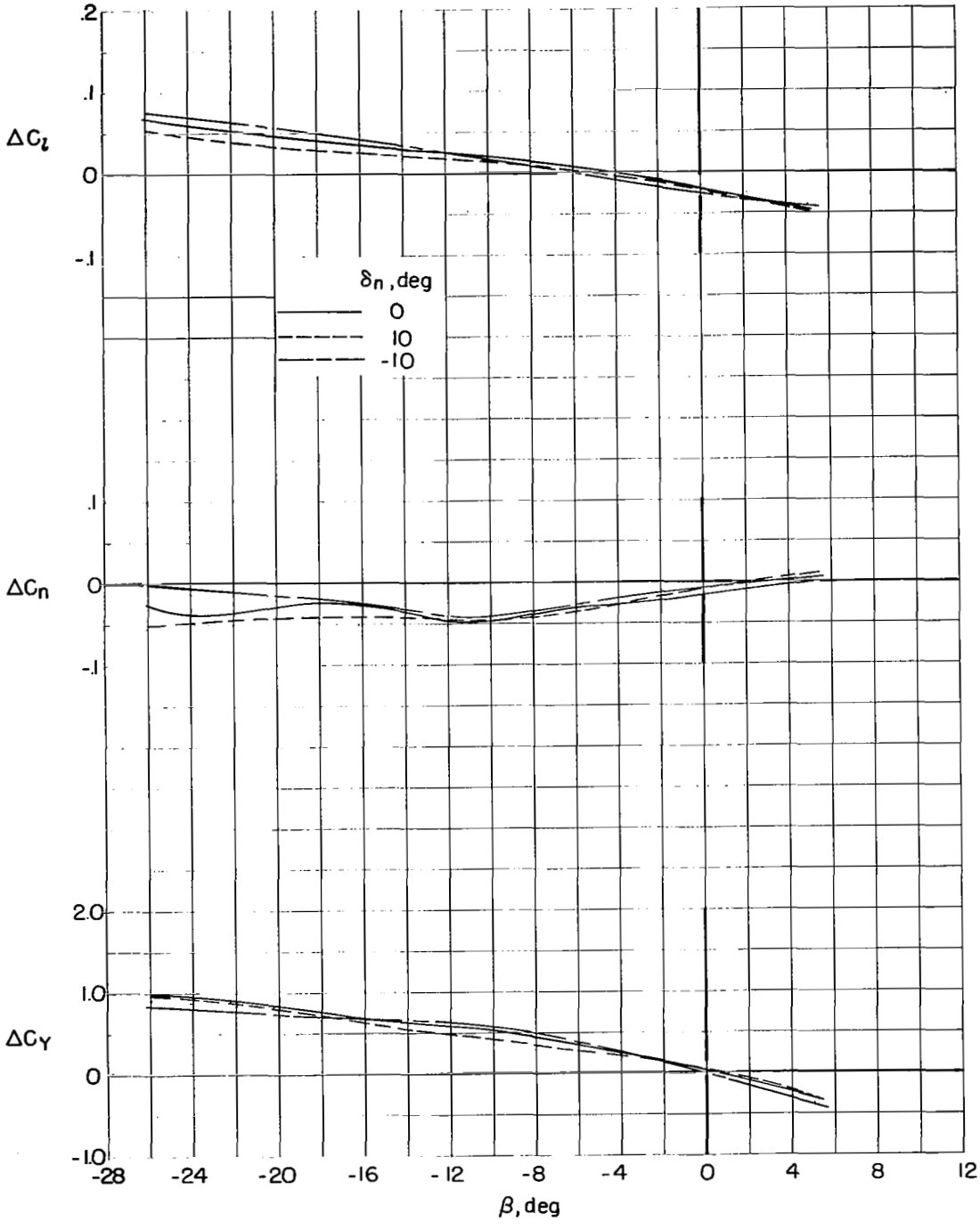


(b) Lateral-directional interference increments.

Figure 15.- Continued.

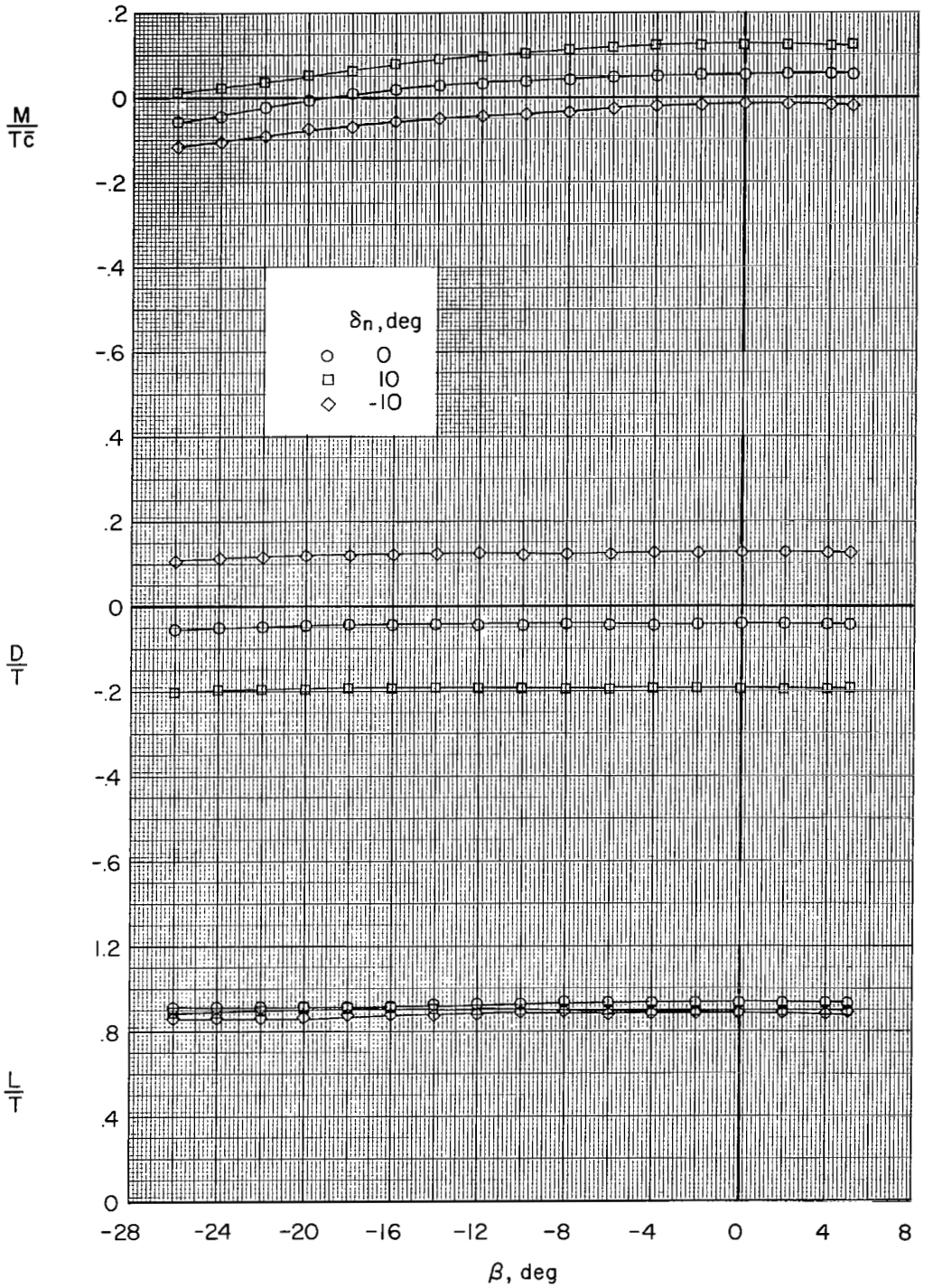


(c) Measured longitudinal characteristics

Figure 15.- Continued.

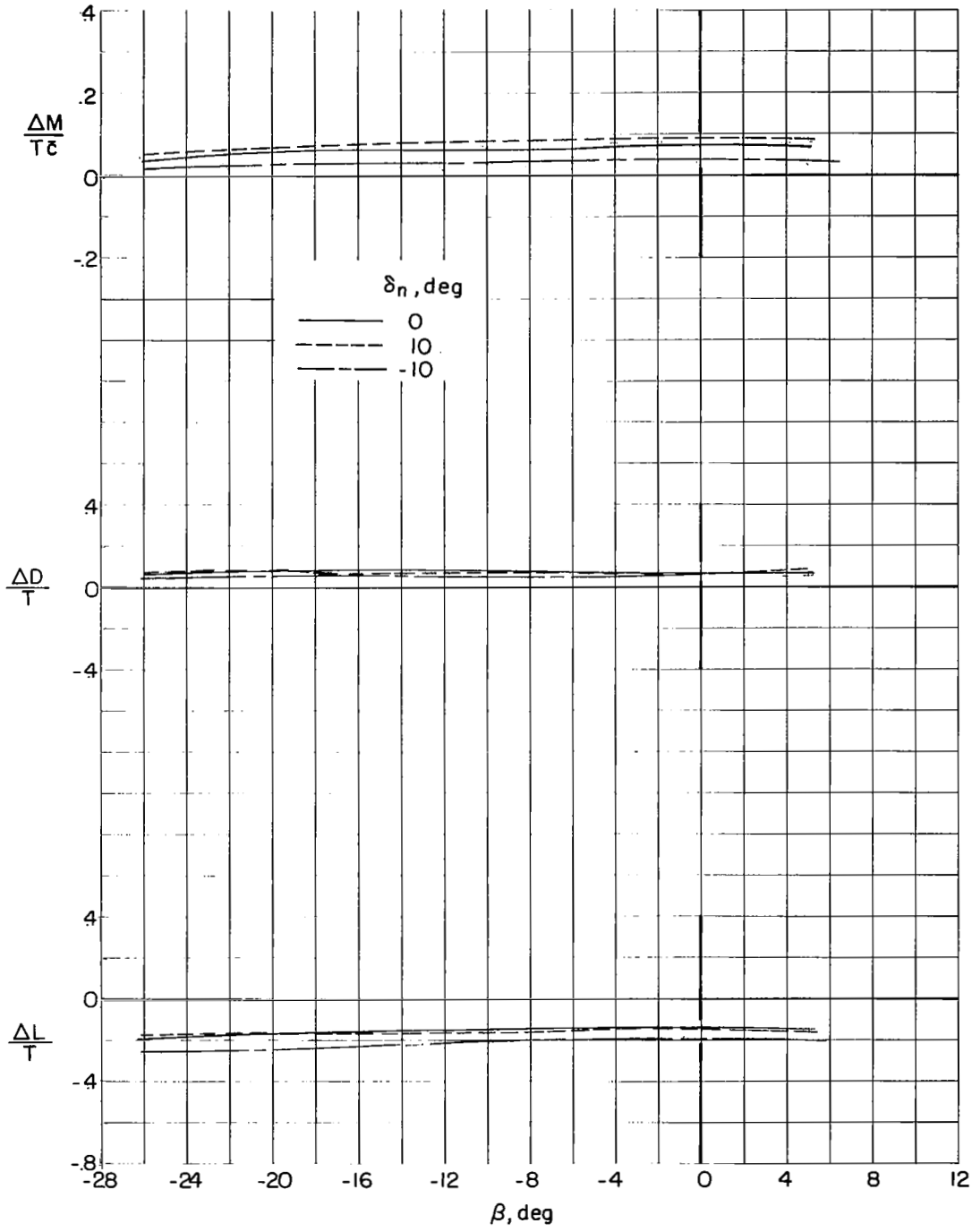


(d) Longitudinal interference increments.

Figure 15.- Concluded.

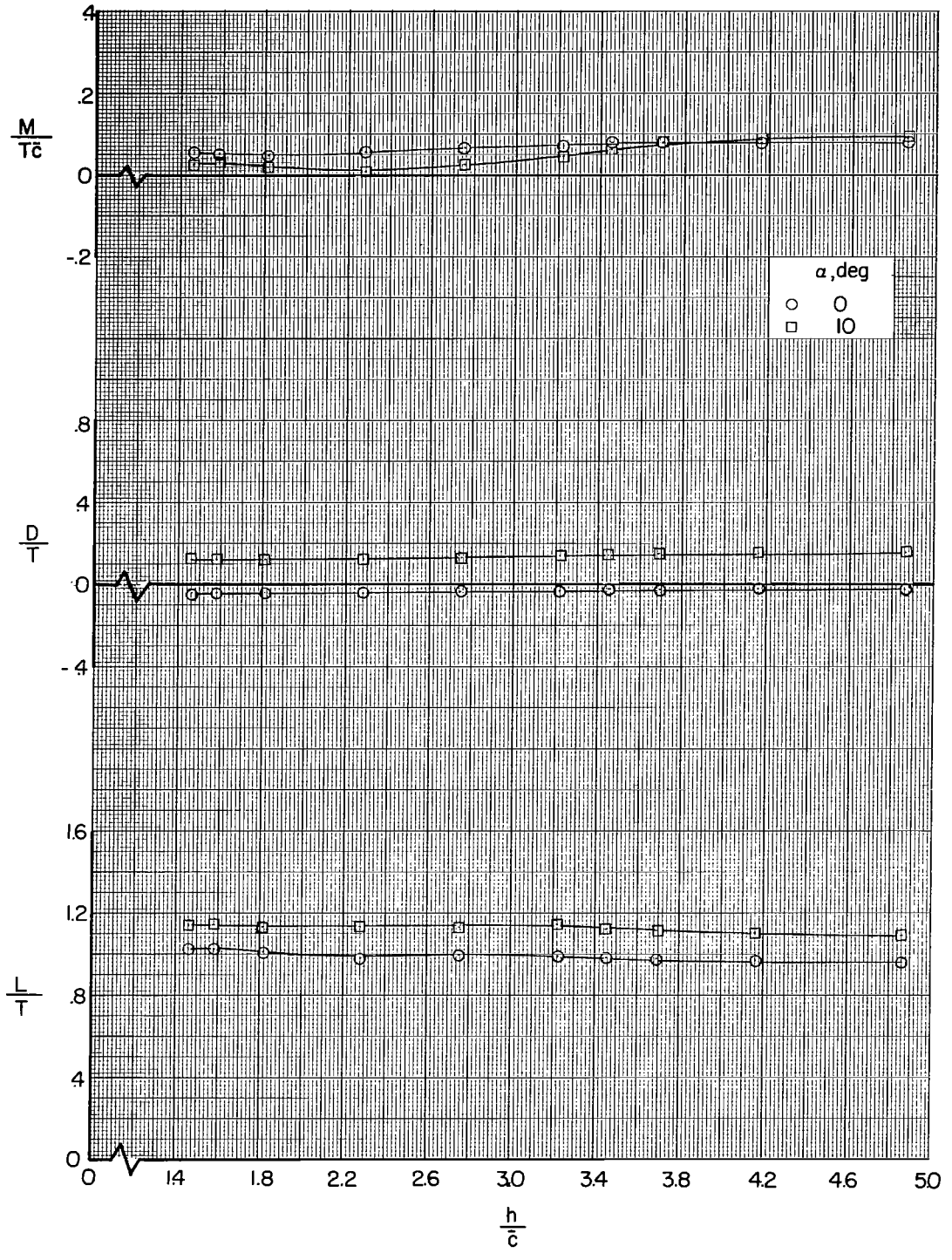


(a) Measured characteristics.

Figure 16.- Variation of $M/T\bar{c}$, D/T, and L/T with $h/\bar{c}$. Six lift engines; effective velocity ratio, 0.115; $\delta_n = 0^0$; landing gear and auxiliary horizontal tail on.

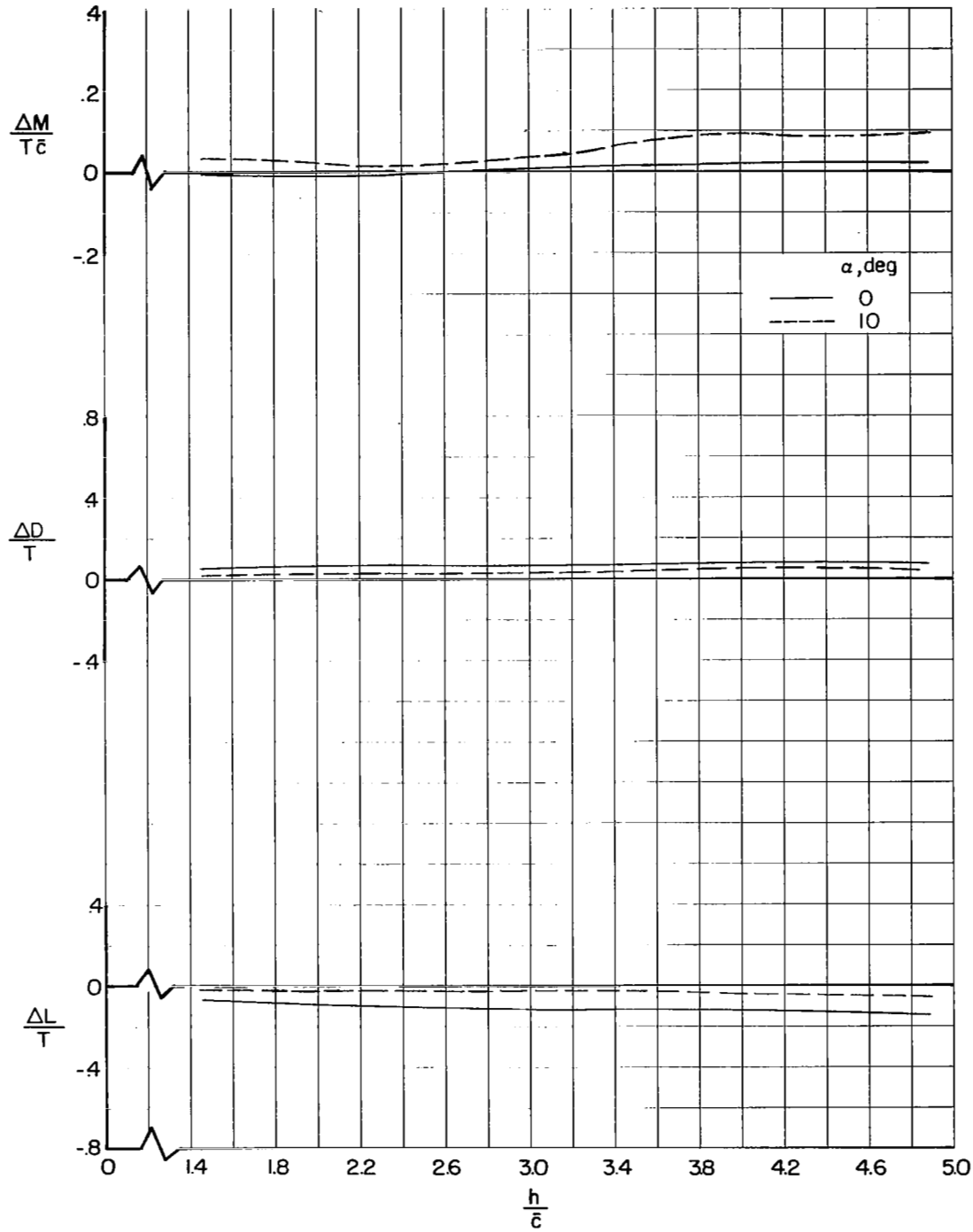


(b) Interference increments.

Figure 16.- Concluded.

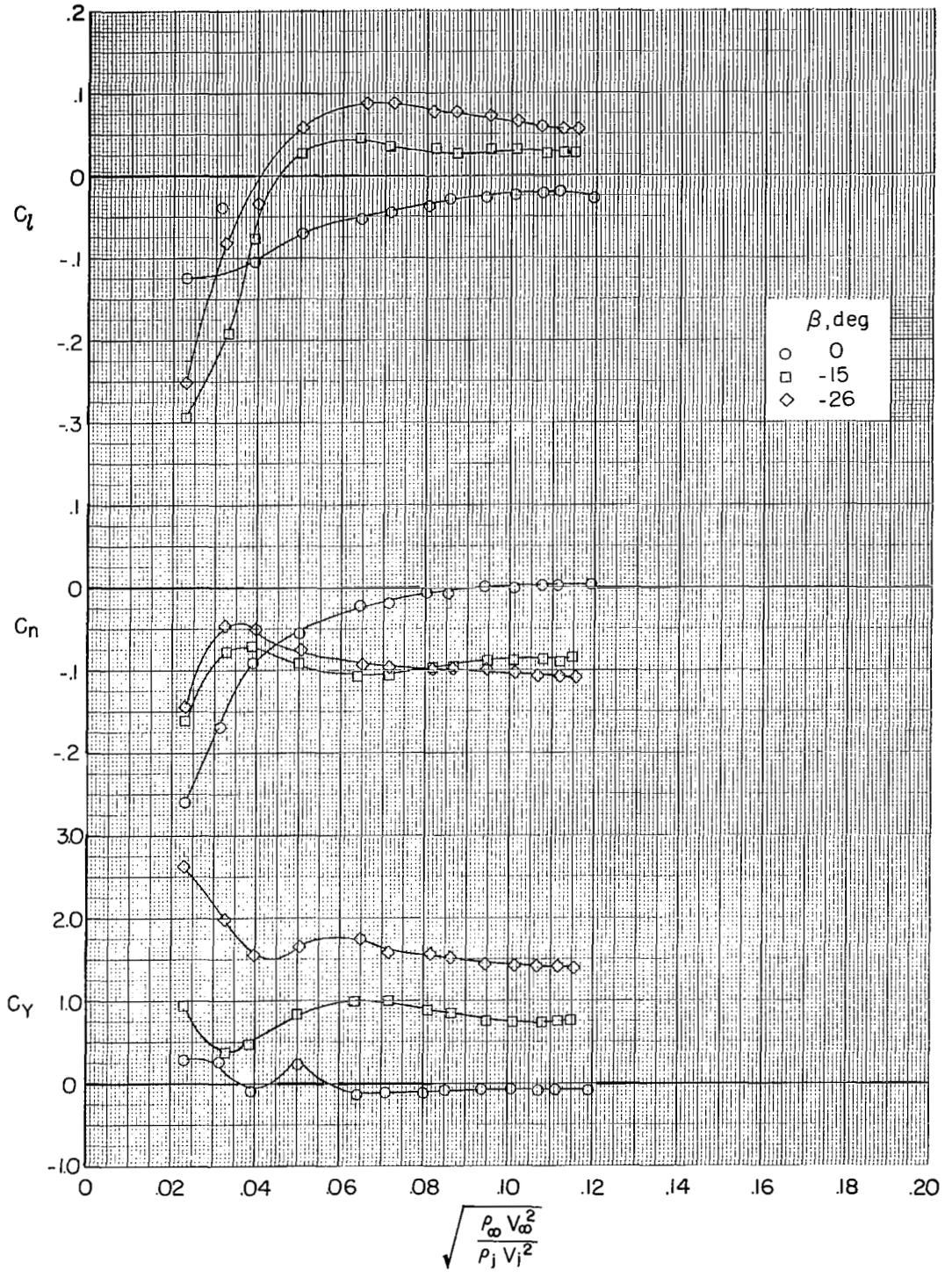


(a) Measured lateral-directional characteristics.

Figure 17.- Variation of $C_l$, $C_n$, and $C_Y$ with effective velocity ratio (in ground effect) showing effect of sideslip angle. Six lift engines; landing gear and auxiliary horizontal tail on; $\alpha = 0^0$; $\delta_n = 0^0$; $h/\bar{c} = 3.45$.

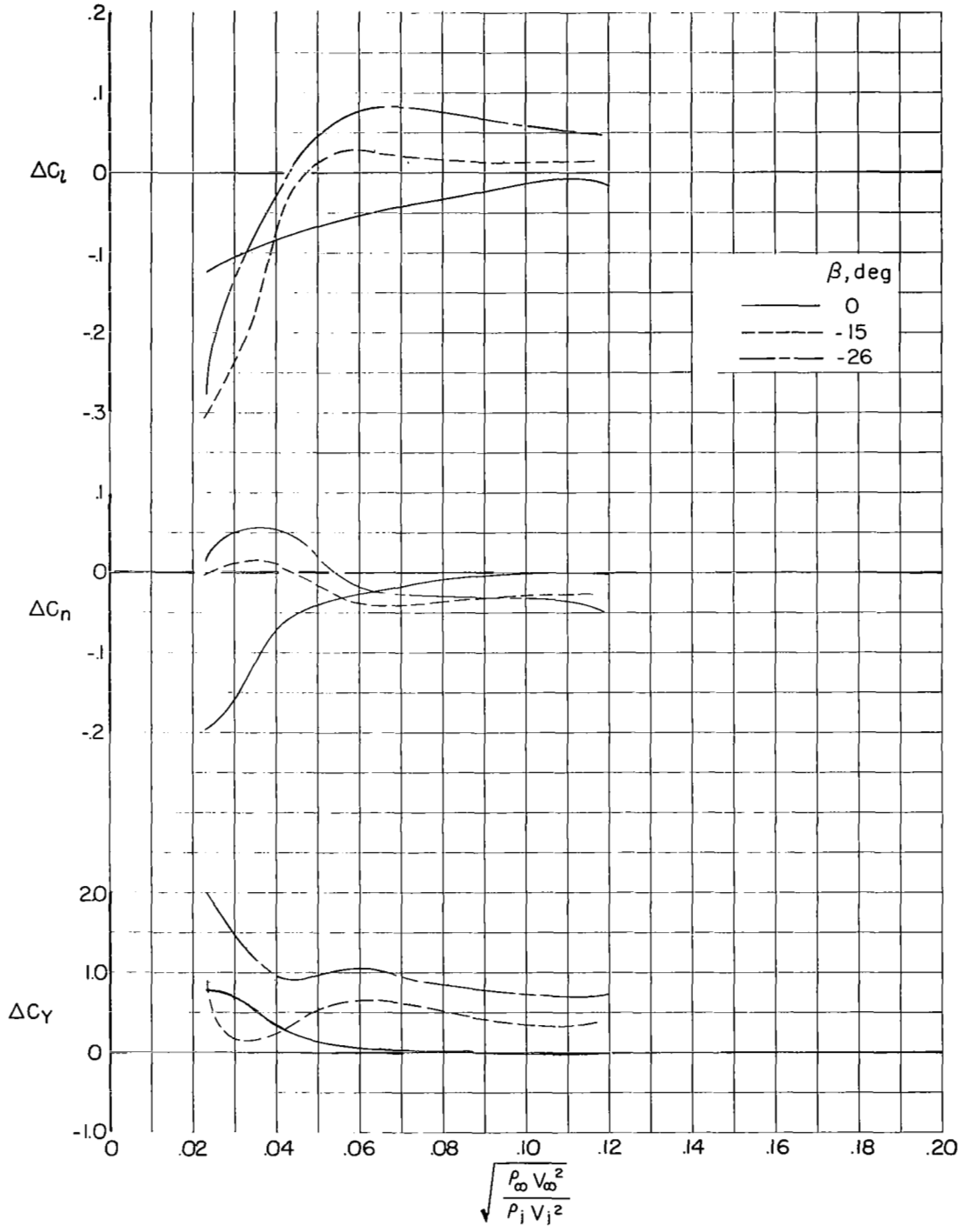


(b) Lateral-directional interference increments.

Figure 17.- Continued.

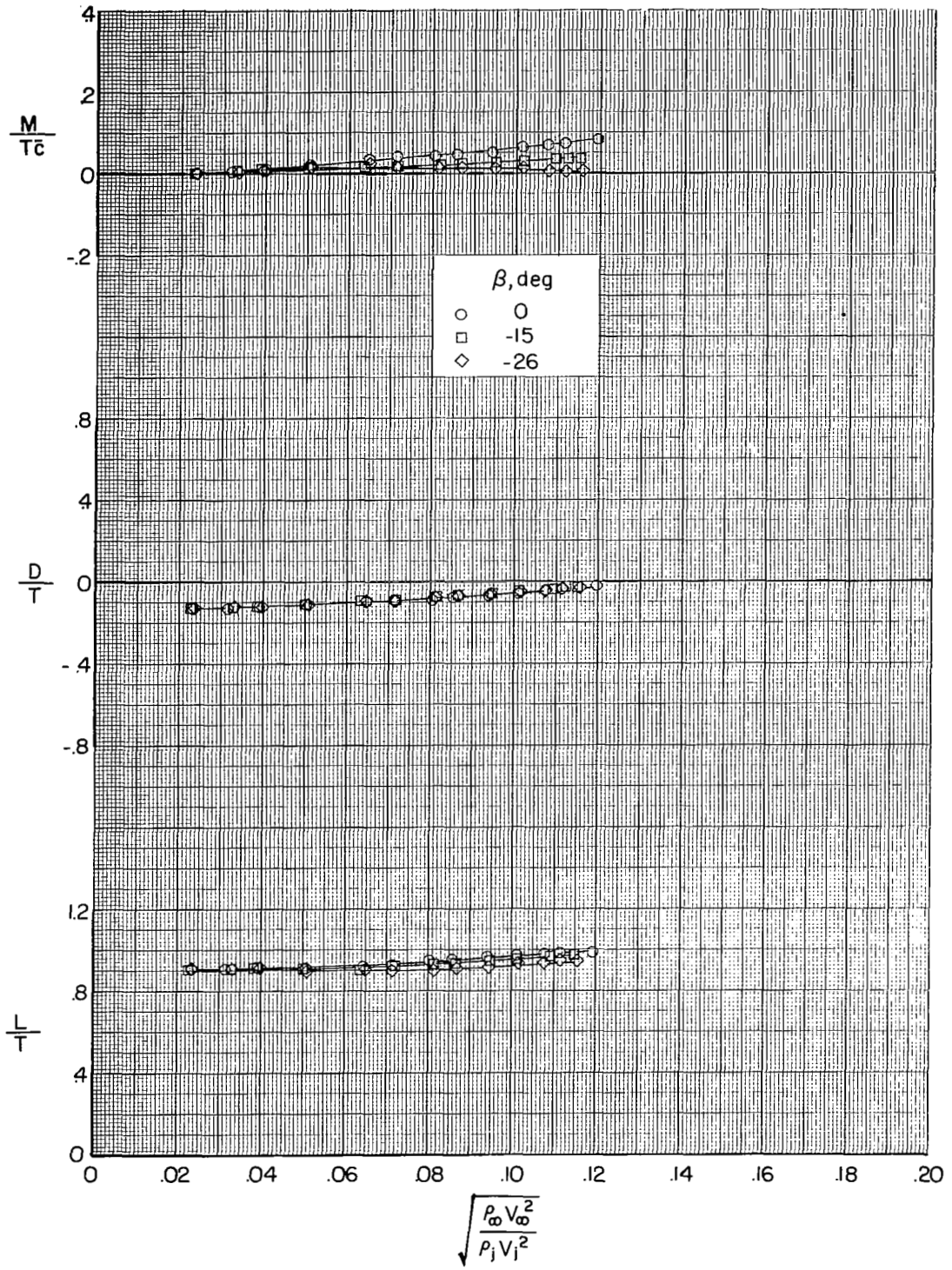


(c) Measured longitudinal characteristics.

Figure 17.- Continued.

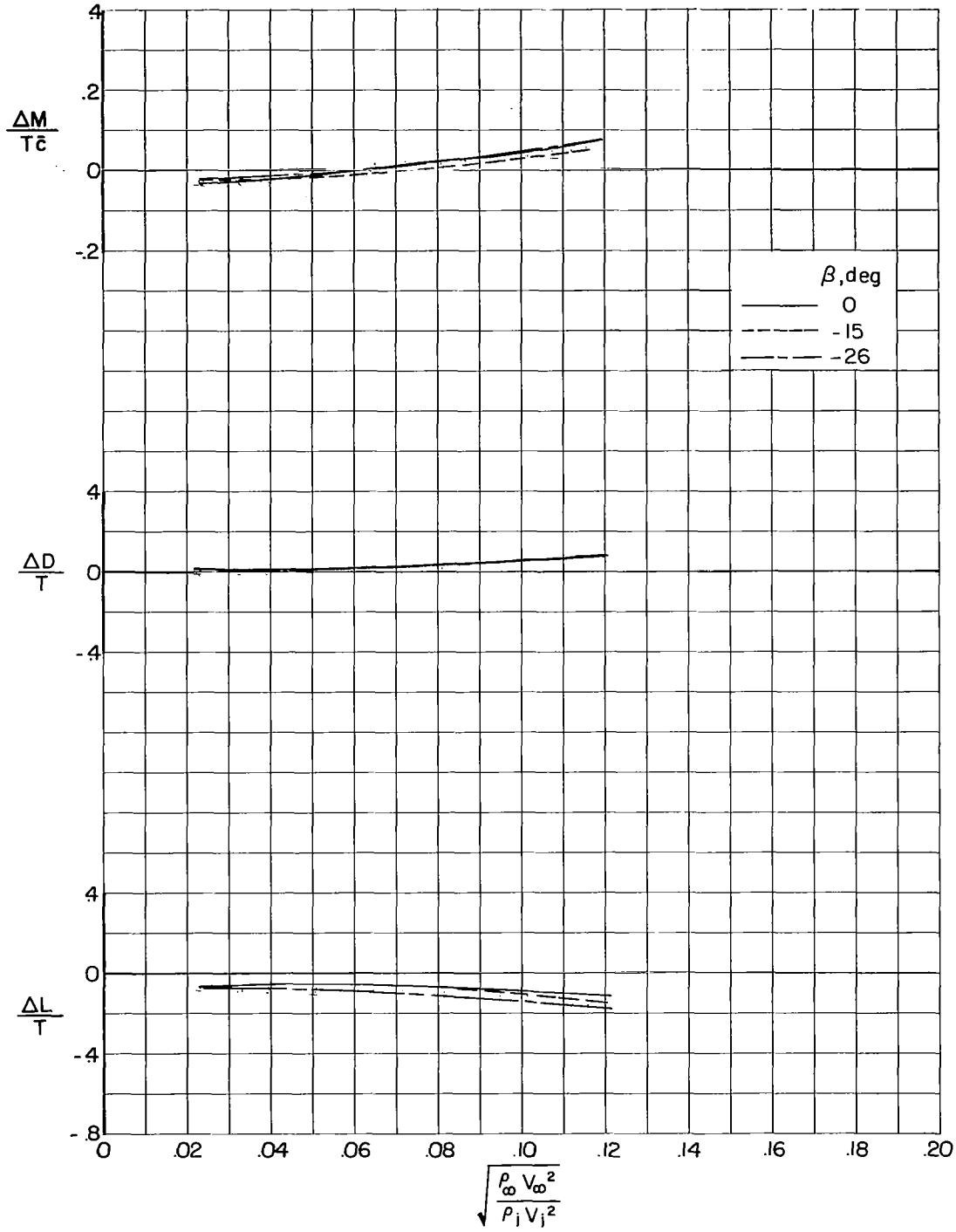


(d) Longitudinal interference increments.

Figure 17.- Concluded.

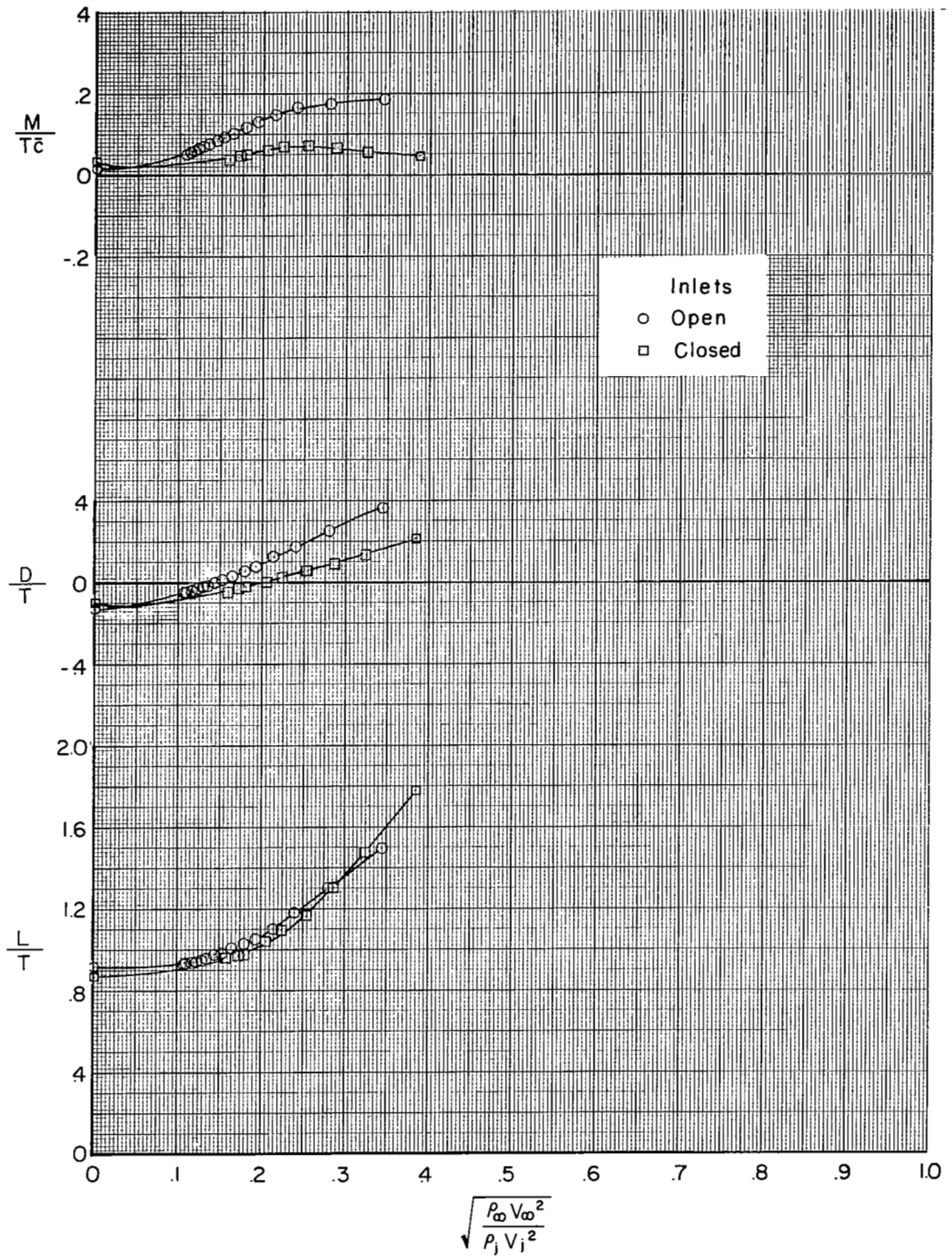


(a) Measured characteristics.

Figure 18.- Variation of $M/T\bar{c}$, D/T, and L/T with effective velocity ratio showing effect of inlet mass flow. Six lift engines; $\alpha = 0^0$; $\beta = 0^0$; $\delta_n = 0^0$.

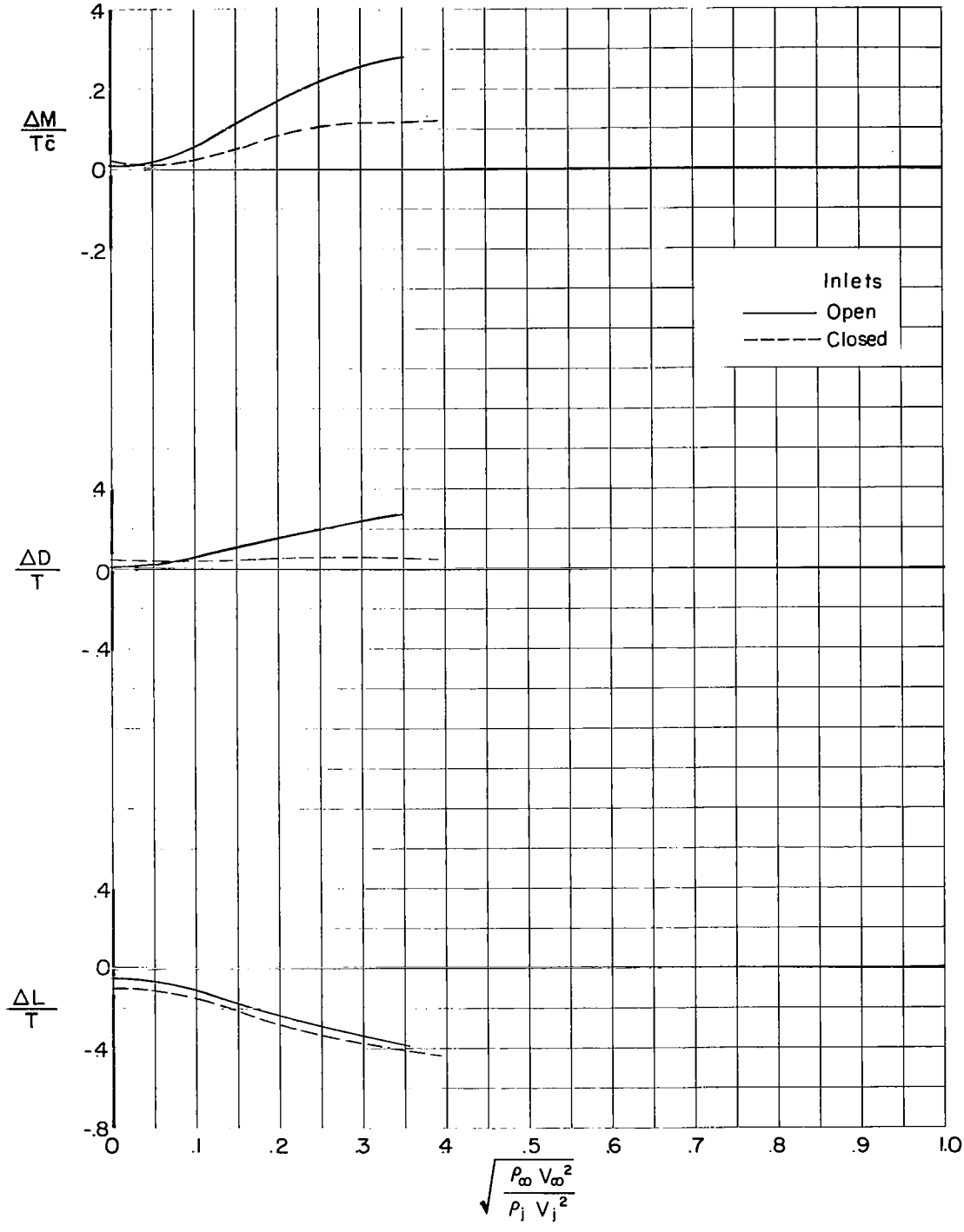


(b) Interference increments.

Figure 18.- Concluded.

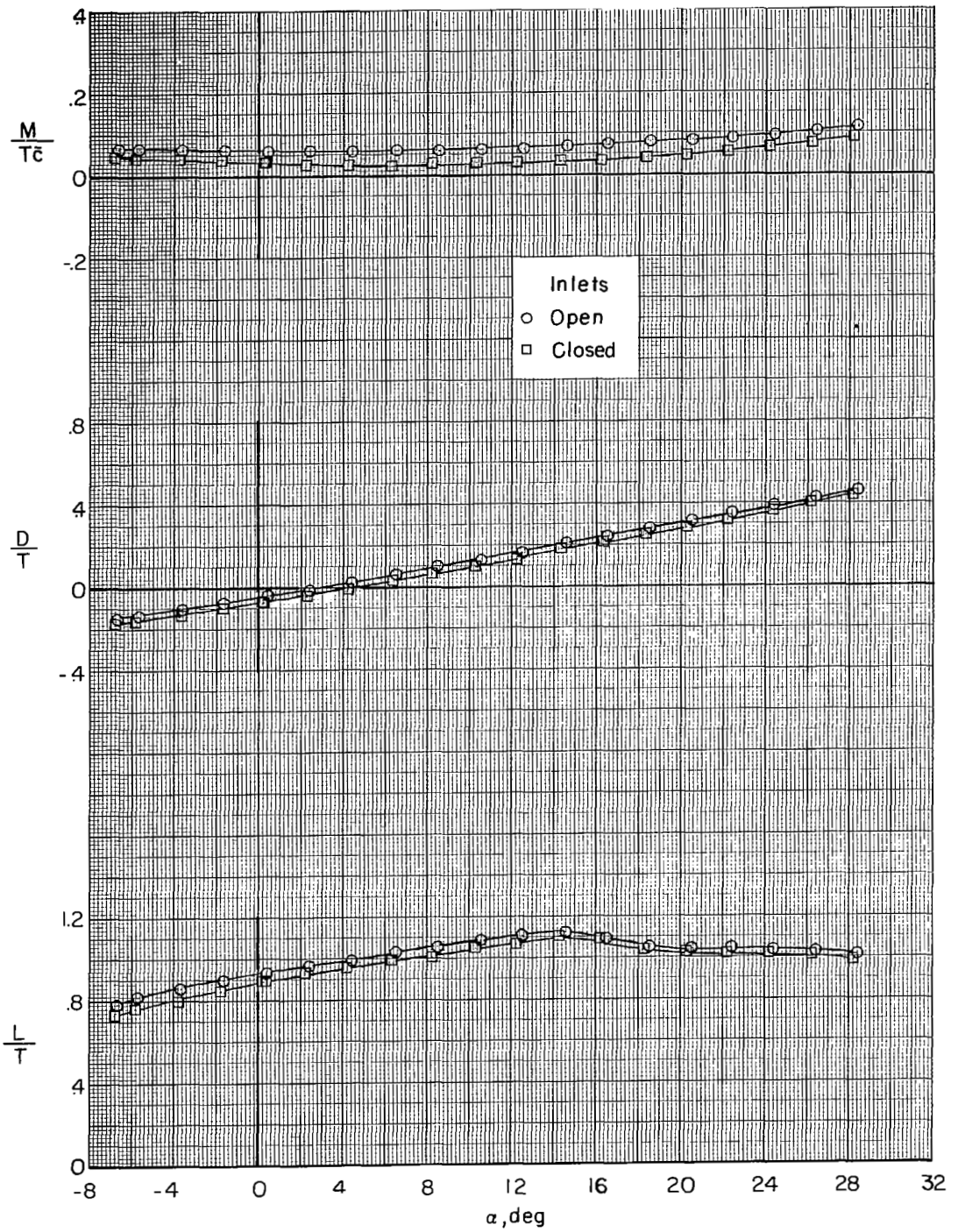


(a) Measured characteristics.

Figure 19.- Variation of $M/T\bar{c}$, D/T, and L/T with angle of attack showing effect of inlet mass flow. Six lift engines; effective velocity ratio, 0.115; $\beta = 0^0$; $\delta_n = 0^0$.

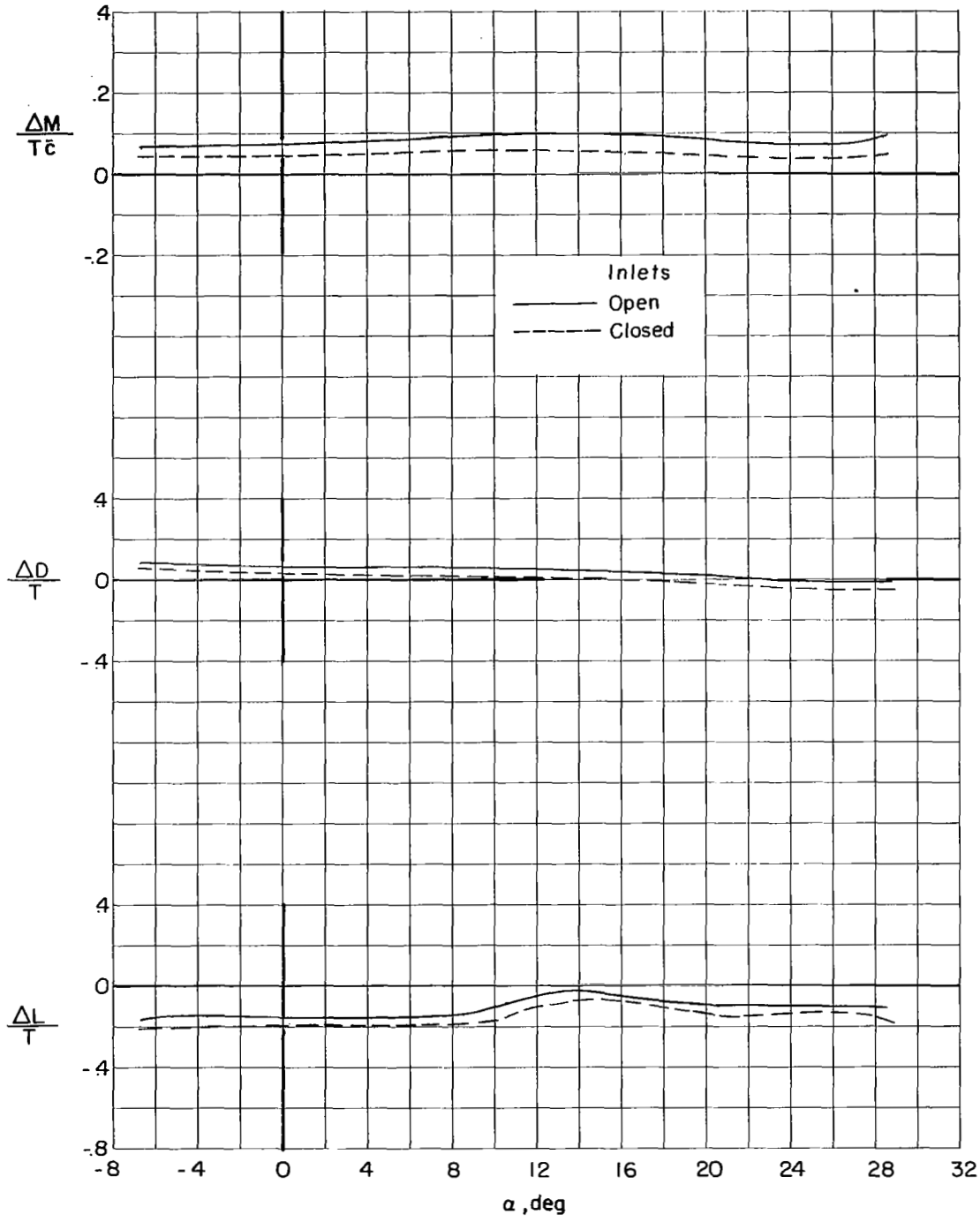


(b) Interference increments.

Figure 19.- Concluded.

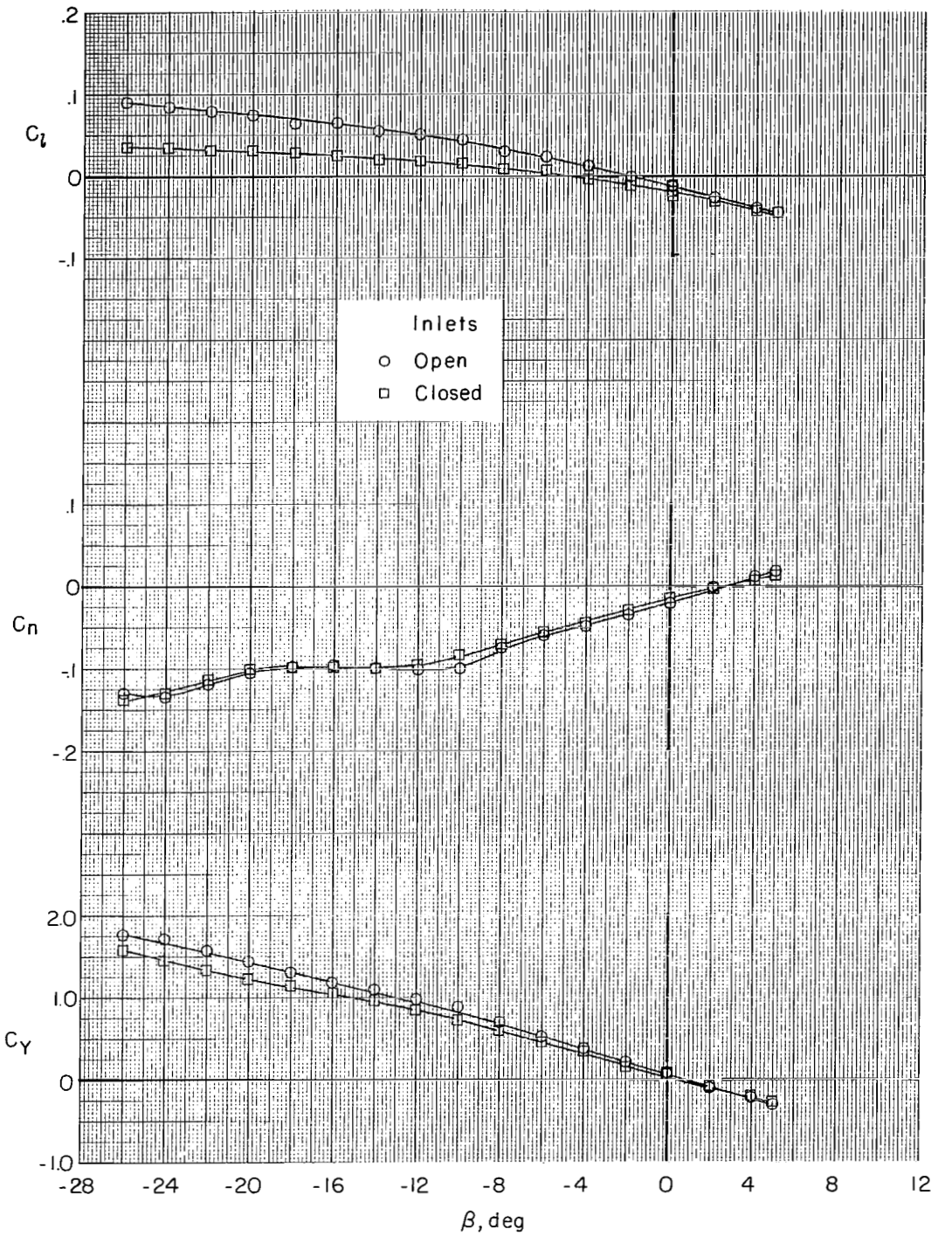


(a) Measured lateral-directional characteristics.

Figure 20.- Aerodynamic characteristics in sideslip showing effect of inlet mass flow. Six lift engines; effective velocity ratio, 0.115; $\alpha = 0^0$; $\delta_n = 0^0$.

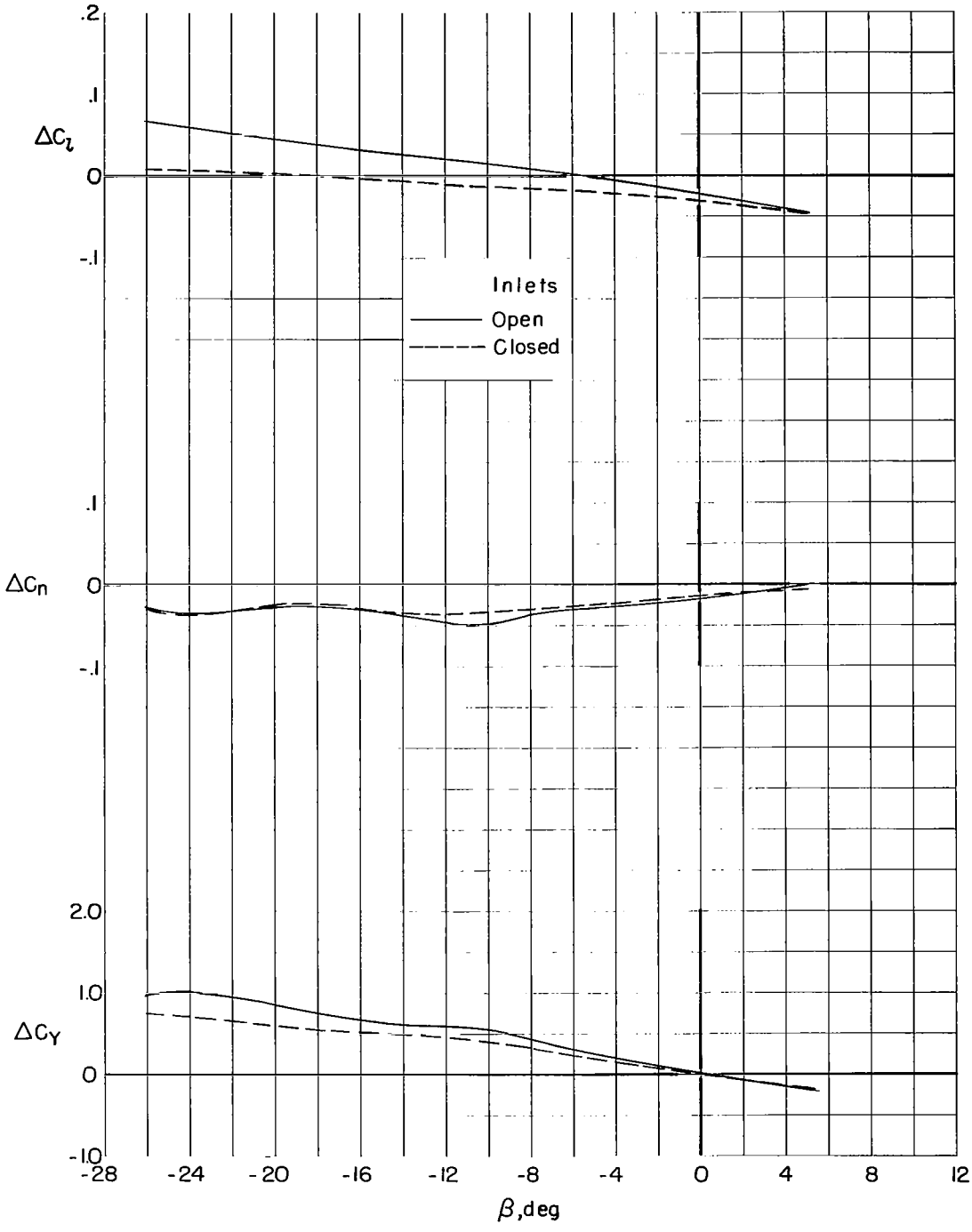


(b) Lateral-directional interference increments.

Figure 20.- Continued.

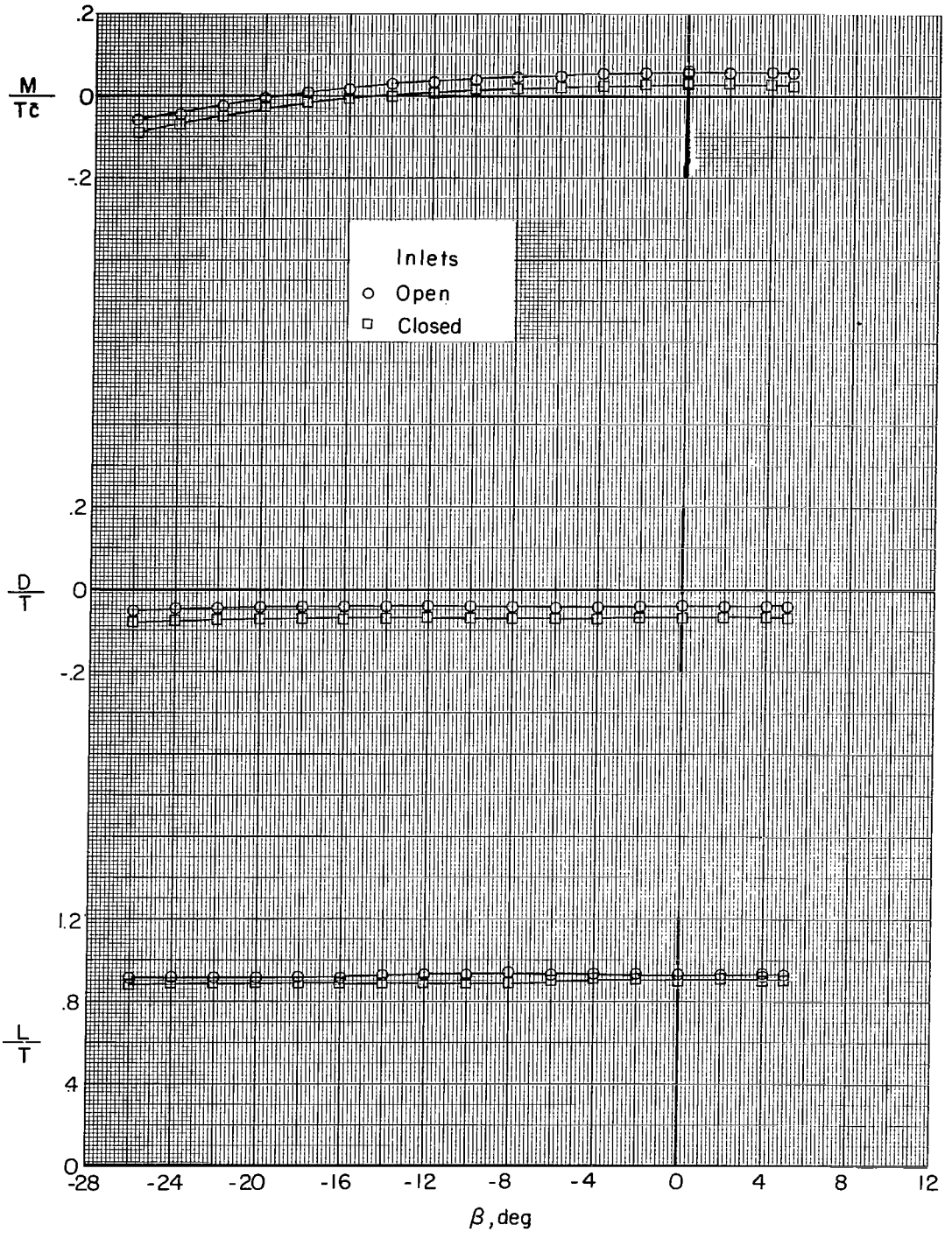


(c) Measured longitudinal characteristics.

Figure 20.- Continued.

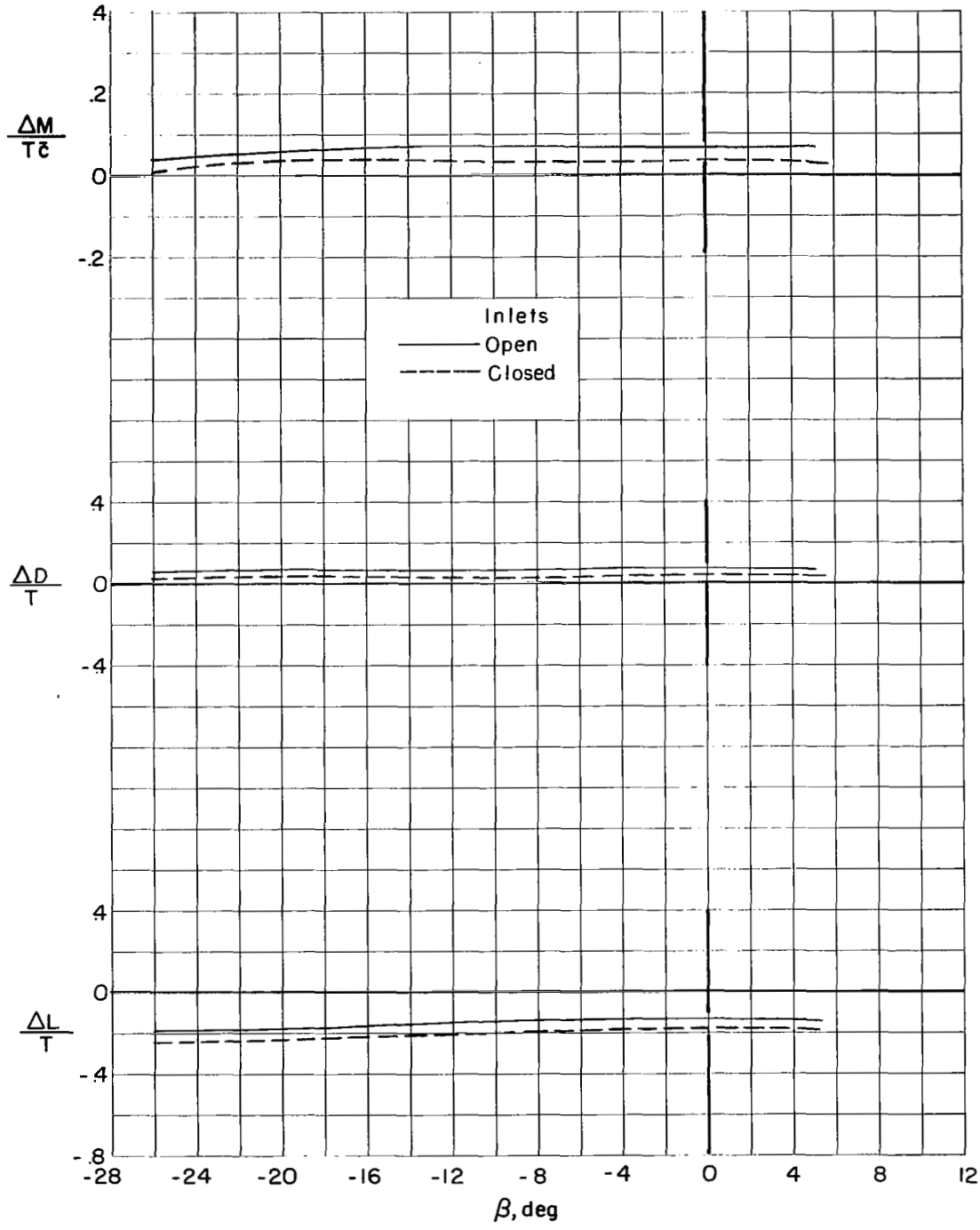


(d) Longitudinal interference increments.

Figure 20.- Concluded.



NASA-Langley, 1970 — 1 L-6921